A LABORATORY EVALUATION OF ALIGNMENT TOLERANCES FOR DOWEL BARS AND THEIR EFFECT ON JOINT OPENING BEHAVIOR

Final Report

Submitted to
MICHIGAN DEPARTMENT OF TRANSPORTATION
Construction and Technology Division
Lansing, Michigan

by
Neeraj Buch (Principal Investigator)
Amit H. Varma (Co-Principal Investigator, Purdue University)
Milind L. Prabhu (Graduate Research Assistant)

Department of Civil and Environmental Engineering
Michigan State University
East Lansing, MI 48824-1226

February 2007

Technical Report Documentation Page

1. Report No. RC-1487	2. Government Accession No.	3. Recipient's Catalog No.
4. Title and Subtitle A Laboratory evaluation of alignment tolerances for dowel bars and their effect on joint opening behavior.		5. Report Date February 2007
		6. Performing Organization Code
7. Author(s) Neeraj Buch, Amit H. Varma and Milind L. Prabhu		8. Performing Organization Report No.
9. Performing Organization Name Address Michigan State University Department of Civil and Environmental Engineering 3546 Engineering Building East Lansing, MI 48824		10. Work Unit No. (TRAIS)
		11. Contract or Grant No.
12. Sponsoring Agency Name and Address Michigan Department of Transportation Construction and Technology Division Lansing, Michigan		13. Type of Report and Period Covered
		14. Sponsoring Agency Code
15. Supplementary Notes		

16. Abstract

This report presents an experimental and analytical investigation on the fundamental pullout behavior and joint opening behavior of misaligned dowel bars in concrete pavement joints. Experimental investigations were conducted to determine the fundamental joint opening behavior of concrete pavements, and to evaluate the effects of dowel misalignment on joint opening behavior. The parameters included in the experimental investigations were the number of dowel bars (1, 2, 3, or 5) at the joint, the dowel misalignment type (horizontal, vertical, and combined), misalignment magnitude (0, 1/36, 1/18, 1/12, 1/9 radians.), and uniformity across the joint. The effects of these parameters were evaluated on the joint opening behavior and structural distresses observed in the specimens. Numerous instrumented laboratory-scale specimens of pavement slabs with doweled joints were tested. The second task focused on the development of 3D finite element models for computing the complex stress states and resulting damage in concrete pavement joints with misaligned dowels, and their validation using experimental results. The concrete pavement is modeled using a damage-plasticity material model, which uses concepts of damaged plasticity formulation in compression and cracking combined with damage elasticity in tension. The longitudinal bond between the steel dowel and the concrete is modeled in two parts. (i) The longitudinal bond resulting from chemical adhesion, mechanical interlock, and static friction (in the aligned state) is modeled using spring elements. (ii) The longitudinal bond resulting from transverse interaction between steel dowels and the concrete pavement is modeled using surface-to-surface contact-interaction elements and associated friction models. The 3D finite element models are validated using results from the experimental investigations. These validated models provide significant insight into the 3D stress states and principal stresses that develop in concrete pavement joints with misaligned dowels. They are used to evaluate analytically the effects of misalignment type, magnitude, uniformity, and distribution on the 3D stress states and resulting damage in concrete pavements. The analytical results (3D stresses and strains) from the finite element analyses were considered to identify significant limit states and distresses in the concrete pavement joints. Parametric studies were conducted and recommendations on misalignment tolerances based on these parametric studies have been made. A preliminary investigation to capture the effects of misaligned dowel bars combined with wheel loads has also been carried out in this research study.

17. key Words Rigid concrete pavements, finite element analysis, misaligned dowel bars, nonlinear concrete material model		18. Distribution Statement	
19. Security Classif. (of this report) Unclassified	20. Security Classif. (of this page) Unclassified	21. No of Pages 376	22. Price

Form DOT F 1700.7 (8-72) **Reproduction of completed page authorized**

ACKNOWLEDGMENTS

The research project was financially supported by the Michigan Department of Transportation. The project team would also like to acknowledge the technical support offered by the project technical assistance group (TAG).

DISCLAIMER

The contents of this report reflect the views of the authors. The contents do not necessarily reflect the views or policies of the Michigan Department of Transportation. This report does not constitute a standard, specification or regulation.

TABLE OF CONTENTS

LIST OF TABLES……..……..…vii

LIST OF FIGURES ……xii

ABSTRACT …….xx

CHAPTER 1

INTRODUCTION

1.1 Introduction..... 1
1.2 Problem statement..... 2
1.3 Research Objectives..... 2
1.4 Research Plan..... 4
1.5 Layout of the Thesis..... 5

CHAPTER 2

LITERATURE REVIEW

2.1 Introduction..... 7
2.2 Definitions of misalignment, various organizational specifications and construction practices 8
2.2.1 Definitions of misalignment 8
2.2.2 Specifications from various State Highway Authorities..... 11
2.2.3 Construction practices..... 14
2.3 Review of field studies..... 20
2.4 Review of laboratory investigations 23
2.5 Review of analytical studies 32

CHAPTER 3

EXPERIMENTAL INVESTIGATIONS

3.1 Introduction..... 46
3.2 Experimental plan 46
3.2.1 Dowel misalignment type 47
3.2.2 Dowel misalignment magnitude 47
3.2.3 Number of misaligned dowels 47
3.2.4 Orientation of misaligned mowel bars..... 47
3.3 Experimental test setup 53
3.4 Limitations and short comings of the test setup..... 57
3.5 Surveying technique and calculations..... 57
3.5.1 Derivation for measurement of vertical misalignment 58
3.5.2 Derivation for measurement of horizontal misalignment 62
3.6 Material specifications 69

3.7 Instrumentation and data acquisition system 74
3.8 Typical cycle for preparing and testing a specimen..... 78

CHAPTER 4

EXPERIMENTAL RESULTS AND EVALUATION

4.1 Introduction..... 81
4.2 Laboratory test results..... 81
4.2.1 Comparison within a type of misalignment..... 85
4.2.2 Comparisons between the orientation of misaligned dowel bars..... 102
4.2.3 Distresses observed in the test specimen …….....118
4.3 Summary of results 127
4.4 Pullout behavior of misaligned dowel bars..... 127
4.5 Dowel-concrete interaction..... 129

CHAPTER 5

DEVELOPMENT OF 3D FINITE ELEMENT MODELS

5.1 Introduction..... 131
5.2 Need for a 3D Finite element model..... 131
5.3 The 3D Finite element model – element selection..... 132
5.4 Material model – Behavior and Calibration..... 135
5.4.1 Types of concrete material models 135
5.4.1.1 The smeared cracking model 135
5.4.1.2 The cracking model for concrete 137
5.4.1.3 The concrete damage plasticity model..... 137
5.4.2 Features of concrete behavior 139
5.4.3 Input parameters for the concrete material model 143
5.4.4 Steel dowel bar material model..... 147
5.5 Development of the dowel – concrete interaction bond model 147
5.5.1 The longitudinal Bond Behavior..... 148
5.5.2 The transverse Interaction Behavior 150
5.6 Limitations and short comings of the FE model..... 151
5.7 Loading and boundary conditions..... 155
5.8 The 3D Finite element model results..... 156
5.9 Concluding remarks..... 167

CHAPTER 6

THREE DIMENSIONAL FINITE ELEMENT ANALYSIS RESULTS

6.1 Introduction..... 168
6.2 Material events or damage limit states..... 168

6.2.1 Additional discussion and limitations 172
6.3 Discussion of analytical and experimental results 175
6.3.1 Single dowel bar models 177
6.3.2 Two dowel bar models 178
6.3.3 Five dowel bar models 179
6.3.4 Concluding remarks on the 3D Finite element analytical models with events / material damage limit states 196
6.4 Analytical parametric study 197
6.5 Results and discussion 198
6.5.1 One misaligned dowel bar 198
6.5.2 Two misaligned dowel bars 201
6.5.3 Concluding remarks on the results of the analytical parametric studies 209
6.6 Conclusions and recommendations 210

CHAPTER 7

PRELIMINARY INVESTIGATION OF LOAD EFFECTS COMBINED WITH

DOWEL MISALIGNMENTS

7.1 Introduction 212
7.2 Assumptions and limitations of the finite element model 212
7.3 Development of the finite element model 213
7.3.1 Dimensions of the analytical model 214
7.3.2 Material model input parameters 219
7.3.3 Interaction models 220
7.3.4 Loading and boundary conditions 224
7.4 Results and discussion 226
7.4.1 Single dowel bar model 227
7.4.2 Three dowel bar model 234
7.5 Concluding remarks 240

CHAPTER 8

SUMMARY, CONCLUSIONS, RECOMMENDATIONS AND FUTURE RESEARCH

8.1 Introduction 241
8.2 Summary and conclusions based on experimental investigations 241
8.3 Summary and conclusions based on analytical investigations 244
8.4 Summary and conclusions of parametric studies 246
8.5 Summary and conculsions based on the studies for misaligned dowels combined with wheel loading 246
8.6 Recommendations and future research 248

Appendices……...……..250
Refereces…….....……...……350

LIST OF TABLES

Table 2.1(a): Possible Effects of Translational type of Dowel Misalignment on Pavement Performance 9
Table 2.1(b): Possible Effects of Skew type of Dowel Misalignment on Pavement Performance 10
Table 2.2: DOT Tolerance Specifications 13
Table 2.3: Survey of Dowel Bar Installation Specifications..... 14
Table 2.4: Construction Factors affecting Misalignment 18
Table 2.5: Summary of Field Study Results 24
Table 3.2: Experimental Test Investigation Matrix 50
Table 3.3(a) Test Specimen of the single dowel bar experiments conducted..... 51
TABLE 3.3(b) Test Matrix of the two dowel bar experiments conducted 52
TABLE 3.3(c) Test Matrix of the three and five dowel bar experiments conducted 53
Table 3.5: Summary Table showing all angles for horizontal misalignment 66
Table 3.6: Mix Design of Concrete..... 70
Table 3.7: Concrete Properties..... 71
Table 5.1: Case I and Case II input parameters for the various models……..151
Table 6.1(a) Test Matrix of the single dowel bar..... 175
Table 6.1(b) Test Matrix of the two dowel bars 176
Table 6.1(c) Test Matrix of the five dowel bars 176
Table 6.2(a): Summary of the pullout load – joint opening for cases I and II in the 1V18, 1H18 and 1C18 tests 181
Table 6.2(b): Summary of pullout load-joint opening for case (i) and (ii) in the 2V18NU, 2V18U and 2V18AM test 181
Table 6.2(c): Summary of pullout load-joint opening for case (i) and (ii) in the 2H18NU, 2H18U and 2H18AM test 182
Table 6.2(d): Summary of pullout load-joint opening for case (i) and (ii) in the 2C18NU, 2C18U and 2C18AM test..... 182
Table 6.2(e): Summary of the pullout load – joint opening for cases I and II in the 5V18NU and 5V18AM tests..... 183
Table 6.2(f): Summary of the pullout load – joint opening for cases I and II in the 5H18NU and 5H18AM tests..... 183
Table 6.2(g): Summary of the pullout load – joint opening for cases I and II in the 5C18NU and 5C18AM tests 183
Table 6.3: Summary of the Finite Element Analysis conducted 197
Table 6.4(a): Summary of the Damage Limit States and Joint Opening (in.) for Case I 199
Table 6.4(b): Summary of the Damage Limit States and Joint Opening (in.) for Case II 199
Table 6.5(a): Summary of the Damage Limit States and Joint Opening (in.) for Case I with Vertically Misaligned dowel bars 202
Table 6.5(b): Summary of the Damage Limit States and Joint Opening (in.) for Case II with Vertically Misaligned dowel bars 202
Table 6.6(a): Summary of the Damage Limit States and Joint Opening for Case I with Horizontally Misaligned dowel bars 206

Table 6.6(b): Summary of the Damage Limit States and Joint Opening for Case II with Horizontally Misaligned dowel bars 206
Table 7.1: Misalignment cases considered for single and three dowel bar loaded slabs 219
Table 7.2: Material input parameters for the single and three dowel bar finite element models 221
Table A-1. Mix Design Specifications 253
Table A-2: Concrete Specimen strength at 7 days 254
Table A-3. Description of Linear Variable Differential Transducer 257
Table A-4. Description of the Hydraulics (Actuators RC 156 and RC 256) 257
Table B-1. Misalignment Check Summary – One Dowel Tests 265
Table B-2. Misalignment Check Summary – Two Dowel Tests (North Dowel) 266
Table B-3. Misalignment Check Summary – Two Dowel Tests (South Dowel) 266
Table B-3. Misalignment Check Summary – Two Dowel Tests (South Dowel) 267
Table B-4. Misalignment Check Summary – Three and Five Dowel Tests 268
Table B-5. Horizontal Misalignment Summary – One Dowel Tests 269
Table B-6. Horizontal Misalignment Summary – Two Dowel Tests (North Dowel) 269
Table B-7. Horizontal Misalignment Summary – Two Dowel Tests (South Dowel) 270
Table B-8. Horizontal Misalignment Summary – Three and Five Dowel Tests 271
Table C-1: Dowel-Concrete Friction Coefficients; Material Properties used and limit states obtained from the analysis. 273
Table C-2: Summary of Material Failure / Damage Limit States from the analysis 273
Table C-3: Dowel-Concrete Friction Coefficients; Material Properties used and limit states obtained from the analysis. 274
Table C-4: Summary of Material Failure / Damage Limit States from the analysis 274
Table C-5: Dowel-Concrete Friction Coefficients; Material Properties used and limit states obtained from the analysis. 275
Table C-6: Summary of Material Failure / Damage Limit States from the analysis 275
Table C-7: Dowel-Concrete Friction Coefficients; Material Properties used and limit states obtained from the analysis. 276
Table C-8: Summary of Material Failure / Damage Limit States from the analysis 276
Table C-9: Dowel-Concrete Friction Coefficients; Material Properties used and limit states obtained from the analysis. 277
Table C-10: Summary of Material Failure / Damage Limit States from the analysis 277
Table C-11: Dowel-Concrete Friction Coefficients; Material Properties used and limit states obtained from the analysis. 278
Table C-12: Summary of Material Failure / Damage Limit States from the analysis 278
Table C-13: Dowel-Concrete Friction Coefficients; Material Properties used and limit states obtained from the analysis. 279
Table C-14: Summary of Material Failure / Damage Limit States from the analysis 279
Table C-15: Dowel-Concrete Friction Coefficients; Material Properties used and limit states obtained from the analysis. 280
Table C-16: Summary of Material Failure / Damage Limit States from the analysis 280
Table C-17: Dowel-Concrete Friction Coefficients; Material Properties used and limit states obtained from the analysis. 281
Table C-18: Summary of Material Failure / Damage Limit States from the analysis 281

Table C-19: Dowel-Concrete Friction Coefficients; Material Properties used and limit states obtained from the analysis. 282
Table C-20: Summary of Material Failure / Damage Limit States from the analysis 282
Table C-21: Dowel-Concrete Friction Coefficients; Material Properties used and limit states obtained from the analysis. 283
Table C-22: Summary of Material Failure / Damage Limit States from the analysis 283
Table C-23: Dowel-Concrete Friction Coefficients; Material Properties used and limit states obtained from the analysis. 284
Table C-24: Summary of Material Failure / Damage Limit States from the analysis 284
Table C-25: Dowel-Concrete Friction Coefficients; Material Properties used and limit states obtained from the analysis. 285
Table C-26: Summary of Material Failure / Damage Limit States from the analysis 285
Table C-27: Dowel-Concrete Friction Coefficients; Material Properties used and limit states obtained from the analysis. 286
Table C-28: Summary of Material Failure / Damage Limit States from the analysis 286
Table C-29: Dowel-Concrete Friction Coefficients; Material Properties used and limit states obtained from the analysis. 287
Table C-30: Summary of Material Failure / Damage Limit States from the analysis 287
Table C-31: Dowel-Concrete Friction Coefficients; Material Properties used and limit states obtained from the analysis. 288
Table C-32: Summary of Material Failure / Damage Limit States from the analysis 288
Table C-33: Dowel-Concrete Friction Coefficients; Material Properties used and limit states obtained from the analysis. 289
Table C-34: Summary of Material Failure / Damage Limit States from the analysis 289
Table C-35: Dowel-Concrete Friction Coefficients; Material Properties used and limit states obtained from the analysis. 290
Table C-36: Summary of Material Failure / Damage Limit States from the analysis 290
Table C-37: Dowel-Concrete Friction Coefficients; Material Properties used and limit states obtained from the analysis. 291
Table C-38: Summary of Material Failure / Damage Limit States from the analysis 291
Table C-39: Dowel-Concrete Friction Coefficients; Material Properties used and limit states obtained from the analysis. 292
Table C-40: Summary of Material Failure / Damage Limit States from the analysis 292
Table C-41: Dowel-Concrete Friction Coefficients; Material Properties used and limit states obtained from the analysis. 293
Table C-42: Summary of Material Failure / Damage Limit States from the analysis 293
Table C-43: Dowel-Concrete Friction Coefficients; Material Properties used and limit states obtained from the analysis. 294
Table C-44: Summary of Material Failure / Damage Limit States from the analysis 294
Table C-45: Dowel-Concrete Friction Coefficients; Material Properties used and limit states obtained from the analysis. 295
Table C-46: Summary of Material Failure / Damage Limit States from the analysis 295
Table C-47: Dowel-Concrete Friction Coefficients; Material Properties used and limit states obtained from the analysis. 296
Table C-48: Summary of Material Failure / Damage Limit States from the analysis 296

Table C-49: Dowel-Concrete Friction Coefficients; Material Properties used and limit states obtained from the analysis. 297
Table C-50: Summary of Material Failure / Damage Limit States from the analysis 297
Table C-51: Dowel-Concrete Friction Coefficients; Material Properties used and limit states obtained from the analysis. 298
Table C-52: Summary of Material Failure / Damage Limit States from the analysis 298
Table C-53: Dowel-Concrete Friction Coefficients; Material Properties used and limit states obtained from the analysis. 299
Table C-54: Summary of Material Failure / Damage Limit States from the analysis 299
Table C-55: Dowel-Concrete Friction Coefficients; Material Properties used and limit states obtained from the analysis. 300
Table C-56: Summary of Material Failure / Damage Limit States from the analysis 300
Table C-57: Dowel-Concrete Friction Coefficients; Material Properties used and limit states obtained from the analysis. 301
Table C-58: Summary of Material Failure / Damage Limit States from the analysis 301
Table C-59: Dowel-Concrete Friction Coefficients; Material Properties used and limit states obtained from the analysis. 302
Table C-60: Summary of Material Failure / Damage Limit States from the analysis 302
Table C-61: Dowel-Concrete Friction Coefficients; Material Properties used and limit states obtained from the analysis. 303
Table C-62: Summary of Material Failure / Damage Limit States from the analysis 303
Table C-63: Dowel-Concrete Friction Coefficients; Material Properties used and limit states obtained from the analysis. 304
Table C-64: Summary of Material Failure / Damage Limit States from the analysis 304
Table C-65: Dowel-Concrete Friction Coefficients; Material Properties used and limit states obtained from the analysis. 305
Table C-66: Summary of Material Failure / Damage Limit States from the analysis 305
Table C-67: Dowel-Concrete Friction Coefficients; Material Properties used and limit states obtained from the analysis. 306
Table C-68: Summary of Material Failure / Damage Limit States from the analysis 306
Table C-69: Dowel-Concrete Friction Coefficients; Material Properties used and limit states obtained from the analysis. 307
Table C-70: Summary of Material Failure / Damage Limit States from the analysis 307
Table C-71: Dowel-Concrete Friction Coefficients; Material Properties used and limit states obtained from the analysis. 308
Table C-72: Summary of Material Failure / Damage Limit States from the analysis 308
Table C-73: Dowel-Concrete Friction Coefficients; Material Properties used and limit states obtained from the analysis. 309
Table C-74: Summary of Material Failure / Damage Limit States from the analysis 309
Table C-75: Dowel-Concrete Friction Coefficients; Material Properties used and limit states obtained from the analysis. 310
Table C-76: Summary of Material Failure / Damage Limit States from the analysis 310
Table C-77: Dowel-Concrete Friction Coefficients; Material Properties used and limit states obtained from the analysis. 311
Table C-78: Summary of Material Failure / Damage Limit States from the analysis 311

Table C-79: Dowel-Concrete Friction Coefficients; Material Properties used and limit states obtained from the analysis. 312
Table C-80: Summary of Material Failure / Damage Limit States from the analysis 312
Table C-81: Dowel-Concrete Friction Coefficients; Material Properties used and limit states obtained from the analysis. 313
Table C-82: Summary of Material Failure / Damage Limit States from the analysis 313
Table C-83: Dowel-Concrete Friction Coefficients; Material Properties used and limit states obtained from the analysis. 314
Table C-84: Summary of Material Failure / Damage Limit States from the analysis 314
Table C-85: Dowel-Concrete Friction Coefficients; Material Properties used and limit states obtained from the analysis. 315
Table C-86: Summary of Material Failure / Damage Limit States from the analysis 315
Table C-87: Dowel-Concrete Friction Coefficients; Material Properties used and limit states obtained from the analysis. 316
Table C-88: Summary of Material Failure / Damage Limit States from the analysis 316
Table C-89: Dowel-Concrete Friction Coefficients; Material Properties used and limit states obtained from the analysis. 317
Table C-90: Summary of Material Failure / Damage Limit States from the analysis 317
Table C-91: Dowel-Concrete Friction Coefficients; Material Properties used and limit states obtained from the analysis. 318
Table C-92: Summary of Material Failure / Damage Limit States from the analysis 318
Table E-1: Comparison of the fine and coarse mesh joint opening and dowel pullout forces 349

LIST OF FIGURES

Figure 2.1: Typical components of a pavement cross section and truck loading. 7
Figure 2.2: Typical dowel basket assembly used as load transfer devices in JPCP 15
Figure 2.3: Dowel Bar Inserter (Source Gomaco Inc., www.gomaco.com)..... 17
Figure 2.4: Various Non-Destructive Misalignment Measuring Devices 20
Figure 2.5: Pressure Exerted on a Loaded Dowel, Yoder (1975)..... 33
Figure 3.1 Sign Convention for Orientation of the dowel bar (Clockwise (CW) – Positive) 48
Figure 3.2: Concrete slab specimen with misaligned dowel bars..... 49
Figure 3.3: Shop drawings showing the test setup dimensions for one and two dowel bar specimens..... 55
Figure 3.4: Photograph of the various components of the experimental set-up 56
Figure 3.5: Horizontal plane showing angles measured from center of base plate to misalignment..... 59
Figure 3.6: Vertical plane in the center of the plate..... 59
Figure 3.7: Horizontal plane showing angles measured from center of base plate to misalignment..... 61
Figure 3.8: Vertical plane in the center of the plate..... 61
Figure 3.9: Horizontal plane showing angles measured from center of base plate to misalignment..... 63
Figure 3.10: Vertical plane in the center of the plate..... 64
Figure 3.11: Angles in the vertical plane, after forcing the misalignment of H. 64
Figure3.12: Showing the final computation of the horizontal misalignment 65
Figure 3.13: Horizontal plane showing angles measured from center of base plate to misalignment..... 66
Figure 3.14: Vertical plane in the center of the plate..... 67
Figure 3.15: Angles in the vertical plane, after forcing the misalignment of H. 68
Figure 3.16: Showing the final computation of the horizontal misalignment 69
Figure 3.17: Concrete Hardened Properties Test Setup..... 71
Figure 3.18: Standard ½ in. Round Tension Test specimen with 2 in. gage length (ASTM E8-99) 72
Figure 3.19: Stages of Coupon Testing..... 73
Figure 3.20: Typical Stress-Strain Curve for a coupon 73
Figure 3.21: Closeup of Instruments (website: www.omega.com and www.beiduncan.com) 75
Figure 3.22: Typical Instruments and cylinders used in the tests..... 76
Figure 3.23: Five Dowel Instrumentation Setup..... 77
Figure 3.24: Typical cycle of specimen preparation and testing 80
Figure 4.1: Typical Bond Stress versus Joint Opening curve..... 85
Figure 4.2: Comparison of pullout force vs. joint opening behavior for specimens with a single vertically misaligned dowel bar 87
Figure 4.3: Comparison of pullout force vs. joint opening behavior for specimens with two vertically misaligned dowel bars having non-uniform (NU) orientation..... 88
Figure 4.4: Comparison of pullout force vs. joint opening behavior for specimens with two vertically misaligned dowel bars and uniform (U) orientation..... 88

Figure 4.5: Comparison of pullout force vs. joint opening behavior for specimens with two vertically misaligned dowel bars and alternate (AM) orientation 89
Figure 4.6: Comparison of pullout force per bar vs. joint opening behavior for specimens with three vertically misaligned dowel bars 89
Figure 4.7: Comparison of pullout force per bar vs. joint opening behavior for specimens with five vertically misaligned dowel bars (5A, 5V18NU and 5V18AM)..... 90
Figure 4.8: Comparison of pullout force per bar for vertically misaligned dowel bars at ¼ in joint opening 90
Figure 4.9: Comparison of pullout force per bar for vertically misaligned dowel bars at ½ in. joint opening 91
Figure 4.10: Comparison of pullout force vs. joint opening behavior for specimens with a single horizontally misaligned dowel bar 93
Figure 4.11: Comparison of pullout force vs. joint opening behavior for specimens with two horizontally misaligned dowel bars having non-uniform (NU) orientation 93
Figure 4.12: Comparison of pullout force vs. joint opening behavior for specimens with two horizontally misaligned dowel bars having uniform (U) orientation..... 94
Figure 4.13: Comparison of pullout force vs. joint opening behavior for specimens with two horizontally misaligned dowel bars having alternate (AM) orientation 94
Figure 4.14: Comparison of pullout force per bar vs. joint opening behavior for specimens with three horizontally misaligned dowel bars 95
Figure 4.15: Comparison of pullout force per bar vs. joint opening behavior for specimens with five horizontally misaligned dowel bars (5A, 5H18NU and 5H18AM). 95
Figure 4.16: Comparison of pullout force per bar for horizontally misaligned dowel bars at ¼ in. joint opening 96
Figure 4.17: Comparison of pullout force per bar for horizontally misaligned dowel bars at ½ in. joint opening 96
Figure 4.18: Comparison of pullout force vs. joint opening behavior for specimens with a single combined misaligned dowel bar..... 98
Figure 4.19: Comparison of pullout force vs. joint opening behavior for specimens with two combined misaligned dowel bars having non-uniform (NU) orientation..... 99
Figure 4.20: Comparison of pullout force vs. joint opening behavior for specimens with two combined misaligned dowel bars having non-uniform (U) orientation..... 99
Figure 4.21: Comparison of pullout force vs. joint opening behavior for specimens with two combined misaligned dowel bars having alternate (AM) orientation..... 100
Figure 4.22: Comparison of pullout force vs. joint opening behavior for specimens with three combined misaligned dowel bars..... 100
Figure 4.23: Comparison of pullout force vs. joint opening behavior for specimens with five combined misaligned dowel bars (5A, 5C18NU and 5C18AM)..... 101
Figure 4.24: Comparison of pullout force per bar for combined misaligned dowel bars at ¼ in. joint opening 101
Figure 4.25: Comparison of pullout force per bar for combined misaligned dowel bars at ½ in. joint opening 102
Figure 4.26: Comparison of pullout force vs. joint opening curves of 2-dowel ½ in. Horizontal Misalignment (2H18NU, 2H18U, and 2H18AM)..... 104
Figure 4.27 Comparison of pullout force vs. joint opening curves of 2-dowel ½ in. Vertical Misalignment (2V18NU, 2V18U, and 2V18AM) 105

Figure 4.28: Comparison of pullout force vs. joint opening curves of 2-dowel ½ in. Combined Misalignment (2C18NU, 2C18U, and 2C18AM) 105
Figure 4.29: Comparison of pullout force vs. joint opening curves of 2-dowel ¾ in. Horizontal Misalignment (2H12NU and 2H12AM) 106
Figure 4.30: Comparison of pullout force vs. joint opening curves of 2-dowel ¾ in. Vertical Misalignment (2V12NU and 2V12AM) 106
Figure 4.31 Comparison of pullout load vs. joint opening curves of 2-dowel ¾ in. Combined Misalignment (2C12NU and 2C12AM) 107
Figure 4.32 Comparison of pullout load vs. joint opening curves of 5H18NU and 5H18AM 107
Figure 4.33 Comparison of pullout force vs. joint opening curves of 5V18NU and 5V18AM 108
Figure 4.34 Comparison of pullout force vs. joint opening curves of 5C18NU and 5C18AM 108
Figure 4.35 Comparison of pullout force vs. joint opening curves of 1H18 and 2-dowel ½ in. Horizontal Misalignment (2H18NU, 2H18U, 2H18AM) 110
Figure 4.36 Comparison of pullout force vs. joint opening curves of 1H9 and 2-dowel 1 in. Horizontal Misalignment (2H9NU, 2H9U) 110
Figure 4.37 Comparison of pullout force vs. joint opening curves of 3H18NU and 5H18NU 111
Figure 4.38: Comparison of pullout force vs. joint opening curves of 1V18 and 2-dowel ½ in. Vertical Misalignment (2V18NU, 2V18U, 2V18AM) 112
Figure 4.39 Comparison of pullout force vs. joint opening curves of 1V9 and 2-dowel 1 in. Vertical Misalignment (2V9NU, 2V9U) 112
Figure 4.40 Comparison of pullout force vs. joint opening curves of 3V18NU and 5V18NU 113
Figure 4.41: Comparison of pullout force vs. joint opening curves of 1C18 and 2-dowel ½ in. Combined Misalignment (2C18NU, 2C18U) 114
Figure 4.42: Comparison of pullout force vs. joint opening curves of 1C9 and 2-dowel 1 in. Combined Misalignment (2C9NU, 2C9U) 115
Figure 4.43 Comparison of pullout force vs. joint opening curves of 3C18NU and 5C18NU 115
Figure 4.44: Comparison of loads at ¼ in. across different tests of misalignment 116
Figure 4.45: Comparison of loads at ½ in. across different tests of misalignment 117
Figure 4.46: Vertical Uplift (2V9NU) 119
Figure 4.47: Diagrammatic representation of Crack in 5V18NU 119
Figure 4.48: Spalling in the 2H9U test 120
Figure 4.49: Joint opening as a function of distance along the joint (2H1U) 121
Figure 4.50: Cracking in 2H12NU 122
Figure 4.51: Crack pattern and Initial dimensions in 2H9NU 123
Figure 4.52: Cracking in 2C12NU 125
Figure 4.53: Corner Cracking in 2C9NU on west side 126
Figure 4.54: Aligned dowel bar in concrete pavement slab 128
Figure 4.55: Misaligned dowel bar in a concrete pavement slab 128
Figure 4.56: Forces on a misaligned dowel and surrounding concrete 130
Figure 5.1: Abaqus Solid element Library (Abaqus User Manual 2004) 133

Figure 5.2: Finite Element Model discretization of the concrete slab and dowel bar. ... 134
Figure 5.3: Uniaxial behavior of plain concrete (Abaqus User Manual 2004)..... 136
Figure 5.4: Typical concrete uniaxial stress –strain curve in tension and compression (Abaqus User Manual 2004)..... 138
Figure 5.5: A plasticity hardening model for concrete (Chen and Han, 1995)..... 140
Figure 5.6: Schematic of yield surface and flow in the meridinal plane. (Abaqus User Manual 2004)..... 141
Figure 5.8: Typical uniaxial compressive strength of concrete, Collins et al (1992)..... 144
Figure 5.9: Typical Post failure Stress – Displacement curve using fracture energy criterion..... 145
Figure 5.10: Typical tensile post failure stress-strain curves using the fracture energy criterion..... 146
Figure 5.11: Spring model derived from the control test specimen (aligned single dowel bar)..... 149
Figure 5.12: Distribution of spring forces along half length of the dowel bar 149
Figure 5.13: Typical spring forces (lbs) at ¼ in joint opening in the 1V18 model..... 150
Figure 5.14 Summary of the Pullout force per bar at debonding limit state (A) and the debonding stress for the aligned and misaligned test cases 153
Figure 5.15: Step I – Dead (gravity / self weight) Load due to the concrete and dowel 155
Figure 5.16: Step II – Displacement Control step simulating joint opening 156
Figure 5.17: Comparison of finite element results and experimental data for a single misaligned 1/18 radians dowel bar. 158
Figure 5.18: Comparison of finite element results and experimental data for two vertically misaligned 1/18 radians dowel bar. 160
Figure 5.19: Comparison of finite element results and experimental data for two horizontally misaligned 1/18 radians dowel bar. 162
Figure 5.20: Comparison of finite element results and experimental data for five vertically misaligned 1/18 radians dowel bar. 164
Figure 5.21: Comparison of finite element results and experimental data for five horizontally misaligned 1/18 radians dowel bar. 165
Figure 5.22: Typical stress contours at material damage / limit state (C) in the FE model for Case I input parameters at 0.05 in. joint opening..... 166
Figure 6.1: Typical location of initial slip state (A) for single and two aligned dowel bars 169
Figure 6.2: Identification of various limit states on the concrete compression – tension stress-strain curves 172
Figure 6.3: Comparison of the FEM model with the experimental data for a single dowel bar specimen 185
Figure 6.4: Comparison of FEM and experimental data for a two dowel bars with vertical misalignment..... 187
Figure 6.5: Comparison of FEM and experimental data for a two dowel bars with horizontal misalignment..... 189
Figure 6.6: Comparison of FEM and experimental data for a two dowel bars with combined misalignment 191
Figure 6.7: Comparison of FEM and experimental data for five dowel bars with vertical misalignment..... 193

Figure 6.8: Comparison of FEM and experimental data for five dowel bars with horizontal misalignment 194
Figure 6.9: Comparison of FEM and experimental data for five dowel bars with combined misalignment 196
Figure 6.10: Summary of Joint Opening Behavior and Limit States of single misaligned dowel bars 200
Figure 6.12: Case II analysis summary of Joint Opening Behavior and Limit States of two vertically misaligned dowel bars 204
Figure 6.13: Case I analysis summary of Joint Opening Behavior and Limit States of two horizontally misaligned dowel bars 207
Figure 6.14: Case II analysis summary of Joint Opening Behavior and Limit States of two horizontally misaligned dowel bars 208
Figure 7.1: Dimensions and location of various parts of the pavement slab and wheel base in the finite element model 216
Figure 7.2: Spring Force vs. Joint Opening behavior used in the finite element models 222
Figure 7.3: Typical constraint conditions used for the finite element model 223
Figure 7.4: Typical Boundary and Loading conditions on the pavement system 226
Figure 7.5: Loaded and unloaded sides of the concrete slab 227
Figure 7.6: Compressive stress zones in the concrete for 1V72 FE model 229
Figure 7.7 Compressive stress zones in the concrete for 1H72 FE model 229
Figure 7.8 Results at location (i) and (ii) for single vertically misaligned dowel bar at 1/8" joint opening 230
Figure 7.9 Results at location (i) and (ii) for single horizontally misaligned dowel bar at 1/8" joint opening 232
Figure 7.10: Stress concentration zones formed in concrete due to misaligned dowel bars and at joint opening (1/8 in) 235
Figure 7.11: Formation of bearing stress zones in the concrete due to load application 236
Figure 7.12: Stress concentration zones formed in concrete due to misaligned dowel bars and at joint opening (1/8 in) 237
Figure 7.13: Formation of bearing stress zones in the concrete due to load application 238
Figure 7.14: Compressive stresses in the three dowel bar FE models 239
Figure A-1. Cross section of the small mold for pullout test 251
Figure A-2. Plan of the small mold with outside dimensions 251
Figure A-3. Typical sectional view of the big mold 252
Figure A-4. Typical plan view of mold with 5 dowel bars 252
Figure A-5. Calibration of 1.5 in. slider-1 258
Figure A-6. Calibration of 1.5 in. slider-2 258
Figure A-7. Calibration of 1.0 in. slider-1 258
Figure A-8. Calibration of 1.0 in. slider-2 258
Figure A-9. Calibration of 1.0 in. slider-3 259
Figure A-10. Calibration of 1.0 in. slider-4 259
Figure A-11. Calibration of LVDT-1 259
Figure A-12. Calibration of LVDT-2 259
Figure A-13. Calibration of LVDT-3 260
Figure A-14. Calibration of RC156 Actuator 1 260
Figure A-15. Calibration of RC256 Actuator 1 260

Figure A-16. Calibration of RC156 Actuator 2 260
Figure A-17. Calibration of RC256 Actuator 2 261
Figure A-18. Data Flow 262
Figure C-1: Comparison of the FEM model with the experimental data for 1A specimen 273
Figure C-2: Comparison of the FEM model with the experimental data for 1V18 specimen 274
Figure C-3: Comparison of the FEM model with the experimental data for 1V36 specimen 275
Figure C-4: Comparison of the FEM model with the experimental data for 1V72 specimen 276
Figure C-5: Comparison of the FEM model with the experimental data for 1H18 specimen 277
Figure C-6: Comparison of the FEM model with the experimental data for 1H36 specimen 278
Figure C-7: Comparison of the FEM model with the experimental data for 1H72 specimen 279
Figure C-8: Comparison of the FEM model with the experimental data for 1C18 specimen 280
Figure C-9: Comparison of the FEM model with the experimental data for 1C36 specimen 281
Figure C-10: Comparison of the FEM model with the experimental data for 2A specimen 282
Figure C-11: Comparison of the FEM model with the experimental data for 2V18NU specimen 283
Figure C-12: Comparison of the FEM model with the experimental data for 2V18U specimen 284
Figure C-13: Comparison of the FEM model with the experimental data for 2V18AM specimen 285
Figure C-14: Comparison of the FEM model with the experimental data for 2V36NU specimen 286
Figure C-15: Comparison of the FEM model with the experimental data for 2V36U specimen 287
Figure C-16: Comparison of the FEM model with the experimental data for 2V36AM specimen 288
Figure C-17: Comparison of the FEM model with the experimental data for 2V72NU specimen 289
Figure C-18: Comparison of the FEM model with the experimental data for 2V72U specimen 290
Figure C-19: Comparison of the FEM model with the experimental data for 2V72AM specimen 291
Figure C-20: Comparison of the FEM model with the experimental data for 2H18NU specimen 292
Figure C-21: Comparison of the FEM model with the experimental data for 2H18U specimen 293

Figure C-22: Comparison of the FEM model with the experimental data for 2H18AM specimen 294
Figure C-23: Comparison of the FEM model with the experimental data for 2H36NU specimen 295
Figure C-24: Comparison of the FEM model with the experimental data for 2H36U specimen 296
Figure C-25: Comparison of the FEM model with the experimental data for 2H36AM specimen 297
Figure C-26: Comparison of the FEM model with the experimental data for 2H72NU specimen 298
Figure C-27: Comparison of the FEM model with the experimental data for 2H72U specimen 299
Figure C-28: Comparison of the FEM model with the experimental data for 2H72AM specimen 300
Figure C-29: Comparison of the FEM model with the experimental data for 2C18NU specimen 301
Figure C-30: Comparison of the FEM model with the experimental data for 2C18U specimen 302
Figure C-31: Comparison of the FEM model with the experimental data for 2C18AM specimen 303
Figure C-32: Comparison of the FEM model with the experimental data for 2C36NU specimen 304
Figure C-33: Comparison of the FEM model with the experimental data for 3A specimen 305
Figure C-34: Comparison of the FEM model with the experimental data for 3V18NU specimen 306
Figure C-35: Comparison of the FEM model with the experimental data for 3H18NU specimen 307
Figure C-36: Comparison of the FEM model with the experimental data for 3C18NU specimen 308
Figure C-37: Comparison of the FEM model with the experimental data for 5A specimen 309
Figure C-38: Comparison of the FEM model with the experimental data for 5V18NU specimen 310
Figure C-39: Comparison of the FEM model with the experimental data for 5V18AM specimen 311
Figure C-40: Comparison of the FEM model with the experimental data for 5V36AM specimen 312
Figure C-41: Comparison of the FEM model with the experimental data for 5H18NU specimen 313
Figure C-42: Comparison of the FEM model with the experimental data for 5H18AM specimen 314
Figure C-43: Comparison of the FEM model with the experimental data for 5H36AM specimen 315
Figure C-44: Comparison of the FEM model with the experimental data for 5C18NU specimen 316

Figure C-45: Comparison of the FEM model with the experimental data for 5C18AM specimen 317
Figure C-46: Comparison of the FEM model with the experimental data for 5C36AM specimen 318
Figure D-1: Stress and Strains for 3A slab model at joint opening of 1/8 in..... 321
Figure D-2: Stresses and Strains for 3A model after load application 322
Figure D-3: Stress and Strains for 3V36NU slab model at joint opening of 1/8 in..... 324
Figure D-4: Stresses and Strains for 3V36NU model after load application..... 325
Figure D-5: Stress and Strains for 3V36AM slab model at joint opening of 1/8 in. 327
Figure D-6: Stresses and Strains for 3V72NU model after load application..... 328
Figure D-7: Stress and Strains for 3V36AM slab model at joint opening of 1/8 in. 330
Figure D-8: Stresses and Strains for 3V36AM model after load application..... 331
Figure D-9: Stress and Strains for 3V72AM slab model at joint opening of 1/8 in. 333
Figure D-10: Stresses and Strains for 3V72AM model after load application..... 334
Figure D-11: Stress and Strains for 3H36NU slab model at joint opening of 1/8 in..... 336
Figure D-12: Stresses and Strains for 3H36NU model after load application..... 337
Figure D-13: Stress and Strains for 3H72NU slab model at joint opening of 1/8 in..... 339
Figure D-14: Stresses and Strains for 3H72NU model after load application..... 340
Figure D-15: Stress and Strains for 3H36AM slab model at joint opening of 1/8 in. 342
Figure D-16: Stresses and Strains for 3H36AM model after load application..... 343
Figure D-17: Stress and Strains for 3H72AM slab model at joint opening of 1/8 in. 345
Figure D-18: Stresses and Strains for 3H72AM model after load application..... 346
Figure E-1: Comparison of dowel pullout force-joint opening behavior for the 2V18NU coarse and fine mesh finite element model..... 349

ABSTRACT

This report presents an experimental and analytical investigation on the fundamental pullout behavior and joint opening behavior of misaligned dowel bars in concrete pavement joints. Experimental investigations were conducted to determine the fundamental joint opening behavior of concrete pavements, and to evaluate the effects of dowel misalignment on joint opening behavior. The parameters included in the experimental investigations were the number of dowel bars (1, 2, 3, or 5) at the joint, the dowel misalignment type (horizontal, vertical, and combined), misalignment magnitude (0, 1/36, 1/18, 1/12, 1/9 radians.), and uniformity across the joint. The effects of these parameters were evaluated on the joint opening behavior and structural distresses observed in the specimens. Numerous instrumented laboratory-scale specimens of pavement slabs with doweled joints were tested. The second task focused on the development of 3D finite element models for computing the complex stress states and resulting damage in concrete pavement joints with misaligned dowels, and their validation using experimental results. The concrete pavement is modeled using a damage-plasticity material model, which uses concepts of damaged plasticity formulation in compression and cracking combined with damage elasticity in tension. The longitudinal bond between the steel dowel and the concrete is modeled in two parts. (i) The longitudinal bond resulting from chemical adhesion, mechanical interlock, and static friction (in the aligned state) is modeled using spring elements. (ii) The longitudinal bond resulting from transverse interaction between steel dowels and the concrete pavement is modeled using surface-to-surface contact-interaction elements and associated friction models. The 3D finite element models are validated using results from the experimental

investigations. These validated models provide significant insight into the 3D stress states and principal stresses that develop in concrete pavement joints with misaligned dowels. They are used to evaluate analytically the effects of misalignment type, magnitude, uniformity, and distribution on the 3D stress states and resulting damage in concrete pavements. The analytical results (3D stresses and strains) from the finite element analyses were considered to identify significant limit states and distresses in the concrete pavement joints. Parametric studies were conducted and recommendations on misalignment tolerances based on these parametric studies have been made. A preliminary investigation to capture the effects of misaligned dowel bars combined with wheel loads has also been carried out in this research study.

CHAPTER 1

INTRODUCTION

1.1 INTRODUCTION

Jointed Plain Concrete pavements (JPCP) have been widely used in the United States and many developing countries both for roadways and airport runways because of their durability and low maintenance requirements. One of the main features of the JPCP is the doweled contraction joint, spaced at 10 – 20 ft intervals to permit contraction of the slabs and control crack locations. To ensure long term performance of highway pavements subjected to heavy traffic mechanical load transfer devices such as dowel bars are necessary. Dowel bars are placed across joints to provide additional load transfer without restricting horizontal joint movement. They also assist in maintaining the horizontal and vertical alignment of slabs.

From a construction view point, it is important to install the dowel bars properly, i.e., in the horizontal plane and parallel to the pavement centerline. Dowel bars can become misaligned during construction. The misaligned dowel bars restrain the horizontal movement of the joint which leads to joint locking. This causes the effective length of the concrete slabs to increase which increases the stresses due to applied thermal and wheel loads causing transverse slab cracking, corner breaks, and joint spalling (Tayabji 1986).

1.2 PROBLEM STATEMENT

The Michigan Department of Transportation (MDOT) specifications require that the dowel bars should provide adequate load transfer across transverse joints, while allowing horizontal movement without significant restraint. These dowel bars are installed during construction using factory fabricated dowel basket assemblies. DOTs also have recently started using dowel bar inserters (DBI) that mechanically insert the dowels into the "green" or fresh (plastic) concrete during construction. The DOTs use the same allowable misalignment tolerances for dowels placed using basket assemblies or dowel bar inserters as given in the construction specifications. The basis of these misalignment tolerances in the specifications needs to be investigated.

There is sparse experimental data documenting the behavior, effects, and distresses caused by the presence of misaligned dowel bars in a concrete pavement joints. Computational models developed in previous studies to investigate the effects of dowel misalignment had several limitations and assumptions. The experimental investigation and companion finite element models developed in this study will play an important role in the process of developing tolerances for dowel misalignment in jointed concrete pavements.

1.3 RESEARCH OBJECTIVES

The objectives of this research are:

1) To investigate experimentally the fundamental *pullout behavior* of misaligned dowel bars in plain concrete pavements subjected to thermal expansion (joint opening only).

2) To investigate experimentally the behavior and distress of pavement joints with multiple misaligned dowel bars subjected to *joint opening*.
3) To develop and calibrate 3D finite element analytical models that can be used to predict the joint opening behavior and evaluate the distresses of concrete pavement joints with misaligned dowel bars.
4) Conduct parametric studies to evaluate the behavior and potential distress of in-situ pavement joint with multiple misaligned dowel bars.

The experimental investigations cannot provide detailed information regarding the localized interaction between the dowel bar and the surrounding concrete. Hence computational models were developed based on the laboratory investigations and validated using experimental results. The computational models and results provide a deeper understanding of the mechanics of dowel-concrete interaction, the 3D stresses, and the distress (damage) produced by misaligned dowels in the pavement specimens. The computational models were 3D finite element models developed using ABAQUS, which is a commercially available finite element software (ABAQUS 2004).

1.4 RESEARCH PLAN

The research objectives were achieved by systematically conducting the following tasks:

1) Task I: Pullout Behavior of single misaligned dowel bars

Task-1 focused on the fundamental pullout behavior of a misaligned dowel bar in a concrete pavement joint. The pullout behavior of single dowel bars with various misalignment types and magnitudes were determined experimentally. Three-dimensional (3D) finite element models were developed to investigate the pullout behavior of single

misaligned dowel bars from the experimental investigation. The experimental results were used to further calibrate and verify the overall behavior predicted by the finite element models.

2) Task 2: Opening behavior of joints with multiple misaligned dowel bars

Task-2 focused on the joint opening behavior of concrete pavement joints with multiple misaligned dowel bars. Experimental investigations were conducted to determine the joint opening behavior of concrete pavement joints with uniformly, non-uniformly or alternately misaligned dowel bars. Three dimensional finite element models were developed and calibrated to predict the overall force – joint opening behavior and to provide insight into the localized stresses and observed distresses. The calibrated models were used to further investigate the behavior of 'realistic' concrete pavement joints with possible and 'typical' dowel bar misalignments. The behavior of these pavement joints were examined for the cases of uniform, non-uniform and random dowel bar misalignments.

1.5 LAYOUT OF THE REPORT

This report, "Experimental and Analytical Investigations of the Mechanistic Effects of Dowel Misalignment in Jointed Concrete Pavements" is outlined as follows:

Chapter 2 contains a detailed literature review of the technical papers, reports and thesis on experimental and analytical studies of dowel bars. This chapter defines misalignment and discusses various construction practices. It discusses the ways for measuring misalignment in the field. The experimental studies conducted by researchers,

their test setups and limitations are also presented in this chapter. A detailed study of the various 2D and 3D finite element models that were developed over the years for rigid pavements is presented. This defines the current state-of-the-art and identifies the modeling strategies used by other researchers in the rigid pavement design field.

Chapter 3 provides a detailed description of the experimental plan and procedure, the test matrix, research parameters such as misalignment magnitudes, type and orientation. The nomenclature used to identify the laboratory test specimens and the finite element models are explained. The instrumentation, hydraulics and data acquisition used in the experimental investigation and their calibration and accuracy are presented.

Chapter 4 presents the results of the experimental investigations. Various cases of dowel pullout forces vs. joint opening behavior are compared to identify trends from the experimental results. A hypothesis regarding the mechanics of dowel misalignment and its impact on surrounding concrete is presented. This chapter also presents a rationale for developing computational models that can be calibrated and validated using data from the experimental investigation.

Chapter 5 shows the development of the 3D finite element model. The ABAQUS concrete damage plasticity model was used in this research study. The features and detailed description of this model including various parameters are presented in this chapter. The development and calibration of the model for the bond between the dowel bar and surrounding concrete is presented. This chapter also includes some comparisons of the overall dowel pullout force-joint opening behavior from the experiment and analysis to verify the model.

Chapter 6 presents a detailed discussion on the various material failure or damage limit states that occur in the analytical models. The chapter presents results from the 3D finite element analyses and parametric studies evaluating effects of various misalignment parameters on the joint behavior. Some recommendations on the misalignment tolerances are made based upon the results of the parametric study.

Chapter 7 presents some preliminary investigations of the effects of wheel loads combined with dowel misalignments and joint opening. This chapter focuses on the development of the finite element model, the loading and boundary conditions and the effects of dowel misalignment and wheel load on joint opening behavior.

Chapter 8 presents the summary and conclusions of this research study. It includes the conclusions from the experimental and analytical investigations and recommendations for future work.

CHAPTER 2

LITERATURE REVIEW

2.1 INTRODUCTION

In general a Jointed Plain Concrete Pavement (JPCP) consists of several components, as shown in figure 2.1 (Davids, 1998)

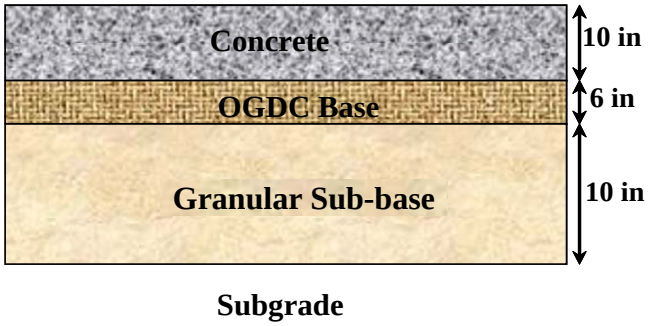

(a) Typical pavement cross-section

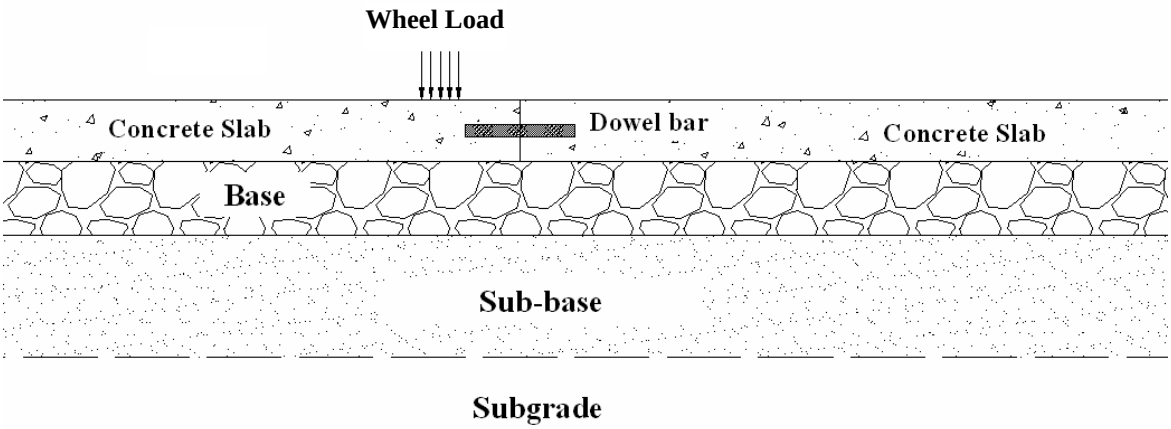

(b) Typical Pavement and loading in longitudinal direction

Figure 2.1: Typical components of a pavement cross section and truck loading.

JPCPs are constructed with contraction joints to accommodate slab movements due to temperature and moisture variations. A combination of steel dowel bars and aggregate interlock are used across joints to maintain continuity between slabs. In this chapter a comprehensive literature review is presented on all aspects of experimental investigation and numerical modeling of dowel bar misalignments.

2.2 DEFINITIONS OF MISALIGNMENT, VARIOUS ORGANIZATIONAL SPECIFICATIONS AND CONSTRUCTION PRACTICES

2.2.1 DEFINITIONS OF MISALIGNMENT

There are two basic types of dowel misalignments that can occur in concrete pavements, namely, the skew and translation type of misalignment. Table 2.1 shows the misalignment types and the effect of these misalignments on the pavement performance. The distresses observed include spalling, cracking and loss of load transfer efficiency. Distresses exhibited are attributable to high levels of stress or deflection (Snyder 1989) and they tend to appear in the vicinity of slab edges and corners. Excessive dowel-concrete bearing stresses may also result in spalling and faulting of concrete surrounding the dowel bars at the joint (Ionnides et al. 1990). From the information provided in table 2.1, the skew types of misalignments are more detrimental and they can cause all three types of distresses at the pavement joints. This research focuses on the effects of the skew type of misalignments.

Table 2.1(a): Possible Effects of Translational type of Dowel Misalignment on Pavement Performance

Type of Alignment		Effect on			Distress Observed
Translation		Spalling	Cracking	Load Transfer	
Horizontal	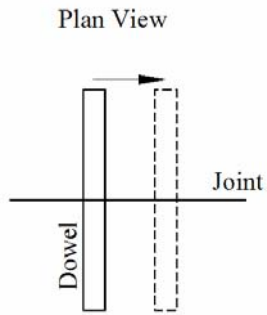	-	-	Yes	Depends on magnitude of Translation
Longitudinal	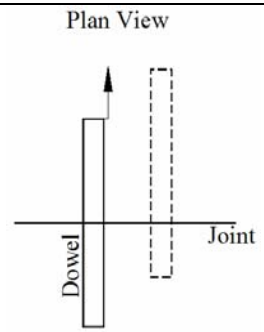	-	-	Yes	
Vertical	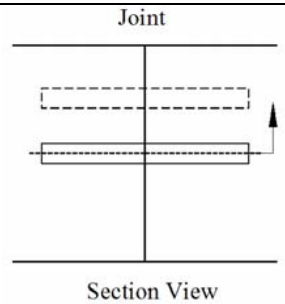	Yes	-	Yes	

Table 2.1(b): Possible Effects of Skew type of Dowel Misalignment on Pavement Performance

Type of Alignment		Effect on			Distress Observed
Skew		**Spalling**	**Cracking**	**Load Transfer**	
Horizontal	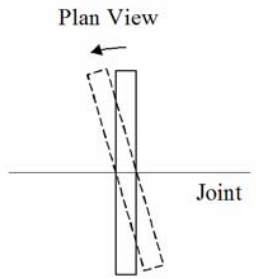	Yes	Yes	Yes	Horizontal rotation or Vertical uplift, depending on magnitude of skew
Vertical	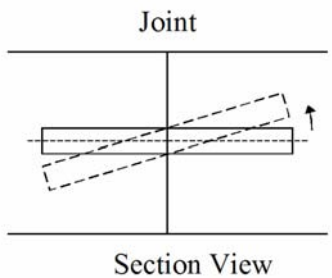	Yes	Yes	Yes	
Combined	Horizontal + Vertical	Yes	Yes	Yes	

2.2.2 SPECIFICATIONS FROM VARIOUS STATE HIGHWAY AUTHORITIES

The American Concrete Paving Association (ACPA) recommends that dowel bars should be used to provide added mechanical load transfer where truck traffic exceeds 120 per day or accumulated design traffic exceeds 4-5 million ESALs. This truck traffic loading condition will require at least an 8 in. thick slab and for most highways, dowels are recommended for 8 in. thick slabs or greater (ACPA 2004).

The American Association of State Highway and Transportation Officials (AASHTO), provisions for joint design include the following parameters; the dowel diameter, embedment length, spacing of joints and dowels so as to limit and control the magnitude of stresses developing in each bar and the deflections in the surrounding concrete. Current DOT practices for dowel and joint design (AASHTO 1993 and Mechanical Emperical Pavement Design Guide), are based on experience and the thumb rule that the diameter of the dowel should be equal to 1/8th of slab thickness. FHWA (1990), Federal Highway Administration, recommends a minimum dowel diameter of 1¼ in. for highways. ACPA (1991) recommends a dowel diameter of 1¼ in. for pavements less than 10 in. thick and 1½ in. for pavements greater than 10 in. thick. The NCHRP 1-37A mechanical empirical design guide methodology is based on the bearing stress of the dowel bar on the surrounding concrete with the dowel bar diameter being a key parameter in the design.

Various highway agencies have their own specific permissible limits. No clear consensus exists as to the level of practical limits on dowel placement tolerances. The Pennsylvania DOT specifies an allowable tolerance of ¼ in. per 18 in. of dowel length in both the horizontal and vertical directions. The Tennessee DOT investigated

misalignment dowels by uncovering dowels in freshly placed concrete and by core drilling in hardened concrete. The recommended limits on horizontal and vertical skew were ½ in. The Michigan DOT recommends the use of Billet steel grade 40 made dowel bars. The dowel bars coated with epoxy have to be placed at 12 in (± ½ in.) centers. As per MDOT specifications, Standard R-40, after the load transfer assembly is set in place, dowel bars shall remain aligned parallel with each other and within ¼ in. anywhere along the length in both the horizontal and vertical planes of the pavement. Indiana DOT and Iowa DOT have specified that dowel bars shall remain aligned parallel with each other and within $\pm 1/8$ in. tolerance limits. Misalignment tolerance specifications for various DOTs have been summarized in table 2.2. A survey of some DOTs, as shown in table 2.3, showed that they have specified some tolerances irrespective of whether the dowel has been placed using a DBI or a basket assembly

Table 2.2: DOT Tolerance Specifications

State	Tolerance	
	Dowel Basket Assembly	**Dowel Bar Inserter**
Michigan (2004)	***Misalignment:*** Dowel bars shall remain aligned (parallel) with each other and ± 1/8 in. in both horizontal and vertical planes. ***Transverse Location and Depth*:** Dowels shall be placed middepth ± ½ in. Dowels shall be centered 1 ft ± ½ in.	***Misalignment:*** ± ¼ in. over the length of the bar in the horizontal and vertical planes. ***Longitudinal Location:*** ± 2 in. of planned longitudinal location.
Wisconsin (2004)	Hold dowel bars in the correct position and alignment using an engineer-approved device during construction	***Misalignment:*** Parallel to the pavement surface and centerline ± ½ in. over 18 in. ***Transverse Location and Depth*:** ± 1 in. of the planned transverse location and depth. ***Longitudinal Location:*** ± 2 in. of planned longitudinal location.
Ohio (2005)	***Misalignment:* ±** ¼ in. per foot. ***Transverse Location and Depth*:** Centerline of individual dowels shall be parallel to each other, the surface and the centerline of the slab. Dowels shall be ± ½ in. on centers. Dowels shall be placed mid-depth of the slab.	
Iowa (2005)	***Misalignment:*** ± 1/8 in. over 18 in. ***Transverse Location and Depth:*** Centerline of individual dowels shall be parallel to the other dowels in the assembly ± 1/8 in. Spacing between dowels shall be 1 ft ± ¼ in. Each assembly shall be placed so that the bars are in a horizontal plane at T/2 ± ½ in.	N/A
California	***Misalignment:*** ± 0.354 in. over 18 in. in both horizontal and vertical directions. ***Transverse Location and Depth*:** Parallel with the pavement lane centerline and surface of the pavement at mid-pavement depth. Transverse location ± 1 in. from planned location. ***Longitudinal Location:*** ± 2 in. of planned longitudinal location.	
Illinois (2002)	***Misalignment:*** ± 1/8 in. over 1 ft. in the horizontal and vertical planes. ***Transverse Location and Depth*:** Dowels, when used, shall be held in position parallel to the surface and centerline of the slab by metal devices.	

Table 2.3: Survey of Dowel Bar Installation Specifications

SHA* / DOT	Basket (% used)	DBI (% used)	Misalignment Tolerance		Quality Control of Misalignment
			DBI	Basket	
Alabama	Yes (100)	No (0)	None	¼ in. over 12 in.	Field Inspection
Colorado	Yes (25)	Yes (75)	Not specific		No requirement
Florida	Yes (100)	No (0)	None	½ in. over 18 in.	Contractor's responsibility
Nevada	Yes (75)	Yes (25)	½ in. over 18 in.		Coring. Also evaluating the the usefulness of MITSCAN
North Carolina	Yes (75)	Yes (25)	½ in. over 18 in.	0.25 in., 0.75 in. opposing skew	MITSCAN
Ohio	Yes (75)	Yes (25)	None	None	Pachometer or coring
Pennsylvania	Yes (25)	Yes (75)	¼ in. over dowel length		Alignment verified prior to concrete placement. Baskets assumed to be rigid.
Virginia	Yes (75)	Yes (25)	Not specific		No requirement
Washington	Yes (75)	Yes (25)	½ in. over 18 in.		Developing specs for MITSCAN
Wisconsin	Yes (50)	Yes (50)	½ in. over 18 in.		Not specific

*SHA: State Highway Association

2.2.3 CONSTRUCTION PRACTICES

Pavements are constructed using fixed form paving and slipform paving. Fixed form paving is used generally for small jobs, complicated geometry pavements, or variable width pavements, while slipform paving is used for larger jobs that require high

production rates. There are two main methods of dowel bar placement in the field: dowel basket assembly and dowel bar inserter (DBI). Slipform paving can accommodate both the methods of dowel bar placement while fixed form paving can accommodate dowel baskets only.

Dowel Baskets

Dowel baskets are simple truss structures used to hold dowel bars at the appropriate height before Portland Cement Concrete (PCC) placement. Typically, dowel baskets span an entire lane width and are fabricated from thick gauge wire. They are left in place after the PCC is placed but do not contribute to the pavement structure. When using dowel baskets, the dowels must be aligned and the dowel basket firmly anchored to the base course. The FHWA recommends that the dowel baskets be secured with steel stakes with a minimum diameter of 0.3 in. embedded at least 4 in. in stabilized bases, 6 in. in treated permeable bases and 10 in. in untreated bases or subgrade. Further, a minimum of 8 stakes per basket is recommended. Figure 2.2 illustrates a typical dowel basket assembly. The dowels come precoated with lubricant from the manufacturer and are welded on alternate sides

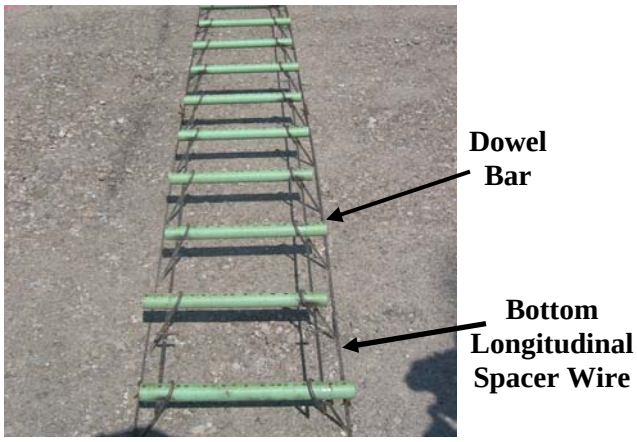

Figure 2.2: Typical dowel basket assembly used as load transfer devices in JPCP

Dowel Bar Inserter

The dowel bar inserter is a device which mounts behind the slipform paver. The DBI can accommodate different dowel spacings, dowel depths, skewed or square contraction joints, etc. as shown in figure 2.3.

(a) Typical Slipform Paver with inbuilt Dowel Bar Inserter

(b) Dowel Bar Magazine in position

Figure 2.3: Dowel Bar Inserter (Source Gomaco Inc., www.gomaco.com)

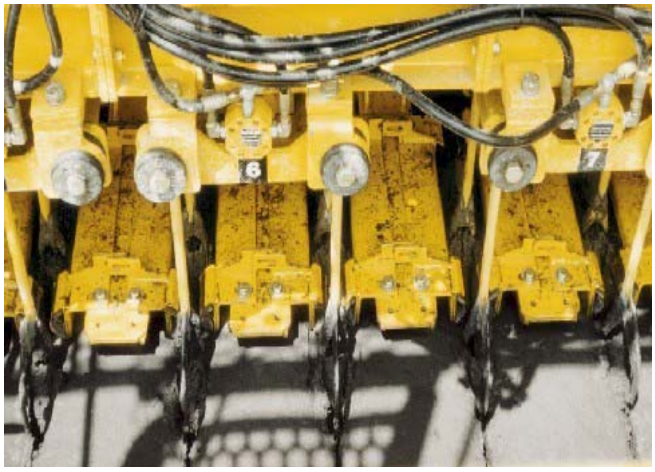

(c) Insertion into Plastic Concrete

Figure 2.3 (cont'd).

When the desired joint location is reached, an automated insertion cycle is activated. A pan mounted dowel distributor shifts allowing the dowels to drop from the magazine through the pan onto the fresh concrete. The vibration-isolated "inserting fork assemblies" then vibrate the bars until they have reached their proper depth in the concrete. Mounted on rubber-isolated beams, the vibrating forks reconsolidate the concrete as the forks are pulled out of the slab. Once the forks have cleared the concrete, the vibration is stopped and DBI and the pan are retracted. Because the dowels are being vibrated intensely and are inserted down to their final resting place under the weight of the dowel inserter assembly and light hydraulic pressure, the concrete has enough time to flow around the bar rather than being displaced (Gomaco, Inc).

Factors affecting misalignment

With either method, care and attention towards many details are required to achieve proper dowel bar alignment (Yu 2005). For dowel baskets, the most critical factor appears to be the manner in which the baskets are secured on the subbase or base prior to paving. If the baskets are not adequately pinned down, the baskets may be shoved,

rotated, or pulled apart during paving, resulting in extreme dowel bar misalignments. The baskets may also get bent during handling or during concrete placement.

For DBI construction, the critical factors are the proper adjustment of the DBI and PCC mix design. When using a DBI, mix optimization is extremely important to ensure the dowel bars do not become displaced after insertion. PCC mix for DBI construction must be stable enough to hold the bars in place without displacing them during paving. Construction factors that may affect misalignment as identified by Tayabji (1986) have been summarized in table 2.4.

Table 2.4: Construction Factors affecting Misalignment*

Dowel Baskets	Dowel Bar Inserter
• Basket rigidity • Quality control during basket fabrication • Care during basket transportation and placement • Fastening of basket to subbase • Location of saw-cut over basket • Paving operation • Field inspection during construction	• Implanting machine operation • Strike-off after dowel placement • Consolidation (vibration) after dowel placement • Location of saw-cut over implanted dowels • Field inspection during construction

*Ref: Tayabji (1986)

Quality Control of Misalignment

There are a few destructive and non-destructive methods used for the detection and measurement of dowel bar misalignment in the field: coring, the pachometer and covermeter, the Ground Penetrating Radar (GPR), and the MIT Scan-2. Coring is the only destructive method among the detection methods and by far, it is the most accurate method but its use is limited. The various devices used in measuring misalignment of dowel bars after construction are shown in figure 2.4.

Pachometer and Covermeter

These are battery-operated magnetic detection devices, which are mainly intended to measure the depth of reinforcement in concrete, and to detect the position of rebars. Its use has been extended to pavements to detect the location of dowel bars. The device emits an electromagnetic field and detects disturbances in the field caused by embedded metals.

Ground Penetrating Radar

The Ground Penetrating Radar (GPR) uses a radio wave source to transmit a pulse of electromagnetic energy into a subsurface (in this case, concrete pavement). The amplitude and arrival time of the reflected electromagnetic pulse (which originates from the top of the dowel) is recorded for analysis (determination of spatial location of the dowel). The GPR signal is characterized primarily by changes in reflection amplitude and changes in the arrival time of specific reflections. The GPR record consists of a continuous graphic display of reflected energy over a preset time interval. The depth to the dowel can then be determined if the propagation velocity, and electromagnetic energy through concrete are known or estimated.

MIT Scan-2

The MIT Scan-2 is a state-of-the-art device for measuring the position of metal bars embedded in concrete. The MIT Scan-2 is based on the magnetic imaging tomography technology and utilizes an array of sensitive detectors and sophisticated data analysis algorithms to produce very accurate results. The device emits a weak, pulsating magnetic signal and detects the transient magnetic response signal induced in metal bars. The methods of magnetic imaging tomography are then used to determine the position of the

metal bars. Unlike other devices that have been used in the past, which are general-purpose instruments adapted to the dowel bar detection application, the MIT Scan-2 was developed specifically for measuring dowel and tie bar alignments. As a result, the device is simple to operate, efficient, and provides real-time results in the field.

(a)Typical Pachometer

(b) Ground Penetrating Radar (GPR)

(c) Close up of MIT Scan-2

(d) Typical Run of MIT Scan-2 in Field

Figure 2.4: Various Non-Destructive Misalignment Measuring Devices

2.3 REVIEW OF FIELD STUDIES

Donahue (2003) in his report on dowel bar placement accuracy with a DBI, carried out field investigation (measurements of alignment) using ground penetrating radar. The findings in his report categorized the misalignments into three groups of skew: $\leq \frac{1}{2}$ in.,

$\frac{1}{2}$ in. $- \leq 1$ in. and > 1 in. Dowel baskets had 70% higher incidence of horizontal dowel misalignments > 1 in. compared to the DBI. Average horizontal skew was 0.49 in. in the DBI and 0.51 in. in the basket assembly. Average vertical skew occurrence was higher in the DBI method compared to using the dowel baskets, but both within acceptable standards close to 90% of ½ in. skew limit. Neither case had occurrences of misalignments over 1 in.

Donahue (2003) states that translation, both horizontal and vertical, does not have as significant an impact as skew. He states that longitudinal translation is a measure of the bar's effective length on the approach and leave slabs. It is not realistic to expect every 18 in. bar to straddle a joint with 9 in. on either side, but it is expected that a bar have at least 6 in. on each side to ensure that it can adequately provide load transfer across the slabs. A study conducted in the late 1950's concluded that the dowel embedment length required to provide full load transfer is five or more times the bar diameter (Teller 1959). A study by Minnesota DOT (Burnham 1999) indicated that an embedment length of only 2.5 in. is sufficient to keep faulting at an acceptable level of ¼ in. and provide load transfer efficiency (LTE) with less variability.

Burati et al. (1983), carried out statistical analysis of the visual surveys and actual measurements recorded of the dowel alignment with an electronic metal detector for both the basket assembly and implanted projects. The visual testing was carried out to record any distress type, rate of occurrence, severity, location of distress, general condition of pavement and any relevant visual imperfections. The metal detector was used to measure the horizontal misalignments. They found that there was no significant difference between the basket assembly and implanted assembly with respect to the joint related

distress. Spalling and raveling was noticeable on the metal inserter projects. The metal insert joints appeared to be the cause of spalling as there was much evidence of corroded insert segments. Strangely, they came up with no statistical proof that either the basket assembly or implanted projects are superior. Though, the overall results, viewed with much skepticism showed that the dowels in the implanted projects, on the average, were better horizontally aligned than the dowels in the basket assembly.

Okamoto et al. (CTL, Inc.) (1989) summarized field evaluations of Texas, Wisconsin and Idaho highways, for both the dowel basket assemblies pinned to the subbase and Guntert & Zimmerman dowel bar inserter joints. Dowel bar depth was generally consistent with both methods of construction. The average depth maintained was plus or minus one inch of slab mid depth. They found that the range of dowel depths at individual joints were 0.8 in. to 0.4 in. for inserter and basket assembly, respectively. The vertical misalignment was generally consistent for both types of construction, though the average ranged from 0.1 in. to 0.2 in per foot. At locations where inserters were used nearly 60% of the dowels were tilted forward (or backwards) in the direction of paving, for the Wisconsin project. For horizontal misalignments, the accuracy was estimated at approximately ¼ in. to ½ in./ft. Also, the direction of paving did not affect the direction of horizontal misalignment. Both uniform and asymmetric horizontal misalignments were observed. Coring data and radar output were used to measure the longitudinal displacement. In Wisconsin, the percentage of dowel displaced were 9.3% and 7.5% for inserter and basket assemblies respectively.

The overall performance and distress of in-service concrete pavements are functions of: (a) the pavement design, (b) environmental conditions including thermal

gradients, (c) joint spacing, (d) applied loads and number of passes (e) the dowel misalignments, (f) material quality and (g) construction. The tolerance limits for dowel misalignment will depend on the other parameters (a - d mentioned here) and the required number of passes (design life) before pavement failure occurs in terms of the distress (spalling, cracking) or performance (load transfer efficiency < 70%). In "in-service" pavements, the structural distresses are probably a combination of the basic types of misalignments. The type and magnitude of skew will impact the concrete-dowel bearing stress which leads to higher cumulative damage at a joint.

Table 2.5 summarizes the results of some of the older and recent field studies comparing the two dowel bar placement methods, i.e. basket assemblies and DBIs, with respect to misalignments and distresses observed.

2.4 REVIEW OF LABORATORY INVESTIGATIONS

Laboratory investigation to study the impact of misaligned dowel bars was started as early as 1938 by Smith and Benham. They conducted laboratory tests of small slab sections incorporating joint and dowels spaced at 12 in. on centers. In these tests, 3/4 in. diameter dowels were placed at different levels of misalignment and loading was applied at 28 days to open the joint. Results indicated that for 6 in. thick slab sections, an alignment error in excess of 1 in. caused spalling when joints were opened ¾ in. For a 5 in. thick slab section, an alignment error of ¼ in. caused slight spalling. Tests also showed that if the joint was not opened more than ½ in., alignment errors upto 1.5 in. could be tolerated without spalling. Generally, the load required to open a contraction

Table 2.5: Summary of Field Study Results

Reference Study and Test Section	Specifications, Method of Measurement and Parameters Monitored	Findings/Conclusions
Georgia DOT (Gary Fowler, 1983) • M-5020 Richmond: Baskets • I-16 Bulloch paved in 1976: DBI • APD-056 Forsyth: DBI Contractor tried placing dowels after the paver had passed resulting in extra finishing, dowel depressions filled with grout, and poor riding surface. The implanter was positioned ahead of the paver after a short period. • Three interstate projects with dowels implanted and two projects with baskets	Dowels 1.25 in. diameter, 18 in. long, 15 in. c/c, joint spacing 20 ft ***Tolerance:*** H, V of ± 1 in. for translation Rotational misalignment was 1-1/8 in. H and 9/16 in. V **Method:** Coring, Electronic Metal Detector **Parameters:** • Depth • Longitudinal alignment • Vertical and horizontal rotation	• 1st project that used an implanter met the specifications in most cases and compared closely to the accuracy of one reference job that utilized baskets. • Utilization of baskets did not eliminate all problems of rotation and especially the problem of longitudinal alignment. • Longitudinal displacement is affected at least as much by location of the sawed joint as it is by actual dowel movement. • Most difficult factor to control with implanting seemed to be the vertical height of dowel. • No dowel related pavement distress occurred in either of the projects. • All dowels were working. The dowel bar paint is ineffective as a coating on the working end of the dowel. However, it does aid in breaking the concrete bond of the dowel.
Missouri DOT (John Donahue, May 2003) US 60 JPCP construction project near Van Buren (G&Z DBI, Baskets)	***Tolerance:*** Be parallel to the subgrade and parallel to the line of the joint Misalignment: ± ½ in. over 18 in. Transverse location: ± 1in. Longitudinal translation: ± 2 in. ***Method:*** Ground penetrating radar (GPR), handheld pachometer ***Parameters:*** • Dowel Skew • Dowel Translation • Dowel depth	• Both tend to have moderate horizontal skew tendencies with the DBI performing a little better. • Both have very good control of vertical skew with the baskets holding a slight edge in performance. • Both have few serious occurrences of high opposite skew between dowel bars in the same joint. • For depth, DBI was more consistent than baskets with respect to surface evaluation. • Average depth and average depth standard deviation was acceptable for both.
Burati et.al.,(1983) Alabama pavements	**Method:** Electronic Metal Detector **Parameters:** • Absolute horizontal rotation • Absolute longitudinal displacement	• No significant difference between DBI and basket projects with respect to joint-related distress. • No significant difference between DBI and basket projects with respect to joint-related distress.

Table 2.5 (contd.)

Reference Study and Test Section	Specifications, Method of Measurement and Parameters Monitored	Findings/Conclusions
Burati et.al.,(1983) Alabama pavements	• Absolute horizontal displacement	• Overall results indicated that the dowels in the implanted projects, on the average, were better aligned than were the dowels in the basket projects. But contractor difference and inconsistency might have contributed to the difference. • Overall results indicated that the dowels in the implanted projects, on the average, were better aligned than were the dowels in the basket projects. But contractor difference and inconsistency might have contributed to the difference. • Individual dowel position had no effect on the alignment achieved. • No effect from pavement grade on dowel alignment or distress was found. • No correlation between misalignment types and distress was found. • Absolute horizontal rotation values were virtually the same for both implanted and basket projects. • Absolute longitudinal and horizontal displacements were noticeably better in implanted projects.
James Parry (Wisconsin DOT) (1987) Three projects each using DBI and baskets on I-90 at Janesville in 1987	***Tolerance:*** Depth of dowel: ½ in. above the mid-depth Vertical/Rotation: ± ½ in. over full length Longitudinal translation: ± 3 in. in either direction **Method:** Coring **Parameters:** • Average depth • Vertical rotation • Horizontal rotation • Ride quality • Voids • Missing dowels	• DBI is capable of consistent satisfactory placement of dowel bars with respect to average depth, vertical and horizontal rotation. • Initial setup of the DBI with respect to depth of dowel placement is critical at the start of each project, and dowel depths should be verified by probing through the fresh concrete. • Accurate marking for sawing joints is important. • Having a magnetic rebar locator available on all doweled PCC construction projects would be useful in aligning sawn joints with the dowel bars and in identifying missing dowels. • Ride quality of 4.6 can be achieved on DBI projects with minimum grinding. • Improved consolidation is required on both projects. • Problems with missing dowels on existing DBI projects appear to be infrequent and isolated, but this problem should be monitored on future projects.

Table 2.5 (contd.)

Reference Study and Test Section	Specifications, Method of Measurement and Parameters Monitored	Findings/Conclusions
Bock, Okamoto (1988) I-86, Idaho (Gomaca DBI) I-45, Texas (Baskets, DBI) I-90, Wisconsin (Baskets, DBI)	**ID**-1.25 in., 18 in. long @ 12 in. c/c. 10 in. PCC, random joint spacing **Tolerance:** ± ¼ in. per 12 in. **TX**-1.25 in., 22 in. long @ 12 in. c/c. 10 in. PCC, 15 ft. joint spacing **WI**-1.25 in., 18 in. long @ 12 in. c/c. 10 in. PCC, random joint spacing **Tolerance:** Dowel depth: mid-depth ± 1 in. Misalignment: ± ½ in. per 18 in. Horizontal Translation: ± 1 in. ***Parameters:*** • Average depth • Vertical Misalignment • Horizontal Misalignment • Longitudinal Displacement (qualitative)	• DBI performed well compared to baskets. • Based on dowel depth, longitudinal displacement, vertical tilt, and horizontal skew, there is no significant difference between DBI and baskets. • Distribution of tilt is more symmetrical for basket joints than inserter joints, indicating that vertical misalignment may not be independent of paving direction. • Horizontal misalignment seems to be independent of paving direction. • Occurrence of longitudinal translation is similar for both types of joints.
Okamato (1987) I-45, South of Dallas, Texas	***Method:*** Ground penetrating radar, Coring ***Parameters:*** • Average depth • Vertical Misalignment • Horizontal Misalignment • Longitudinal Displacement (qualitative)	• Overall, the dowels in the inserter sections tended to be misaligned slightly downward in the leave direction. • Displacement can be introduced if the joint location is not marked correctly for sawing, or if the saw cut does not follow the marked joint location. • Average dowel depths appear to be uniform for both methods. • DBI performance is better than basket in terms of both degree of vertical misalignment and variability of vertical misalignment with each joint. • If other sources of variability, such as accuracy of joint locating and sawing are assumed to be constant, it appears that more longitudinal displacement was detected in the DBI sections than basket sections. Number of occurrences was, however, small in comparison to the number of dowels evaluated.

Table 2.5: (contd.) Summary of Field Study Results

Reference Study and Test Section	Specifications, Method of Measurement and Parameters Monitored	Findings/Conclusions
Yu, Khazanovich (2003) One section each using DBI and baskets, totaling 100 joints each, on I-15 reconstruction project near Victorville, California	***Tolerance:*** Horizontal and vertical misalignment: ± ¼ in. per 1 ft Lateral dowel position: ±1 in. ***Method:*** MIT Scan-2 ***Parameters:*** Horizontal and vertical misalignment	• Dowel alignment in the DBI section is no worse than that in the basket section. • In terms of number of bars misaligned, the basket section performed better (15.2 % vs 19.1 %) • In terms of the risk of the improper dowel alignment causing joint problems, the DBI section may be better because the greater percentage of the out-of-spec bars in the DBI section was due entirely to the higher percentage of misaligned bars in the 0.35 to 0.6 in. range. • In both of the more severe misalignment categories (0.6 to 0.8 in.; and >0.8 in.), the basket section had a higher percentage of misaligned bars than the DBI section.

joint by ½ in. did not exceed 3,000 lb per dowel. Also, the load necessary to close an expansion joint to a width of 0.25 in. in no case exceeded 4000 lbs per bar.

Segner and Cobb (1967), tested slab sections 6 ft wide, 5-1/2 ft long, and 10 in. thick. Dowels used were 1.25 in. diameter and 16 in. long. Testing was done at 2 and 7 days. The dowel bar alignment errors in any plane resulted in an increase in the load required to produce a joint opening of ½ in. and ¾ in. A dowel bar alignment error on the order of ¼ in. does not require an appreciable increase in the load to produce these joint opening. Their observation indicated that any misalignment in the vertical and oblique (combined misalignment) plane was more critical than the horizontal plane in terms of the load required to produce a joint opening of ½ in. and ¾ in. A dowel bar misalignment greater than ¼ in. produced severe increase in the load required to produce a corresponding joint opening.

Significant spalling failures were observed for a 3 in. horizontally and 1 in. vertically misaligned dowel bar for a joint opening of 0.9 in. A spalling type failure defines one that pulls, breaks or chips out concrete in the immediate vicinity of the contraction joint. The failure results in large wedge-shaped “chunk” of concrete being torn out of the top of the slab. Another type of failure that occurred with the dowel misaligned specimens was the local crushing of concrete around the periphery of the dowels. This crushing or bearing type failure around the dowels was more severe in the specimens tested at 2 days than those tested at 7 days. This was expected since the additional age probably provided for an increase in the bearing strength of concrete. The crushing of the concrete around the dowels undoubtedly increases slightly the diameter of the dowel cavity in the slab. This increase in the dowel cavity provided some slop or

room for the movement between the dowel and the cavity walls in addition to that provided by the dowel grease which probably loosened the effects of dowel misalignment to some extent.

Load required to open a joint by ½ in. for a 1 in. vertical misalignment of a dowel was about 4,000 lbs and for a 1 in. horizontal misalignment of a dowel the load was about 2,000 lb for the same joint opening. Spalling was produced for a vertical misalignment of 3 in. at a joint opening of about 0.9 in as indicated above.

Tayabji (1989) conducted laboratory study of misaligned dowel bars using a slab section of 3ft wide by 7ft. The depths of the slab sections were 8 in. and 10 in. with misalignment levels (per 18 in length) being 0, ¼ ,½ , 1, 2 and 4 in. Both categories of misalignment, i.e. horizontal and vertical, were carried out. Pullout loads were applied gradually and uniformly to obtain a joint opening of 0.25 in. in about 1 minute. Chairs were used to keep the dowel bars in place and a 1/8 in. thick steel plate used to form the joint. Typical relationship between joint opening and pullout load were shown. A large portion of the pullout load is required to open the joint 0.01 in. After the joint was opened to about 0.05 in, there is no further increase in the pullout load.

For each of the tests that they performed, they applied pullout load three times. After each pullout, the slab was pushed back to close the joint and the pullout test was repeated. The maximum pullout load was always obtained under the first test. For the second and third test, the maximum pullout load obtained was less than half that obtained for the first test. Maximum average pullout load for the various misalignments of single dowel bar in an 8 in. slab with max joint opening of 0.25 in. was 1237 lbs.

Testing of a pair of misaligned dowel bars with the same level of misalignment was carried out but the misalignment was in the opposite direction to cancel out any tendency of pulled slab to tilt horizontally or vertically. Both the 8 in. thick and 10 in. thick slab sections were tested with the load applied gradually and uniformly to obtain a joint opening of 0.25 in. In their tests they observed that there was an increase in the pullout load with increased level of dowel misalignment. The absolute magnitude of pullout force was 1000 lbs for dowel misalignments less than 1 in. The magnitude of the pullout load increased to 4000 lbs when the dowel misalignment exceeded 1 in. A very important fact worth mentioning was that there was no spalling around the dowel bars at the joint face for specimens having dowels with misalignments less than 1 in.

Weaver et al. (1970) carried out laboratory studies on the effects of the misalignment of dowel bars. The concept they used was that the effect of a misaligned dowel bar in a joint when opening or closing can be studied in a joint containing a single dowel bar, aligned normal to the joint, by the application of a shear force across the joint in a direction parallel to the plane of the joint. This method of study had the advantage that specimens containing precisely aligned dowel bars were produced easily and tested by varying the deflection across the joint. As a result of change in magnitude of the shear force applied to the joint, of known width (a) and deflection (Δ), a series of equivalent misalignments Δ/a were simulated until failure eventually occurred.

The authors tested joints of various widths with plane and interlocking joint faces. Tests were conducted on 10 in. thick specimens and 1 in. dowel diameters. Dowel bars were coated over half their length with a bond preventing compound and joints were produced using brass or steel sheets. The joints were loaded initially to an equivalent

misalignment of 4%, then unloaded and reloaded to the same equivalent misalignment. This was followed by 2 similar cycles but to an equivalent misalignment of 8%, which were followed by a cycle to 16%. The second and fourth cycles were performed as checks on the results of the first and third cycles. Relationships between dowel bar rigidity, $\left(\lambda = P/\Delta\right)$, and equivalent misalignment were plotted for various joint widths and overall they all exhibited the same characteristic shape. On initial application of the load to the joint, high dowel bar rigidity is noted, which rapidly decreases until an equivalent misalignment of 3% is reached and then it becomes a constant. A very important observation from the comparison of the results stated that as the joint width is increased the dowel bar rigidity decreased. The measured rigidity of dowel bars in a joint increased up to an age of 7 days and then little difference was detected between specimens of ages 7 and 28 days.

They observed that when a joint is loaded with a shear force, the concrete in the face of the joint around the uncoated half of the dowel bar is stressed in a complex fashion. The tensile strains across the horizontal axis through the dowel bar increased until at a strain of about 100 x 10^{-6} was reached and cracking occurred. After cracking occurred they found that the load - deflection curve became linear, the dowel bar rigidity was constant and the width of the crack recorded as strain in the joint face increased linearly. When a crack originates at the dowel bar due to traffic or misalignment, the condition is stable and will not progress until the load or effect of misalignment is exceeded; progression of cracks to the surface of the specimen were noted at equivalent misalignments of 25%.

The experimental and field investigations could not provide any information on the internal stresses that developed due to misaligned dowel bars. The field and experimental studies did not provide any knowledge on the mechanics of dowel-concrete interaction and how the distresses were produced due to misaligned dowel bars. A comprehensive study on some of the analytical investigations carried out in the past and recent years is presented in the next section.

2.5 REVIEW OF ANALYTICAL STUDIES

The determination of stresses and deflections, using analytical finite element methods, in concrete pavements with joints containing dowel bars as load transfer devices has been investigated in detail since the late 1970s. Analytical solutions and theories presented in the 1930s by Westergaard (1926) based on many simplified assumptions presented equations of stresses and displacements of infinite length slabs resting on a Winkler foundations and static loads.

The stress analysis of dowels is based upon the work presented by Timoshenko (1925). Dowel bar stresses result from shear, bending and bearing. These stresses can be analyzed analytically to determine factors that affect load-transfer characteristics. According to Timoshenko (1925), a dowel bar encased in concrete will deflect as shown in figure 2.5. When a load is applied at the end of the dowel bar it will deflect downward exerting pressure at the lower face of the dowel for a distance designated as A to B in figure 2.5.

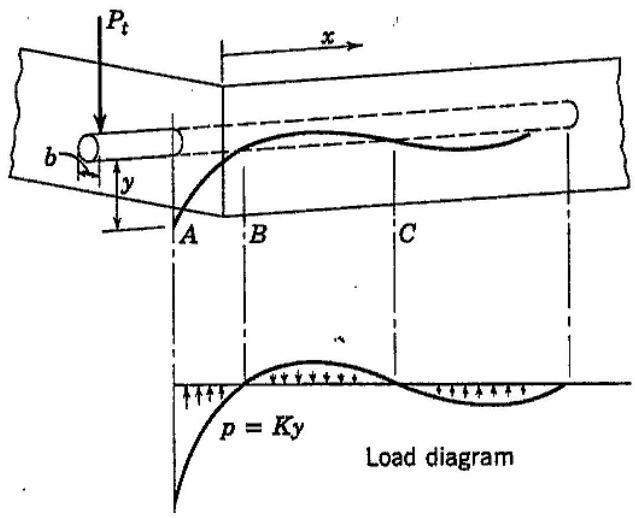

Figure 2.5: Pressure Exerted on a Loaded Dowel, Yoder (1975).

At this point of contra flexure, resulting bearing stress is on the top of the dowel and then at some distance beyond this, bearing again on the bottom of the dowel bar. For the purpose of analysis, it is necessary to assume that the dowel bar is infinite in length, extending into an elastic body. This assumption, can however, be simplified by neglecting the small pressures exerted on the bar at some distance on the elastic body.

Bradbury (1938) and Friberg (1940) have presented mathematical analysis of dowel design, which are all based upon the principles presented by Timoshenko. The relative stiffness of the bar embedded in concrete is given by

$$\beta = \sqrt[4]{\frac{K\ b}{4\ E\ I}} \quad \text{.....Equation 2.1}$$

where,

K = modulus of dowel support (*pci*) = 300,000 to 1,500,000 pci

b = diameter of the dowel

E = modulus of elasticity of the dowel

I = moment of inertia of the dowel

According to Timoshenko, the deflection of the bar resulting from the load P_t is:

$$y = \frac{e^{-\beta x}}{2\beta^2 EI}[P_t \cos(\beta x) - \beta M_o(\cos\beta x - \sin\beta x)] \text{.....Equation 2.2}$$

where,

e = natural logarithm base

x = distance along dowel from face of concrete

M_o = bending moment on dowel at face of concrete

P_t = transferred load

Friberg (1940) adopted the above equation to dowels for design purpose. Bending moment and shear in the dowel can be expressed as following equations

$$-EI\frac{d^2y}{dx^2} = M = -\frac{e^{-\beta x}}{\beta}[P_t \sin\beta x - \beta M_o\ (\sin\beta x + \cos\beta x)]$$

.....Equation 2.3

$$\frac{dM}{dx} = V = -e^{-\beta x}[(2\beta M_o - P_t)\ \sin\beta x + P_t\ \cos\beta x] \text{..... Equation 2.4}$$

If the joint-width opening is designated z and since the concrete is very stiff compared to the steel bar, the moment at the dowel – concrete interface as:

$$M_o = -\frac{P_t z}{2} \text{.....Equation 2.5}$$

for x = 0, and $M_o = -\frac{P_t z}{2}$ the deflection of the dowel joint is

$$y_o = \frac{P_t}{4\beta^3 EI}(2 + \beta z) \text{.....Equation 2.6}$$

The bearing pressure on concrete at the joint face is

$$\sigma = Ky_O = \frac{P_t}{4\,\beta^3\,EI}(2+\beta\,z) \text{ ..... Equation 2.7}$$

Maximum moment occurs where the shear is equal to zero $\left(\frac{dM}{dx}=0\right)$ and can be written as

$$M = -\frac{P_t\,e^{-\beta\,x}}{2\,\beta}\sqrt{1+(1+\beta\,z)^2} \text{ ..... Equation 2.8}$$

The above equations for bearing pressure and maximum moment are directly applicable to stress computations. In each case P_t is the transferred load on the dowel and is less than the design load as a portion of the load is transferred by the pavement to the subgrade.

The bearing stress on the concrete at the face of the joint is critical for the proper function of the dowel bar in concrete. If the bearing stress on the concrete becomes too large the concrete will begin to break away where it contacts the dowel bar. Repetitive high-stress loadings of the dowel bar concrete interface will create a void. This void creates an additional amount of deflection in the system before the dowel bar begins to take on the applied load. This additional deflection creates a loss in the efficiency of the dowel bar to transfer load across the joint. This loss in efficiency must now be carried by the subgrade, which puts additional stress on the subgrade and creates the possibility for differential settlement of the adjacent slabs.

The bearing stress at the face of the joint is given as

$$\sigma = Ky_O = \frac{P_t}{4\,\beta^3\,EI}(2+\beta\,z) \text{ ..... Equation 2.9}$$

The bearing stress on the concrete should be less that the crushing of concrete. According to the American Concrete Institutes (ACI) Committee 325 (1956), the allowable bearing stress on the concrete is equivalent to

$$\sigma_a = \left(\frac{4-b}{3}\right) f'_c \quad \text{.....Equation 2.10}$$

where,

σ_a = allowable bearing stress (psi)

b = dowel bar width, i.e., diameter (in.)

f'_c = compressive strength of concrete (psi)

This equation provides a factor of safety of approximately three. The dowel bars immediately under the applied load assume a major portion of the load with other dowel bars assuming progressively lesser amounts of load. According to the theoretical analysis, maximum negative moment occurs at a distance of 1.8 l from the load, where l is the radius of relative stiffness.

Finite element methods were first employed to model response of rigid pavements in the 1970's. The fast growth of computer capabilities has enabled researchers to make use of the complicated computational techniques into many engineering applications. Finite element analysis has proved to be one such tool that has been molded into a powerful tool to solve complex pavement engineering problems. The following is a summary of the various studies that have been conducted using finite element analysis to model the dowel bar and the dowel – concrete interaction in JPCP joints.

Tabatabaie, et al. (1979), developed a 2D finite element program that is commercially available, modified later and still used, called ILLISLAB written in Fortran IV. This FEM code uses elastic material properties, can model load transfer systems such

as dowel bars and aggregate interlock and effects of using different types of base layers and variety of traffic loading on the slab system. The concrete slab and the base are modeled using elastic homogenous medium thick plates. The subgrade is modeled as a Winkler foundation using springs and dashpots. The dowel bars are modeled as beam elements and the relative deformation between the dowel bar and surrounding concrete was incorporated using spring elements. The authors compared and verified the accuracy of the finite element program with analytical solutions found before 1978, i.e., Westergaards (1926) equations and the Pickett and Ray charts.

Majidzadeh, et al. (1981), presented the development of stress analysis model called RIGMUL. Features of their model were variables such as slab thickness, effects of curling, warping and load transfer across joints, etc. The authors coupled finite element plate theory with multilayer elastic layer theory using two layer rigid slabs for concrete resting on three semi-infinite layers of elastic solid foundation. The model was verified by comparing results for different loading conditions from Westergaard's theory. RIGMUL was capable of analyzing load transfer effects of aligned dowel bars between slabs. The authors after conducting many parametric studies, concluded with engineering judgment and experience that their model worked well for cases with change in dowel bar diameter and spacing on the slab stresses and displacements.

Kukreti et al. (1992) presented a finite element procedure for the dynamic analysis of rigid airport pavements with discontinuities. Their overall aim was to model the dynamic interaction between the aircraft and a rigid pavement. To model the concrete pavement, rectangular, thin plate elements, having three degrees of freedom at each of the four corner nodes, namely vertical displacement and rotations about the in-plane, x and y,

axes. The discontinuities in the pavement such as joints were represented as vertical spring elements connecting two nodes having the same global coordinates in the mesh. They assumed that the load is transferred across the joint by shear. The equivalent spring stiffness is dependent on the dowel properties, dowel spacing, joint opening and dowel concrete interaction. They identified the interaction between the dowel and concrete as a parameter known as modulus of dowel support. The subgrade was modeled as a Winkler foundation consisting of a uniformly distributed springs and dashpots. To verify their model, parametric studies were carried out by varying mesh type, loading condition, slab thickness, changing modulus of dowel support and modulus of subgrade reaction. By changing the modulus of dowel support from 3×10^5 to 8×10^6 psi/in., the load transfer efficiency increased from 50 – 87%, meaning that by increasing the modulus of dowel support, the concrete supporting the dowel bar became more rigid. Increasing the slab thickness from 8 – 24 in., the load transfer efficiency decreased from 77 – 63%. This is due to the fact that the equivalent spring stiffness of the joint became smaller relative to the slab thickness. They did not study the effects on load transfer efficiency due to misalignment of dowel bars, slab curling or warping due to temperature gradients.

Channakeshava et al. (1993), presented a nonlinear finite element analysis of dowel jointed concrete pavement. Material nonlinearity, geometric nonlinearity and nonlinear loading conditions were considered by the authors. Nonlinear concrete cracking in tension, yielding in compression and nonlinear response of subgrade soils were considered in the material nonlinearities. The variables considered in the model were loss of support due to pumping of the material, expansion and curling of slabs under temperature gradients and the resulting joint closure and partial loss of support were

incorporated in the model as geometric nonlinearities. Behavior of nonlinear concrete material under static loading and effects due to loss of support and temperature curling were considered. To accurately model the nonlinear behavior of concrete, the authors identified the following four parameters that have to be calibrated; the uniaxial strength of concrete in compression (f'_c); uniaxial strength of concrete in tension (f'_t); equal biaxial compressive strength of concrete (f_{bc}) and point on the failure envelope corresponding to the hydrostatic and deviatoric stresses. The subgrade was represented as a set of three orthogonal springs. These springs were capable of resisting the compressive forces to prevent lift-offs and to simulate in-plane frictional effects between the subgrade and pavement slab (not considered in this paper). To simulate loss of support the authors assumed that the subgrade springs loose their stiffness over a certain width of the pavement adjacent to the joint; different widths were assumed in their analysis. For the dowel bars, beam elements were used and only elastic behavior was assumed. In order to simulate small gaps around the dowel (dowel looseness), interface spring elements connecting the beam nodes and isoparametric quadratic solid element concrete nodes were used. To model the dowel concrete interface, a localized joint response analysis was performed. The authors stated that the dowel bars embedded in concrete on either side of the joint bear against concrete in shear as the slab is loaded. The bearing strength of concrete is limited and due to the repetition of heavy loads, high level of stresses is induced on the concrete around the dowel at the joint. Their study did not consider the effects of misaligned dowel bars as the finite element meshes had to be coarse for computational efficiency. The authors concluded that load (shear) transfer efficiency of

the joint is reduced due to the local deformations of concrete around the dowels at the joint due to high stress concentrations.

Guo et al. (1995), presented a component dowel bar model to simulate the doweled joint in Portland Cement Concrete (PCC) pavements. The model developed by the authors is a further modification to the dowel concrete interaction models used by Tabatabaie et al. (1979) and Nishizawa et al. (1989). The component dowel bar model consists of two bending beams of finite length, embedded in concrete connected by a shear – bending beam. To verify the accuracy of their model the authors compared the model to results obtained from JSLAB, developed by Tayabji and Colley. The results for longitudinal edge stresses and bending moments of the dowel bars predicted were found to be in close comparison with both the analytical and experimental results.

Zaman et al. (1995), developed a finite element algorithm to model the multiple jointed concrete pavements to moving aircraft loads. The authors presented a special joint element developed to accurately model the dowel pavement joints based on contact theory. They idealized the finite element model using rectangular thin plate elements and the soil using Winkler springs and dashpots. For the dowel bars, massless plane frame elements were considered with the dowel – concrete interaction represented by contact elements between the dowel bar and concrete. For simulating aggregate interlock, vertical spring elements were used. In the model and parametric studies they did not consider misaligned dowel bars as a load transfer mechanism. The contact element between the dowel and surrounding concrete was developed based on the Lagrangian Multiplier Method. In their model they assumed one side of dowel to be fully embedded in the pavement and not allowed to move, whereas the other side is allowed to move vertically

or slide simulating dowel looseness. The contact forces developed in the embedded end are normal and tangential forces, and similar forces are developed on the free end. The Coulomb friction law was used in addition to the tangential forces. The plane frame element considered has three degrees of freedom per node, namely, vertical deflection and rotations about in-plane axes. The contact elements used are such that common points between the dowel and surrounding concrete are in contact. The authors verified the accuracy of their model with parametric studies to understand the contact element behavior. A specific study on dowel looseness showed that the joint efficiency decreases from 99 – 70% with an increase in dowel looseness from 0 – 0.005 in.

Kuo et al. (1995), developed a 3D finite element model called 3DPAVE to analyze many complex factors that influence the concrete pavement using Abaqus. Factors such as base thickness and stiffness, interface bond and friction, slab curling and warping due to temperature and moisture gradients were considered. Using C3D20R and C3D27R, a bilinear quadratic three dimensional continuum element, they were able to model the temperature gradient through the depth of the slab. Interface elements were used to model the separation between the concrete and the underlying layers. Using Abaqus infinite elements the subgrade was modeled as an elastic foundation. Straight dowel bars were modeled as beam elements to model dowel load transfer mechanism. Aggregate interlock at the joints was modeled using shear springs. The 3DPAVE model was validated with full scale field test data such as the AASHO Road test, PCA Tests and the Arlington Road test. The authors presented results obtained from the 3DPAVE model that matched well with the above tests in terms of measured stress and strains, deflections at load position, etc.

Bhatti et al. (1998), presented a finite element model for nonlinear analysis of jointed concrete pavement that allows for modeling of nonlinear concrete material properties, behavior under cyclic loading and nonlinear fatigue damage accumulation. The concrete slab was modeled as a nine noded quadrilateral element formulated using the Mindlin approach for thick plates. The elements they used allowed for accurate monitoring of cracks and fatigue propagation through the thickness of the concrete pavement. The subgrade was modeled as Winkler foundation that can resist only the compressive stresses and involves the pumping of materials due to cyclic loading. The dowel bar was considered as a beam element that accounts for shear deformations. As the slab is loaded at the joint there is relative deformation between the dowel bar and the adjacent concrete slabs as a result of which additional deformations such as deflections, shear forces and bending moments takes place. To account for this generalized springs capable of supporting both axial and rotational deformations were used attached to the ends of the beam element. To assess the model, the authors used examples and validated the results obtained by other finite element programs and analytical solutions. They modeled the slabs such that the dowel bars were straight and did not include any misalignment.

Davids et al. (1998, 1999, 2000, 2003) developed a user friendly three dimensional finite element program that is freely available to a pavement design engineer. The program called EverFE can model multiple slabs with varied loading conditions, dowel mis-location, nonlinear thermal and shrinkage gradients, nonlinear horizontal shear stress transfer between the slabs and base, etc. Twenty noded quadratic hexahedral elements are used to discretize the slab and base layers. The dense liquid

foundation is discretized using eight noded quadratic elements that are meshed with the bottommost layer of the solid elements. The dowel bars are modeled using embedded flexural finite elements. The dowel slab interaction is captured by springs sandwiched between the dowel and slab and the dowel support modulli or the spring stiffness is specified by the user. A note by the author says that dowel bar misalignment solutions are not included in the algorithm and also, the localized stresses in the concrete surrounding the dowels may not be accurately predicted when the embedded length formulation is used. Numerous parametric studies were conducted by changing the dowel concrete spring stiffnesses and load transfer efficiency to ascertain the robustness of the finite element code.

Khazanovich et al. (2001), in a feasibility study for the Michigan Department of Transportation, built 2D finite element models with elastic material properties to explain and understand the pullout behavior of a single and joint opening behavior of multiple dowel bars. They used the general purpose commercially available finite element package ABAQUS. Various cases of misaligned dowel orientation and magnitudes were studied. Their models did predict that the presence of dowel misalignment can significantly affect joint opening behavior and cause subsequent increase in stresses around the dowel in the surrounding concrete pavement at the joint. After carefully examining the model developed by the authors, it was found that the models were based on several assumptions and limitations. To model the dowel concrete interaction, special contact interface elements were used. An initial contact pressure between the dowel and concrete was introduced by assigning a change in dowel temperature. The analytical relationship

between the pullout force and joint opening could not be validated with experimental results.

Kim et al. (2003), presented various aspects of the structural behavior of doweled joints in load transfer using nonlinear three dimensional finite element methods. They basically considered two concrete slab segments connected by dowel and supported by layers of continuum three dimensional solid elements. In the paper presented they state that by using solid continuum elements they were able to capture the severe deformation of the slabs compared to the classical plate elements. Also using solid elements as supporting layers (subgrade), a better representation of the materials was seen compared to using Winkler foundation made of springs and dashpots. Beam elements were used to model the dowels which were primarily considered straight with no misalignment. The dowel beam elements were directly connected to solid elements for an intact joint. The dowel elements were embedded in the solid concrete elements so the interaction between the dowel and slab is through mechanical contact. To simulate the loose dowels, a gap contact algorithm was considered. This approach assumes that there is a physical gap between the dowel bar and concrete. As the dowel bar deforms, the gap closes and the bar bears on the surrounding concrete transferring stresses. A parametric study was conducted on load levels (single wheel and multiple wheels), dowel spacing, slab thickness, dowel looseness, etc. Their analyses clearly showed that thicker slabs engage more dowels in load transfer. The load transfer ratio was found to decrease with an increase in applied wheel load for multiple wheel slabs. Without a doubt, they were able to show that dowel looseness, with small gaps between the dowel and surrounding

concrete, reduces the load transfer efficiency significantly and magnified the bending stresses.

Rarely has any one in the past studied or investigated experimentally and analytically the behavior of misaligned dowel bars. The purpose of this research is to examine and incorporate the effects of misaligned dowel bars and use the knowledge gained from previous literature to better model a joint in a concrete pavement system.

CHAPTER 3

EXPERIMENTAL INVESTIGATIONS

3.1 INTRODUCTION

A comprehensive laboratory experimental investigation was carried out to study the joint opening behavior of misaligned dowel bars placed in contraction joints. The instrumented pavement slab specimens were subjected to simulated thermal joint expansion and the various distresses that occurred due to misalignment were documented. This chapter presents the experimental plan, definition, type and sign convention of misalignment used in this research study. A complete description of the test setup, the surveying techniques used and an example of the calculations to demonstrate the misalignment calculation is shown. The casting process including MDOT approved concrete mix design and fresh and hardened properties of concrete are presented. Additionally, a description of the various test equipment, instrumentation and data acquisition system is presented.

3.2 EXPERIMENTAL PLAN

An extensive experimental investigation was carried out to study the effects of skew type misalignment on the opening of transverse joints subjected to thermal expansion. The effects of the following parameters on the joint opening characteristics were investigated:

- Dowel misalignment types
- Varying the dowel misalignment magnitude
- Varying the number of dowels misaligned in a test specimen
- The orientation of misalignment

3.2.1 DOWEL MISALIGNMENT TYPE

There are three types of skew misalignments, namely, the vertical, horizontal and combined misalignment types, as shown in table 2.1(b). The combined form of misalignment, formed with equal magnitude of skew in the vertical and horizontal direction, was also considered.

3.2.2 DOWEL MISALIGNMENT MAGNITUDE

The misalignment magnitude in the test specimens were measured over half the length of the dowel bar (9 in.). The misalignment magnitudes that were considered were 0 (aligned), ¼ in., ½ in., ¾ in. and 1 in. The misalignment magnitudes were considered as skew angles measured in radians. A misalignment of $1/18$ radians translated to a misalignment magnitude of ½ in. measured over 9 in. length of the dowel bar. Similarly, $1/9$ radians, $1/12$ radians and $1/36$ radians relate to a misalignment magnitude of 1 in., ¾ in. and ¼ in. measured over 9 in. length of the dowel bar, respectively.

3.2.3 NUMBER OF MISALIGNED DOWELS

As shown in table 3.2, the one-, two-, three- and five- dowels were considered in the test matrix. The tests were carried out in two slab sizes, explained later in the experimental test setup. The smaller slab (overall dimensions 48 in. x 48 in. x 10 in.) could accommodate one- and two- dowel bars. The larger slab (overall dimensions 96 in. x 72 in. x 10 in.) could accommodate three- and five- dowel bars. The dowel bars in each test specimen could be all aligned or misaligned or have a certain misalignment orientation.

3.2.4 ORIENTATION OF MISALIGNED DOWEL BARS

In the case of multiple misaligned dowel bars in a test specimen, the orientation of a dowel bar with the adjacent bars was considered. The orientation of a dowel was

measured with respect to the skew angle. For example in a test specimen, all the dowel bars could be misaligned having uniform skew, non-uniform skew or alternate skew angles. The sign convention for measuring the skew angle is shown in figure 3.1, a clockwise skew (CW) is considered positive and counter-clockwise skew (CCW) is considered negative angle of orientation.

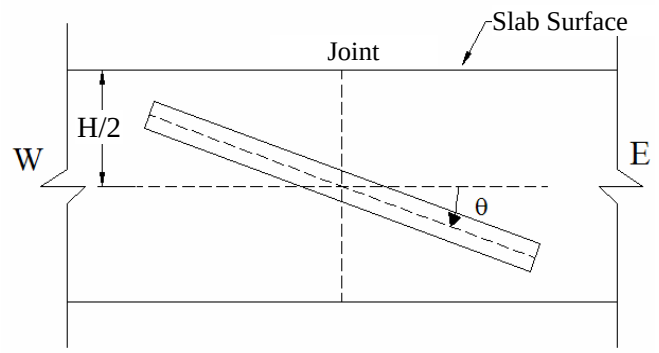

(a) Slab Specimen - Section View

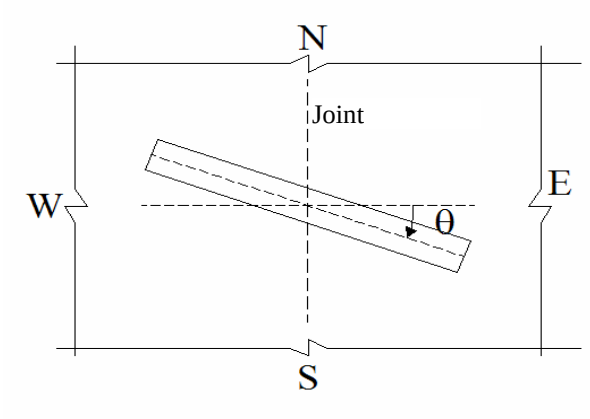

(b) Slab Specimen – Plan View

FIGURE 3.1 Sign Convention for Orientation of the dowel bar (Clockwise (CW) – Positive)

Therefore, in case of a test specimen with non-uniform misaligned dowel bars, shown in figure 3.2 (a), the bars will have opposite angles of skew with respect to each other. In case of uniform misaligned dowel bar test specimen, shown in figure 3.2 (b), the dowel bars will have the same angle of skew with respect to each other and for alternate misaligned dowel bars, shown in figure 3.2 (c), an aligned dowel bar is placed adjacent to

the misaligned dowel bar and the misaligned dowel bars in the test specimen will have opposite skew with respect to each other.

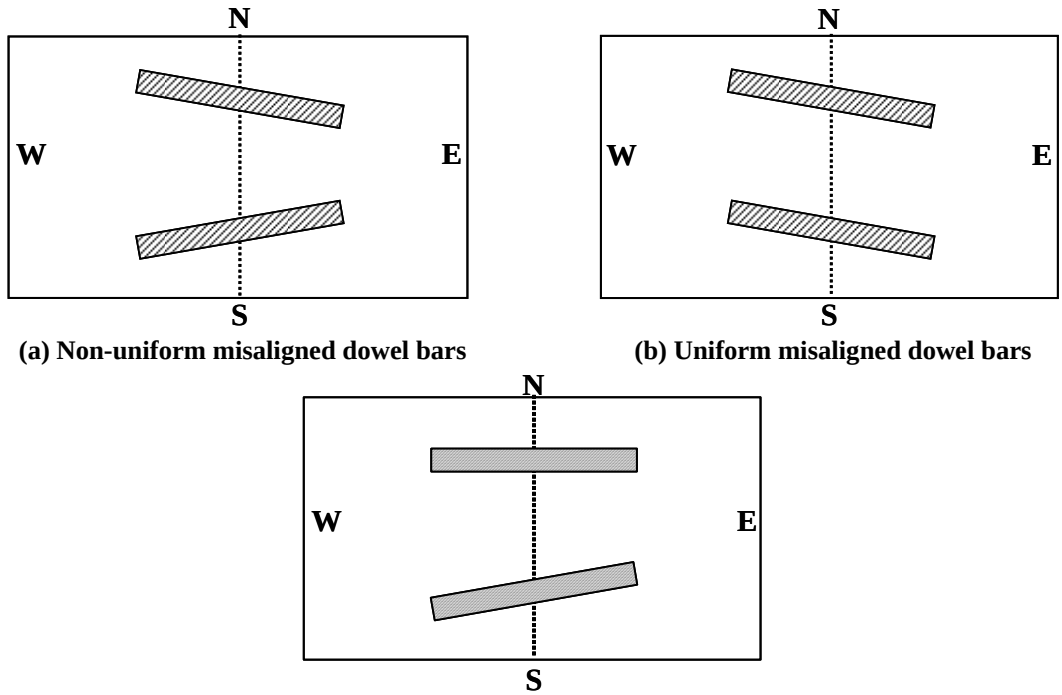

(a) Non-uniform misaligned dowel bars **(b) Uniform misaligned dowel bars**

(c) Alternate misaligned dowel bars

Figure 3.2: Concrete slab specimen with misaligned dowel bars

A nomenclature was developed to identify a test specimen. The specimen identification (ID), for example, 2V18NU, consisted first of the number of dowel bars in a test specimen, one-, two-, three- or five-. The second letter is the misalignment type, aligned (A), vertical (V), horizontal (H) or combined (C). The numbers following the misalignment type is the misalignment magnitude measured in radians (18 represents $1/18$ radians, ½ in. magnitude of misalignment measured over 9 in. length). In case of multiple dowel bars test specimen, following the misalignment magnitude is the misalignment orientation, NU (Non-Uniform), U (Uniform) and AM (alternate misaligned).

Table 3.2, shows the experimental matrix that was developed for the laboratory investigation. In all, 67 laboratory tests on slab specimens were carried out which included limited repetitions.

Table 3.2: Experimental Test Investigation Matrix

Orientation	Magnitude		1 bar	2 bars			3 bars	5 bars	
	(in in.)	(in rad.)		U	NU	AM	NU	AM	NU
Aligned	0	0	x	x			x	x	
Vertical (V)	1	9	x	x	x				
	3/4	12	x		x	x			
	1/2	18	x	x	x	x	x	x	x
	1/4	36	x	x	x			x	
Horizontal (H)	1	9	x	x	x				
	3/4	12	x		x	x			
	1/2	18	x	x	x	x	x	x	x
	1/4	36	x	x	x			x	
Combined (C)	1	9	x	x	x				
	3/4	12	x		x	x			
	1/2	18	x	x	x	x	x	x	x
	1/4	36	x		x			x	
		Total	13	9	13	6	3	6	4

Table 3.3 (a), (b) and (c), presents the slab specimen dimensions, the number of dowels in a test specimen, specimen ID, misalignment type and misalignment magnitude measured in radians.

TABLE 3.3(a) Test Specimen of the single dowel bar experiments conducted

Slab Dimensions	Number of Dowels	ID	Misalignment	Magnitude (in rad.)	Magnitude (in in.)
2 slabs each (48 in. x 24 in. x 10 in.)	1	1A	Aligned	0	0
		1V9	Vertical	$1/9$	1 in. over 9 in.
		1V12		$1/12$	$3/4$ in. over 9 in.
		1V18		$1/18$	$1/2$ in. over 9 in.
		1V36		$1/36$	$1/4$ in. over 9 in.
		1H9	Horizontal	$1/9$	1 in. over 9 in.
		1H12		$1/12$	$3/4$ in. over 9 in.
		1H18		$1/18$	$1/2$ in. over 9 in.
		1H36		$1/36$	$1/4$ in. over 9 in.
		1C9	Combined	$1/9$	1 in. over 9 in.
		1C12		$1/12$	$3/4$ in. over 9 in.
		1C18		$1/18$	$1/2$ in. over 9 in.
		1C36		$1/36$	$1/4$ in. over 9 in.

TABLE 3.3(b) Test Matrix of the two dowel bar experiments conducted

Slab Dimensions	Number of Dowels	ID	Misalignment	Magnitude (in rad.)	Magnitude (in in.)
2 slabs each (48 in. x 24 in. x 10 in.)	2 (Uniform)	2A	Aligned	0	None
		2V9U	Vertical	$+1/9$; $+1/9$	1 in. over 9 in.
		2V18U		$+1/18$; $+1/18$	$1/2$ in. over 9 in.
		2V36U		$+1/36$; $+1/36$	$1/4$ in. over 9 in.
		2H9U	Horizontal	$+1/9$; $+1/9$	1 in. over 9 in.
		2H18U		$+1/18$; $+1/18$	$1/2$ in. over 9 in.
		2H36U		$+1/36$; $+1/36$	$1/4$ in. over 9 in.
		2C9U	Combined	$+1/9$; $+1/9$	1 in. over 9 in.
		2C18U		$+1/18$; $+1/18$	$1/2$ in. over 9 in.
	2 (Non - Uniform)	2V9NU	Vertical	$+1/9$; $-1/9$	1 in. over 9 in.
		2V12NU		$+1/12$; $-1/12$	$3/4$ in. over 9 in.
		2V18NU		$+1/18$; $-1/18$	$1/2$ in. over 9 in.
		2V36NU		$+1/36$; $-1/36$	$1/4$ in. over 9 in.
		2H9NU	Horizontal	$+1/9$; $-1/9$	1 in. over 9 in.
		2H12NU		$+1/12$; $-1/12$	$3/4$ in. over 9 in.
		2H18NU		$+1/18$; $-1/18$	$1/2$ in. over 9 in.
		2H36NU		$+1/36$; $-1/36$	$1/4$ in. over 9 in.
		2C9NU	Combined	$+1/9$; $-1/9$	1 in. over 9 in.
		2C12NU		$+1/12$; $-1/12$	$3/4$ in. over 9 in.
		2C18NU		$+1/18$; $-1/18$	$1/2$ in. over 9 in.
		2C36NU		$+1/36$; $-1/36$	$1/4$ in. over 9 in.
	2 (One Bar Misaligned)	2V12AM	Vertical	$1/12$; 0	$3/4$ in. over 9 in.
		2V18AM		$1/18$; 0	$1/2$ in. over 9 in.
		2H12AM	Horizontal	$1/12$; 0	$3/4$ in. over 9 in.
		2H18AM		$1/18$; 0	$1/2$ in. over 9 in.
		2C12AM	Combined	$1/12$; 0	$3/4$ in. over 9 in.
		2C18AM		$1/18$; 0	$1/2$ in. over 9 in.

TABLE 3.3(c) Test Matrix of the three and five dowel bar experiments conducted

Slab Dimensions	Number of Dowels	ID	Misalignment	Magnitude (in rad.)	Magnitude (in in.)
2 slabs each (96 in. x 36 in. x 10 in.)	3 (Non - Uniform)	3V18NU	Vertical	$+\frac{1}{18}$; $-\frac{1}{18}$; $+\frac{1}{18}$	$\frac{1}{2}$ in. over 9 in.
		3H18NU	Horizontal		
		3C18NU	Combined		
	5 (Non - Uniform)	5V18NU	Vertical	$+\frac{1}{18}$; $-\frac{1}{18}$; $+\frac{1}{18}$; $-\frac{1}{18}$; $+\frac{1}{18}$	$\frac{1}{2}$ in. over 9 in.
		5H18NU	Horizontal		
		5C18NU	Combined		
	5 (Alternate Misaligned)	5V18AM	Vertical	$+\frac{1}{18}$; 0; $-\frac{1}{18}$; 0; $+\frac{1}{18}$	$\frac{1}{2}$ in. over 9 in.
		5H18AM	Horizontal		
		5C18AM	Combined		

3.3 EXPERIMENTAL TEST SETUP

Each laboratory scale pavement specimen consisted of two concrete slabs connected at the joint using steel dowel bars. The steel dowels are smooth round bars 1.25 in. in diameter, 18 in. in length and placed at the mid-depth of the slab. The embedded length is 9 in. on either side of the joint. In case of multiple dowel bars, the bars are placed at 12 in. on center. The number of dowel bars at a joint, the misalignment type, magnitude and uniformity was varied as shown in the experimental plan, tables 3.2 and 3.3.

The test specimen molds were made from structural steel sections and designed using specifications described in the AISC Steel Manual. The test mold consisted, from

ground up, of ½ in. thick steel base plates which had 2 in. diameter solid rollers placed over it. The solid rollers supported a structural steel base plate of ½ in. thickness. The base rails, solid rollers and bottom of the base plate were treated with a special mill finish to obtain a smooth frictionless surface. The structural steel C10x15 channels made up the sides of the mold. The structural steel channels parallel to the joint were left in place during the duration of the test whereas the channels perpendicular to the joint were removed after concrete set.

To form the contraction joint between the two slab specimens, a 1/8 in. thick aluminum separator plate with pre-fabricated holes at mid-height and 12 in. center were used. This aluminum plate was left in place after casting the concrete and it does not hinder the experiment or separation of the slab in any way. A box cut-out made of ¼ in. steel plate was fabricated and placed on either side of the joint. After concrete set and the mold was stripped, hydraulic cylinders were placed in the box cut outs.

To hold the steel dowel bars in alignment before and during the casting process, a simple U shaped hanging assembly was developed. This assembly was primarily made of a light weight structural steel channel section with a 3/8 in. slot drilled along the length. A 3/8 in. diameter threaded steel bar was bent into a U shape to hold the dowel bar. This threaded U shape was then bolted to the supporting steel channel through the slot. The overall dimensions of one and two dowel bars concrete slab test specimen is shown in figure 3.3. Figure 3.4 shows the details of the slab specimen mold, U-shape hanging assembly in the test setup and a cast specimen.

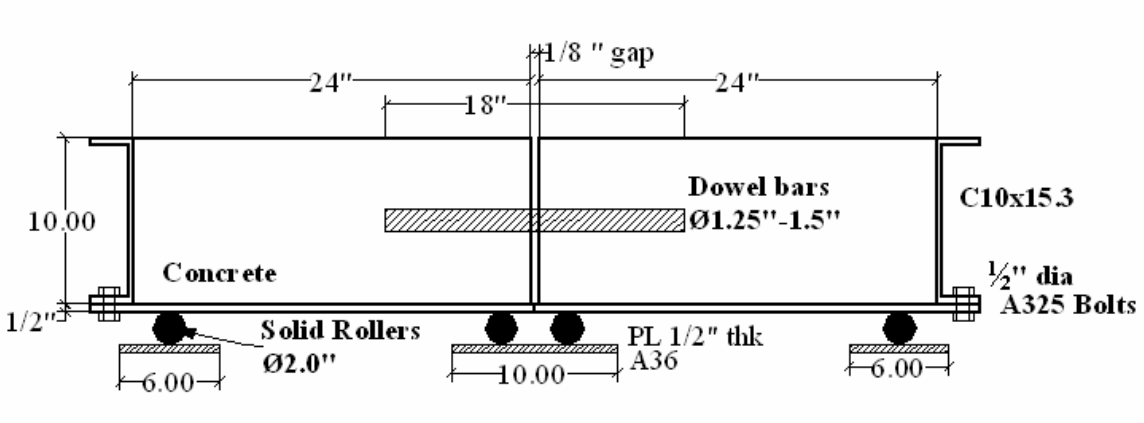

(a) Cross Section view of test setup

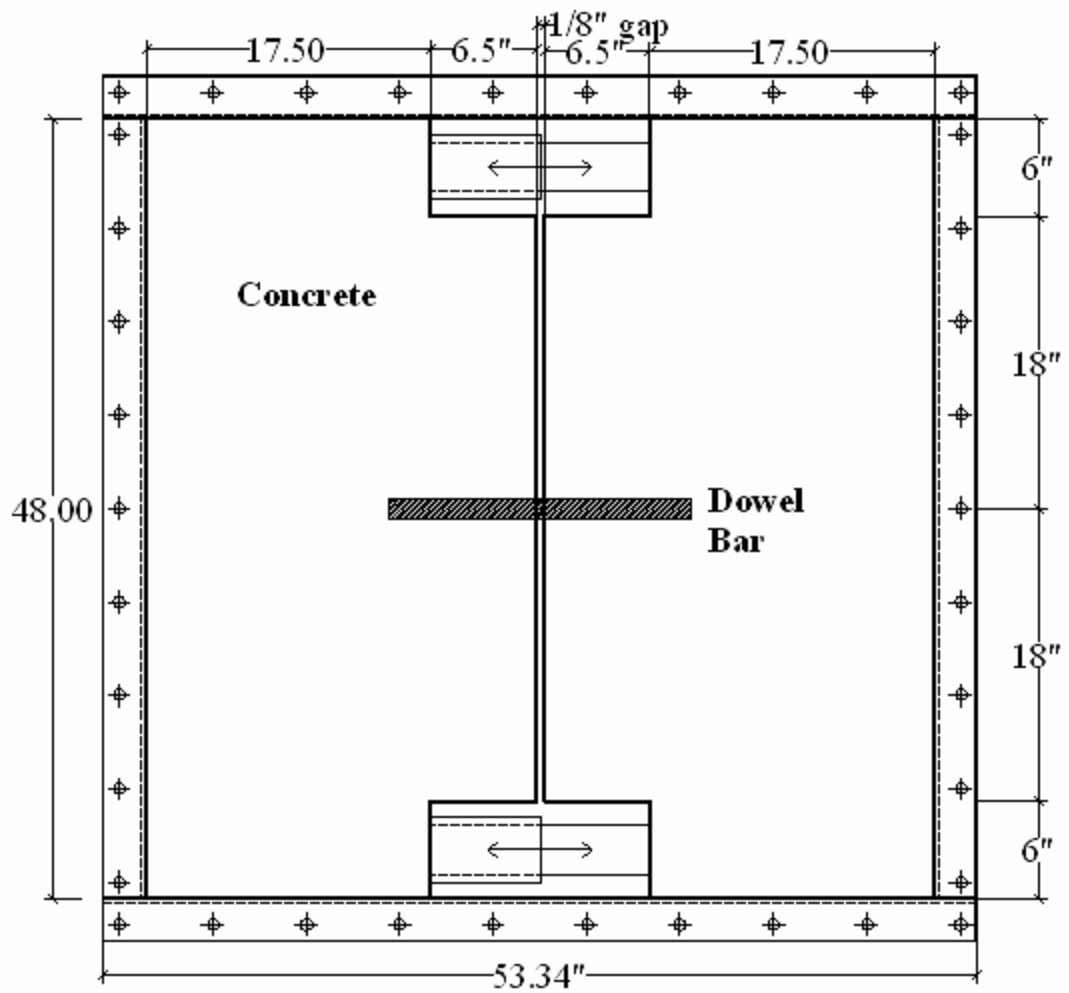

(b) Plan view of the test setup dimensions

Figure 3.3: Shop drawings showing the test setup dimensions for one and two dowel bar specimens

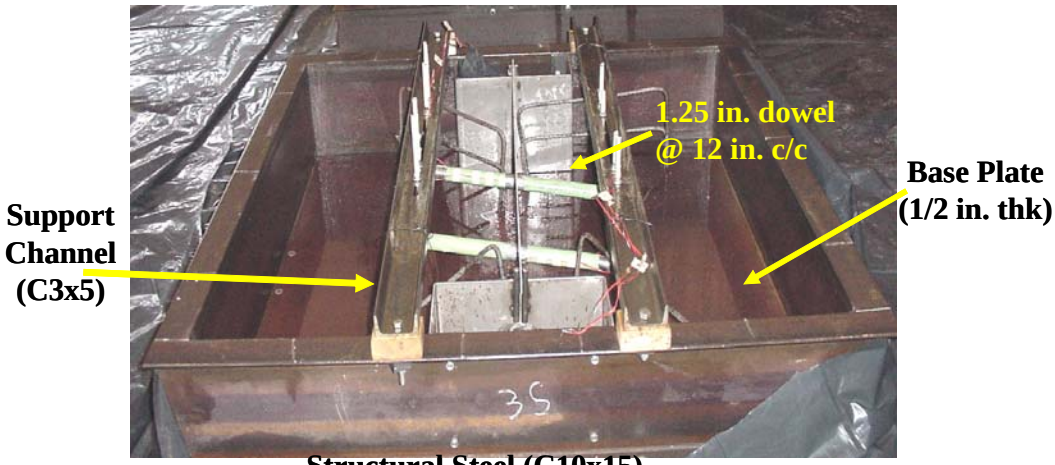

(a) Experimental Setup

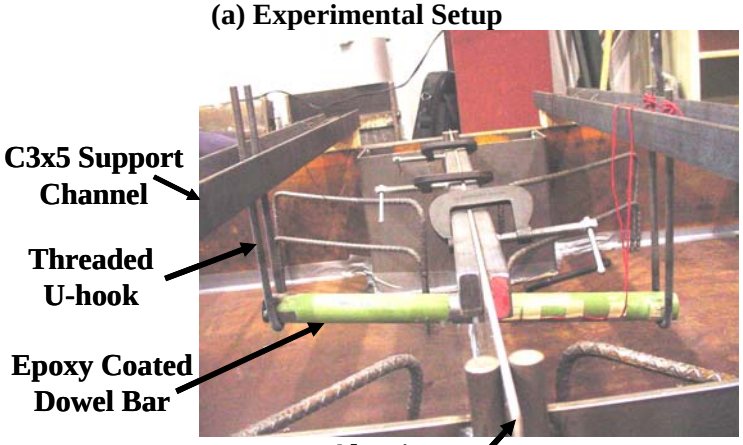

(b) Close up of U-hook Assembly

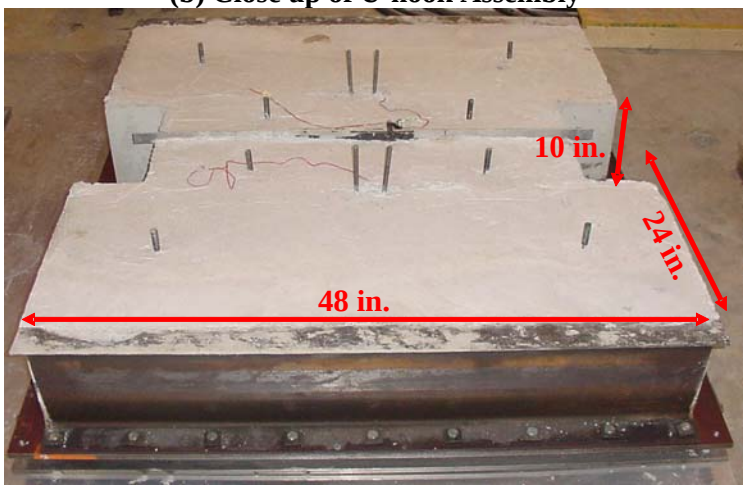

(c) Cast Specimen (48 in. x 24 in. x 10 in.)

Figure 3.4: Photograph of the various components of the experimental set-up

Misalignment accuracy was measured using surveying techniques and instruments such as the total electronic station. Details of the surveying calculations and an example demonstrating the misalignment calculation are shown in a later section of this chapter. The test setup shown in figures 3.3 and 3.4 and dimensions given in table 3.3(c) was modified to study the effects of joint opening on a 12 in. thick slab with five dowel bars of 1.5 in. diameter and placed 12 in. on centers.

3.4 LIMITATIONS AND SHORT COMINGS OF THE TEST SETUP

The research study focuses on the joint opening behavior of concrete pavement slabs with misaligned dowel bars. The joint in the slab specimens was created using a 1/8 in. aluminum separator plate to eliminate effects of aggregate interlock. Joint design is primarily based on the strength of concrete, diameter of dowels and modulus of dowel support.

The scaled test specimens were subjected to controlled joint opening which are related to the thermal expansion of the concrete slabs in the field. The slab specimens in the experimental investigation were cast in steel molds to eliminate effects due to base friction and isolate distresses caused due to misaligned dowel bars. No axle wheel loads are considered in this phase of the experimental investigation but they will be included in future research on a full pavement cross-section.

3.5 SURVEYING TECHNIQUE AND CALCULATIONS

Accurate misalignments of the dowel bars in the test setup were achieved using simple surveying techniques. A Total Electronic Station (Theodolite) was used to measure the

various angles formed between the dowel bar and the horizontal and vertical planes of the mold. To measure one misalignment angle, two theodolite stations were used.

Each misalignment of the dowel bar in the test setup achieved using the theodolite was cross-checked with a tape measure before preparing the specimen to receive concrete. The derivation to achieve the desired misalignments is explained along with sample calculations.

3.5.1 DERIVATION FOR MEASUREMENT OF VERTICAL MISALIGNMENT

Notations:

L = Distance between Station A and Station B

Horizontal Angles

θ_a = from Station A to the base plate (center of the base plate)

θ_b = from Station B to base plate (center of the base plate)

Vertical Angles

α_a = from Station A to the base plate (at the level of the base plate)

α_b = from Station B to base plate (at the level of the base plate)

β_a = from Station A to the dowel bar (at the level of the center of dowel bar)

β_b = from Station B to the dowel bar (at the level of the center of dowel bar)

A = Station A B = Station B

C = Base Plate (center) D = dowel bar (center)

E = height at eye level (center)

Referring to figure 3.5, in the horizontal plane,

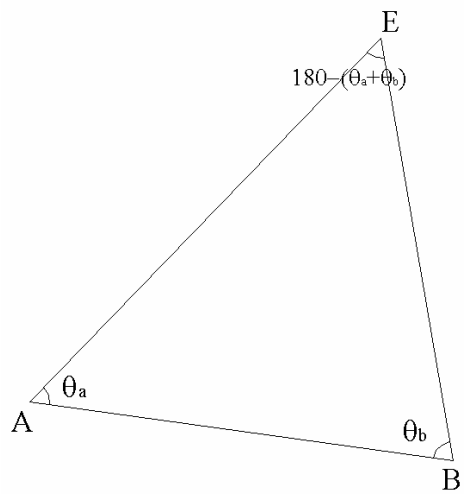

Figure 3.5: Horizontal plane showing angles measured from center of base plate to misalignment

For ΔABE, refer figure 3.5:

Using Sine Rule,

$$AE = L\ Co\sec[\theta_a + \theta_b]\ Sin[\theta_b]$$

Now with respect to the dowel at the center of the plate:

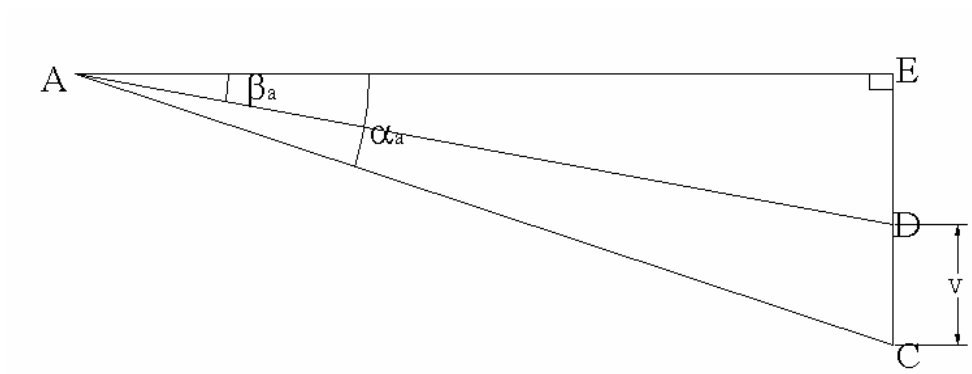

Figure 3.6: Vertical plane in the center of the plate

The vertical height from the eye level to the base plate is

$$EC = AE\ \tan[\alpha_a]$$

The vertical height from the eye level to the center of the dowel bar is:

$$ED = AE \tan[\beta_a]$$

The difference in the height taken from the eye level to the base plate and the center line of the dowel bar will give us the vertical height,

$$V = EC - ED$$

Therefore, vertical misalignment = V – 5 in. (mid height of the dowel).

Sample Calculations for Vertical Misalignment of ½ in:

The sample calculations shows are for a vertical misalignment of ½ in on the East Side of the test setup. The same set of calculation is carried out on the West Side.

Table 3.4: Summary Table showing the various angles

Location	WEST SIDE (L = 10.4')				EAST SIDE (L = 9.2')			
	Theodolite			Theoretical	Theodolite			Theoretical
	Degrees	Minutes	Seconds	Degrees	Degrees	Minutes	Seconds	Degrees
θ_a	62	37	0	62.617	25	12	40	25.211
θ_b	27	53	50	27.897	74	51	0	74.850
α_a	322	27	30	322.458	333	44	20	333.739
α_b	337	52	40	337.878	331	47	20	331.789
β_a	319	12	20	319.206	335	39	40	335.661
β_b	333	15	10	333.253	314	32	10	314.536

Referring to figure 3.7;

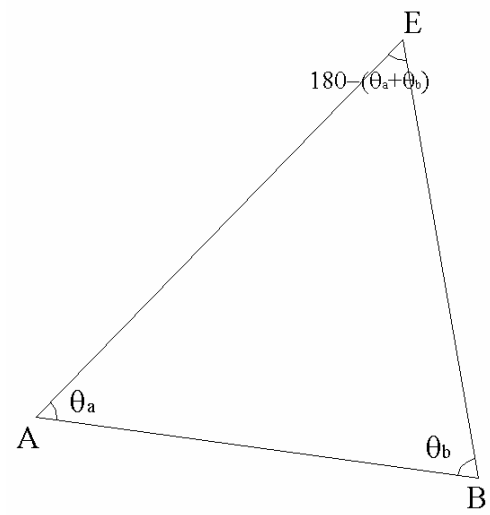

Figure 3.7: Horizontal plane showing angles measured from center of base plate to misalignment

For ΔABE:

Using Sine Rule,

$$AE = L\ Co\sec[\theta_a + \theta_b]\ Sin[\theta_b] = 108.227 \text{ in.}$$

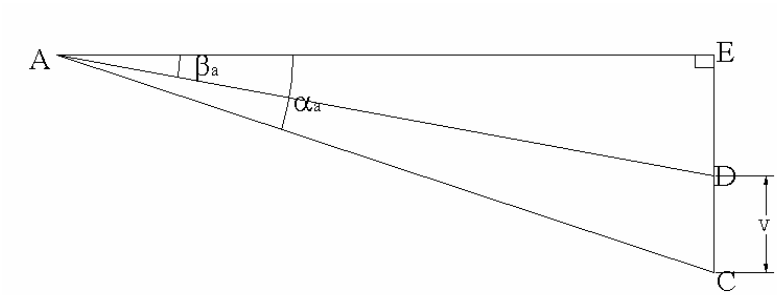

Figure 3.8: Vertical plane in the center of the plate

The vertical height from the eye level to the base plate is:

$$EC = AE\ \tan[\alpha_a] = 53.397 \text{ in.}$$

The vertical height from the eye level to the bottom edge of the dowel bar is:

$$ED = AE\ \tan[\beta_a] = 48.9549 \text{ in.}$$

The difference in the height taken from the eye level to the base plate and dowel bar will give us the distance from the base plate to the bottom edge of the dowel bar,

$V = EC - ED = 4.4429$ in.

A perfectly aligned bar will be at (base plate to center line of dowel bar) = 5 in.

Misalignment = 5 – 4.4429 = 0.557 in. vertical misalignment.

3.5.2 DERIVATION FOR MEASUREMENT OF HORIZONTAL MISALIGNMENT

Notations:

L = Distance between Station A and Station B

Horizontal Angles

θ_a = from Station A to the base plate (center of the base plate)

θ_b = from Station B to base plate (center of the base plate)

γ_a = from Station A to the base plate (horizontal misalignment on the base plate)

γ_b = from Station B to base plate (horizontal misalignment on the base plate)

Vertical Angles

α_a = from Station A to the base plate (at the level of the base plate)

α_b = from Station B to base plate (at the level of the base plate)

β_a = from Station A to the dowel bar (at the level of the center of dowel bar)

β_b = from Station B to the dowel bar (at the level of the center of dowel bar)

A = Station A	B = Station B
C = Base Plate (center)	D = dowel bar (center)
E = height at eye level (center)	E = height at eye level (misaligned)

C’ = Base Plate (misaligned) D = dowel bar (misaligned)

In the following surveying description we are assuming two important measurements:

1. The height of each of the stations is same

2. The two stations are parallel to the horizontal misalignments.

Referring to figure 3.9, in the horizontal plane,

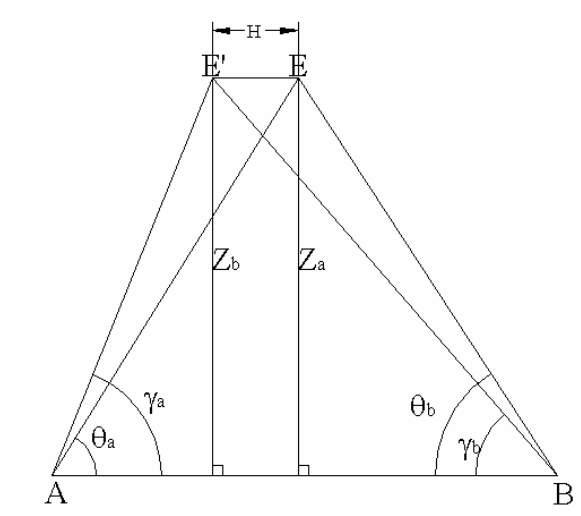

Figure 3.9: Horizontal plane showing angles measured from center of base plate to misalignment

For ΔABE, figure 3.9:

Using Sine Rule,

$$AE = L\ Co\sec[\theta_a + \theta_b]\ Sin[\theta_b]$$

$$BE' = L\ Co\sec[\gamma_a + \gamma_b]\ Sin[\gamma_a]$$

To make sure that the two stations are parallel, we compare the perpendicular distances, Z_a and Z_b:

$$Z_a = AE\ Sin[\theta_a] \qquad \& \qquad Z_b = BE'\ Sin[\gamma_b]$$

If, $Z_a \cong Z_b$, then the two stations are parallel to the horizontal misalignment.

Now with respect to the dowel at the center of the plate:

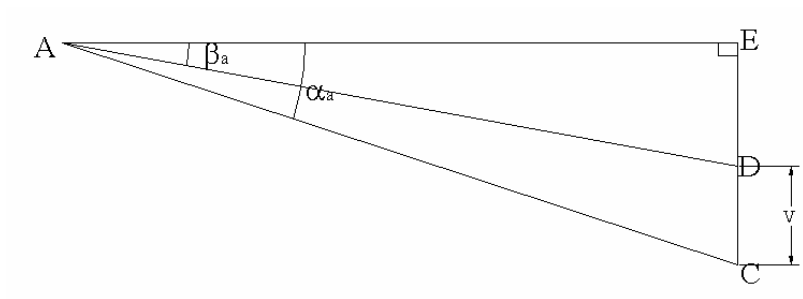

Figure 3.10: Vertical plane in the center of the plate

The vertical height from the eye level to the base plate is, figure 3.10:

$$EC = AE \tan[\alpha_a]$$

The vertical height from the eye level to the center of the dowel bar is

$$ED = AE \tan[\beta_a]$$

The difference in the height taken from the eye level to the base plate and the center line of the dowel bar will give us the vertical height,

$$V = EC - ED$$

Therefore, vertical misalignment = V – 5 in. (mid height of the dowel)

Now to check after forcing a misalignment, H, the vertical distance of the dowel bar from the base plate

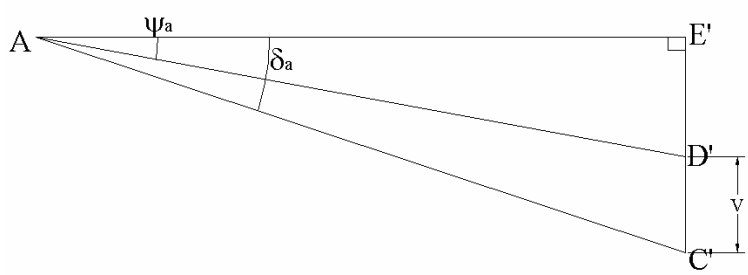

Figure 3.11: Angles in the vertical plane, after forcing the misalignment of H.

The vertical height from the eye level to the base plate is, figure 3.11:

$$E'C' = AE' \tan[\delta_a]$$

The vertical height from the eye level to the center of the dowel bar is

$E'D' = AE' \tan[\psi_a]$

The difference in the height taken from the eye level to the base plate and the center line of the dowel bar will give us the vertical height

$V' = E'C' - E'D'$

Therefore, vertical misalignment after forcing the misalignment in the horizontal plane should be = V' – 5 in. (mid height of the dowel)

For ΔABE', in horizontal plane,

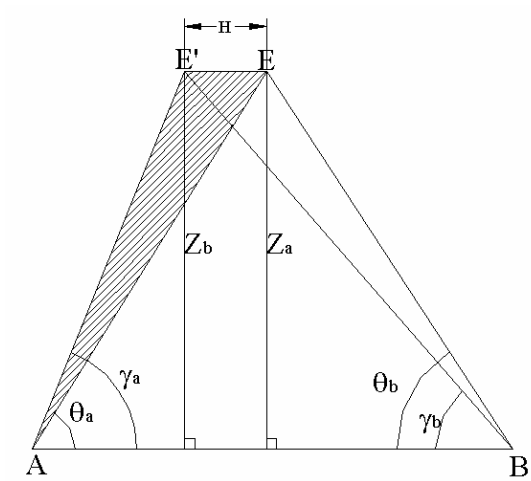

Figure3.12: Showing the final computation of the horizontal misalignment

$AE' = Z \ Co\sec[\gamma_a]$

Using cosine rule for $\Delta AEE'$, figure 3.11:

$$H = \sqrt{(AE)^2 + (AE')^2 - 2\ (AE)\ (AE')Cos[\theta_a - \gamma_a]}$$

The H obtained is then compared with tape measure as a final check.

Sample Calculation for Horizontal Misalignment of ½ in:

Table 3.5: Summary Table showing all angles for horizontal misalignment

Location	NORTH WEST SIDE (L = 5.7')				SOUTH EAST SIDE (L = 5.2')			
	Theodolite			Theoretical	Theodolite			Theoretical
	Degrees	Minutes	Seconds	Degrees	Degrees	Minutes	Seconds	Degrees
θ_a	56	58	40	56.978	57	30	40	57.511
θ_b	49	0	20	49.006	53	19	0	53.317
γ_a	57	30	0	57.500	57	6	40	57.111
γ_b	48	41	40	48.694	53	47	30	53.792
α_a	317	58	30	317.975	319	53	20	319.889
α_b	321	0	30	321.008	321	30	0	321.500
β_a	321	6	40	321.111	323	13	40	323.228
β_b	324	5	10	324.086	324	52	0	324.867
δ_a	317	52	40	317.878	320	3	50	320.064
δ_b	321	11	0	321.183	321	22	20	321.372
ψ_a	321	0	30	321.008	323	24	0	323.400
ψ_b	324	17	50	324.297	324	42	0	324.700

Referring to figure 3.13, in the horizontal plane,

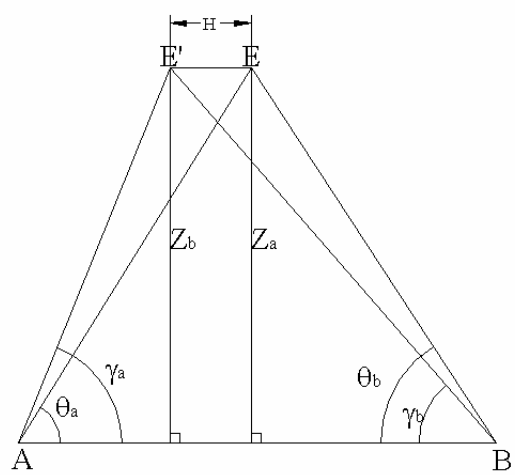

Figure 3.13: Horizontal plane showing angles measured from center of base plate to misalignment

For ΔABE, figure 3.13:

Using Sine Rule,

$$AE = L\ Co\sec[\theta_a + \theta_b]\ Sin[\theta_b] = 53.54 \text{ in.}$$

$$BE' = L\ Co\sec[\gamma_a + \gamma_b]\ Sin[\gamma_a] = 56.09 \text{ in}$$

To make sure that the two stations are parallel, we compare the perpendicular distances, Z_a and Z_b:

$$Z_a = AE\ Sin[\theta_a] = 45.16 \text{ in.} \qquad \& \qquad Z_b = BE'\ Sin[\gamma_b] = 45.27 \text{ in.}$$

If, $Z_a \cong Z_b$, then the two stations are parallel to the horizontal misalignment.

Now with respect to the dowel at the center of the plate:

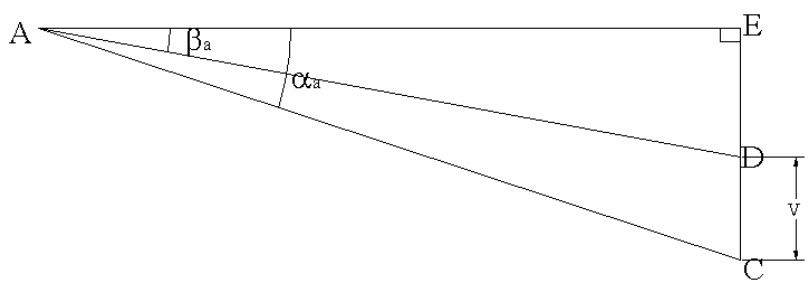

Figure 3.14: Vertical plane in the center of the plate

The vertical height from the eye level to the base plate is, figure 3.14

$$EC = AE\ \tan[\alpha_a] = 45.10 \text{ in.}$$

The vertical height from the eye level to the center of the dowel bar is

$$ED = AE\ \tan[\beta_a] = 40.01 \text{ in.}$$

The difference in the height taken from the eye level to the base plate and the center line of the dowel bar will give us the vertical height,

$$V = EC - ED = 5.09 \text{ in.}$$

Therefore, vertical misalignment = V – 5 in. (mid height of the dowel) = 0.09in

Now to check after forcing a misalignment, H, the vertical distance of the dowel bar from the base plate

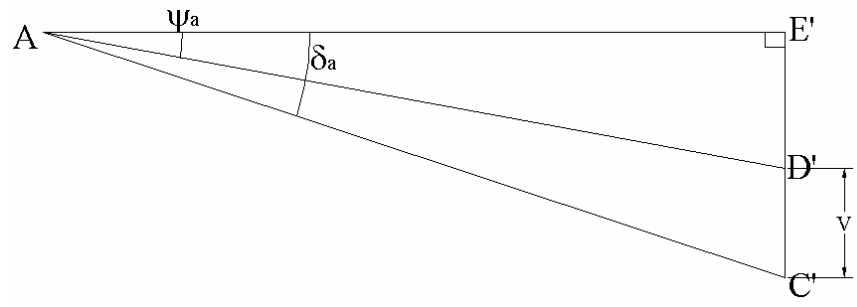

Figure 3.15: Angles in the vertical plane, after forcing the misalignment of H.

The vertical height from the eye level to the base plate is, figure 3.15:

$$E'C' = AE' \tan[\delta_a] = 45.12 \text{ in.}$$

The vertical height from the eye level to the center of the dowel bar is

$$E'D' = AE' \tan[\psi_a] = 40.02 \text{ in.}$$

The difference in the height taken from the eye level to the base plate and the center line of the dowel bar will give us the vertical height,

$$V' = E'C' - E'D' = 5.09 \text{ in.}$$

Therefore, vertical misalignment after forcing the misalignment in the horizontal plane should be = V' – 5 in. (mid height of the dowel) = 0.09 in.

For ΔABE', in horizontal plane,

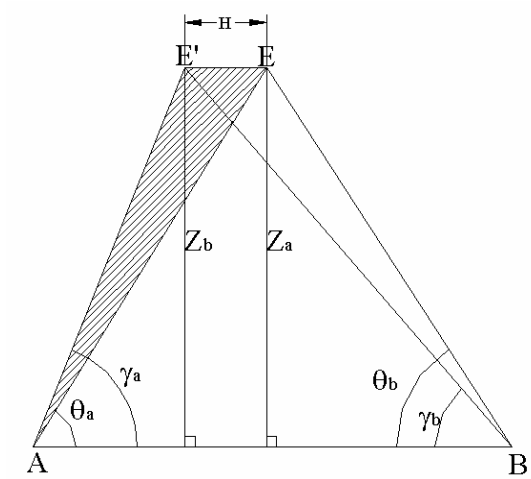

Figure 3.16: Showing the final computation of the horizontal misalignment

$$AE' = Z\ Co\sec[\gamma_a] = 53.89 \text{ in.}$$

Using cosine rule for $\Delta AEE'$, figure 3.15

$$H = \sqrt{(AE)^2 + (AE')^2 - 2\ (AE)\ (AE')Cos[\theta_a - \gamma_a]} = 0.5168 \text{ in.}$$

The H obtained is then compared with tape measure as a final check.

In the next section, material specifications such as the M-DOT approved mix design, fresh and hardened properties of concrete specimens, coupon strengths of the steel dowel bar carried out as per ASTM specifications that were documented are presented.

3.6 MATERIAL SPECIFICATIONS

The concrete used in the fabrication of the pavement slab specimens was a MDOT pavement mix grade P1 supplied by a local pre-approved ready mix plant. The mix design is summarized in table 3.6.

Table 3.6: Mix Design of Concrete

Source of Concrete: Plant 14-East Lansing

Material	Class: Source	SSD Weight (lb/yd^3)	Yield, ft^3
Cement	ASTM C-150 Type I: Essroc	564	2.87
Fine Aggregate	2NS: Builders Aggregates (#34-86)	1275	7.65
Coarse Aggregate	6AA: MLO LS(#71-3)	1720	10.81
Water		256	4.1
Air Content		6.5 %	1.77
		Total	27.2

Admixtures added:

ASTM C-494A Water Reducer Type A	MB 200 N	3.0 oz/c
ASTM C-260 Air Entrainer	MB Microair	1.2 oz/c

Desired Plastic Concrete Properties

Slump	3 in.
Concrete Unit Weight	142 pcf
Air Content	6.5 %

Fresh and hardened properties of concrete were documented. Concrete cylinders (4 in. diameter x 8 in. length) and flexural beams (4 in. x 4 in. x 14 in.) were cast during the slab specimen construction. During the slab specimen casting, fresh concrete properties such as slump (3.6 in. average), air content (6.1 % average), unit weight (144.8 pcf average) and temperature (70.8 ^{o}F) were recorded. The hardened properties were measured at 3-days, 7-days and 28-days corresponding to the day at which demolding took place, day of testing and target compressive strength is achieved, respectively. To measure the compressive strength of concrete, split tensile strength and flexural strength an average was taken of 3 cylinders, 2 cylinders and 2 beams, respectively. The specimens were tested in accordance with ASTM specifications, as shown in Table 3.7 and figure 3.17.

Table 3.7: Concrete Properties

Type of Test	Property Measured	ASTM Standard
Fresh Concrete	Slump (in.)	ASTM C143
	Unit Weight (pcf)	ASTM C138
	Air Content (%)	ASTM C138
	Temperature (^{o}F)	ASTM C1064
Hardened Concrete	Compressive Strength (psi)	ASTM C39
	Split Tensile Strength (psi)	ASTM C496
	Flexural Strength (psi)	ASTM C78

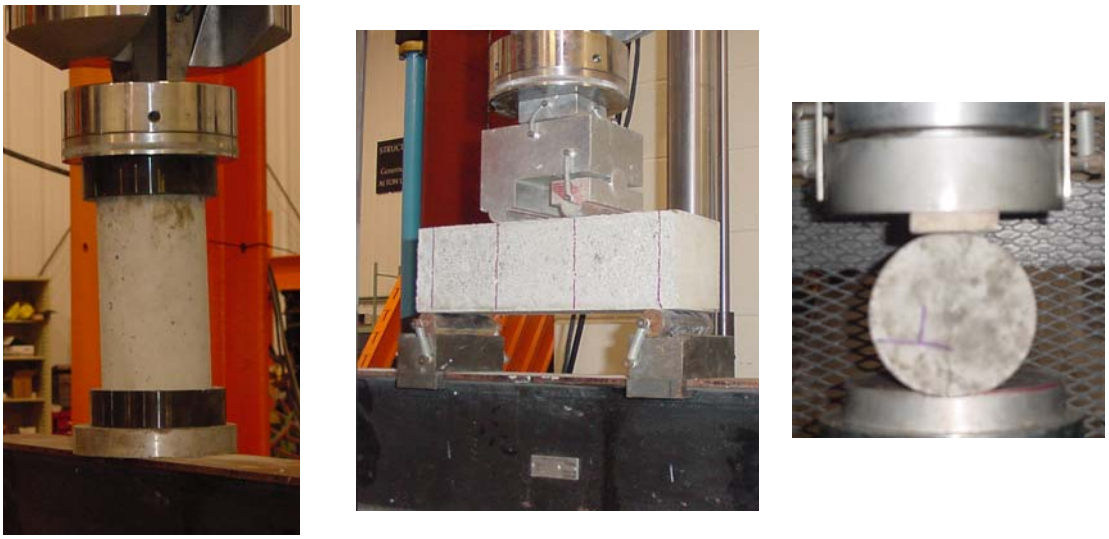

(a) Compression (b) Flexure (c) Split Tension

Figure 3.17: Concrete Hardened Properties Test Setup

The dowel bars used in the tests were made from billet steel grade 40 as per AASHTO M31 specification which says that the minimum yield strength and minimum ultimate strength of the steel coupons should be 40 ksi and 70 ksi respectively. The dowel bars were epoxy coated as per AASHTO M254 and MDOT specifications and obtained from the same heat and batch as far as possible. Tensile coupon tests were fabricated as shown in figure 3.18, according to ASTM E8-99. Using an MTS testing machine, the

yield strength, the ultimate strength and the elastic modulus of steel was determined, figure 3.19 and 3.20. The average yield strength, ultimate tensile strength and elastic modulus of steel obtained were 69 ksi, 95 ksi and 30,270 ksi, respectively.

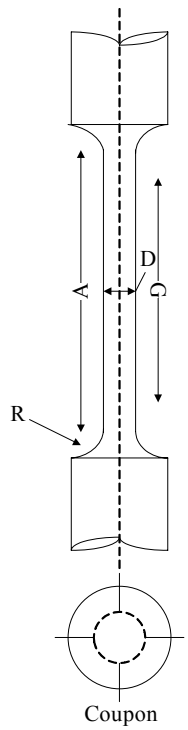

Legend:

D= nominal diameter = 0.500 in.

A= length of reduced section = 2¼ in.

G = gage length = 2.000 ± 0.005 in.

R = radius of fillet = ⅜ in.

Figure 3.18: Standard ½ in. Round Tension Test specimen with 2 in. gage length (ASTM E8-99)

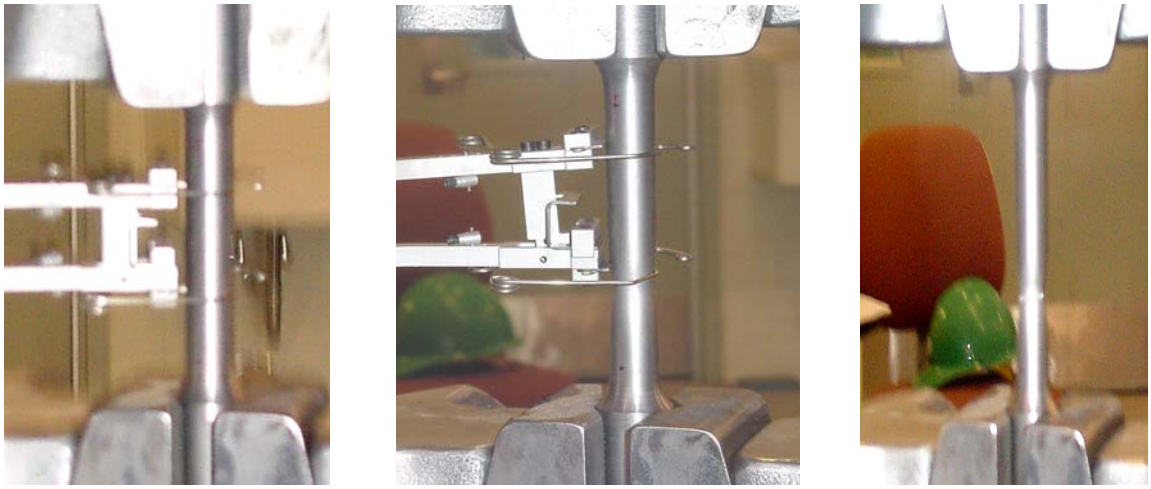

(a) Coupon before testing **(b) Coupon at the Initiation of Necking** **(c) Coupon at Failure**

Figure 3.19: Stages of Coupon Testing

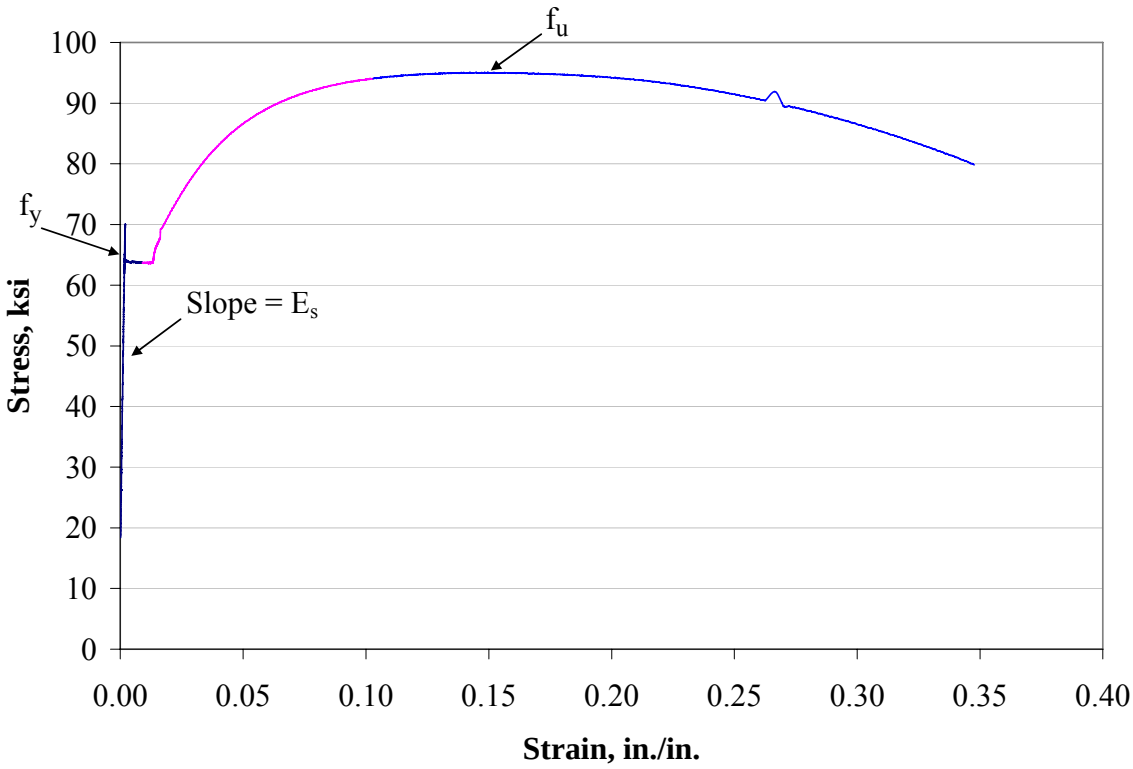

Figure 3.20: Typical Stress-Strain Curve for a coupon

3.7 INSTRUMENTATION AND DATA ACQUISITION SYSTEM

The translational and longitudinal joint opening, uplift and the force applied to push the slabs apart were measured using various instruments. Linear Variable Displacement Transducers (LVDT) and spring-return linear motion sensors (potentiometers) were used to measure various displacements occurring in the slab specimens. Special brackets were designed to hold these instruments plumb and in place during the test. The LVDTs (Omega LD610-15) were a 1.5 in. stroke LVDT placed strategically on top of the dowel bar to measure longitudinal only joint openings. Linear displacement potentiometers (Duncan Electronics 9610 and 9615) of 1.0 in. and 1.5 in. stroke lengths were used to measure the longitudinal joint opening, vertical uplift of the slabs and any translational displacements causing non-uniform joint openings in the slabs. Two pressure transducers (Omega PX303-015G5V) were placed close to the hydraulic cylinders to measure the force that was being applied to cause joint opening. The LVDTs, sliders and pressure transducers used during the testing of the specimens are shown in figure 3.21.

(a) Linear Variable Differential Transducer

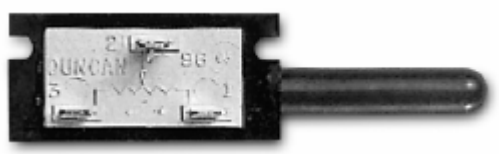

(b) 9610 Linear Motion Position Sensor (1.0 in. stroke)

(c) PX303-015G5V Pressure Transducer

(d) 9615 Linear Motion Position Sensor (1.5 in. stroke)

Figure 3.21: Closeup of Instruments (website: www.omega.com and www.beiduncan.com)

The pullout load was applied using two similar hydraulic cylinders and hand pumps supplied by Enerpac. These cylinders were placed in the box cut out on either side of the slab specimen. For the smaller slab configuration two RC156 (15 ton – 6 in piston stroke) and for the larger slab RC256 (25 ton – 6 in piston stroke) hydraulic cylinders were used. The pressure flow through the hydraulic cylinders was controlled using split flow and needle valves to apply a continuous monotonic loading at a rate of 20 lbs./min. followed by an opening rate of 0.02 in./min. The linear displacement potentiometers and the LVDTs had a measurement sensitivity of 0.02 in. and 4.5 x 10^{-3} in. Some typical photographs of the enerpac hand pump, hydraulic jacks, lvdts and sliders mounted on special designed brackets are shown in figure 3.22.

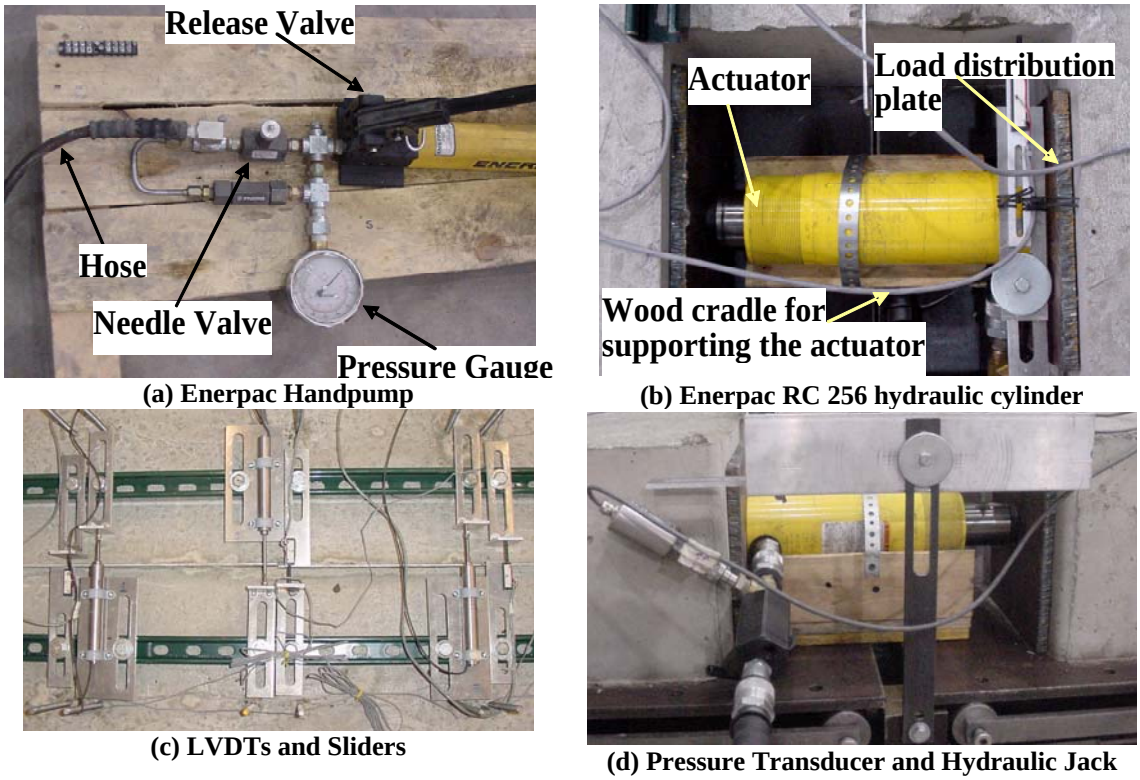

(a) Enerpac Handpump

(b) Enerpac RC 256 hydraulic cylinder

(c) LVDTs and Sliders

(d) Pressure Transducer and Hydraulic Jack

Figure 3.22: Typical Instruments and cylinders used in the tests

All the instruments used during the test were calibrated and the calibrated graph was used to scale the analog signals in the data acquisition system software. The calibration data is provided in Appendix A. The data from various instruments was collected at the rate of nearly 6 – 12 scans per second, using an array of National Instruments Data Acquisition cards. Custom built software called Little General was used to collect and process the data that was later imported into Microsoft Excel for data analysis.

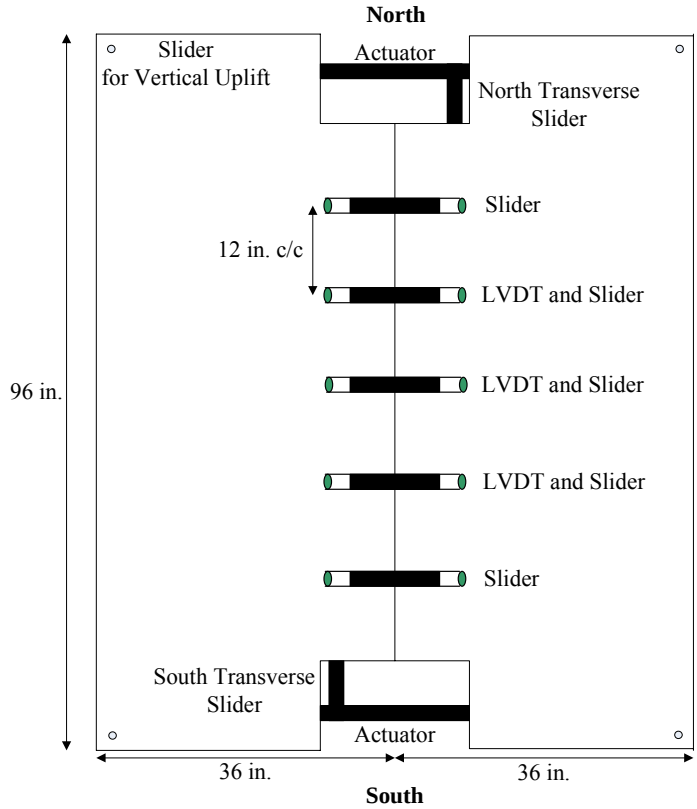

(a) Plan of Instrumentation Setup for 5-dowel test

(b) Actual setup of instrumentation on the slab specimen

Figure 3.23: Five Dowel Instrumentation Setup

3.8 TYPICAL CYCLE FOR PREPARING AND TESTING A SPECIMEN

A typical cycle in fabricating and testing a specimen in the laboratory involved, cleaning and assembling the mold; rough misalignment, surveying and final preparation before casting; casting and material testing and finally demolding and setting up instrumentation and hydraulic cylinders before testing. A typical preparation and testing cycle would take 14 days. All slabs were tested on the 7th day after casting, giving 7 days for preparation time for the next slab specimen.

Step 1: Cleaning and assembling the mold – The mold and all the structural steel sections were first cleaned, placed and assembled. The smooth polished surfaces of the base rails, solid steel rollers and bottom of the base plate were cleaned using rubbing alcohol solution. This was done to remove any debris or small pieces of concrete and to provide a smooth frictionless surface between the base rails, rollers and base plates when the slabs were moved apart. The molds were assembled as per the shop drawings mentioned earlier.

Step 2: Rough Misalignment, surveying and final preparation – Once the assembled mold was placed on the solid rollers, the next step was to thread the rods through the threaded U shapes and the holes fabricated in the 1/8 in thick aluminum separator plate. Using the base plate and the sides of the structural steel sections, a rough misalignment as per the desired combination was achieved using tape measures. After rough misalignment, one side of the dowel bar was greased using MDOT certified grease / bond breaking agent. The other side of the dowel bar was welded using small tack welds to the threaded U shapes. This assembly of the dowels is basically a controlled misalignment provided by a basket assembly.

Accurate dowel misalignments were achieved using two total electronic stations (theodolites), a reference point (the base plate and sides of the mold), trigonometric principles and surveying techniques as explained earlier. The accuracy of the surveying instruments (0.005 radians) was adequate for determining the dowel misalignment angles. The maximum error between the measured and theoretical values of misalignment was $\pm 1/16$ in. On the day of casting, a mold release agent was applied to the insides of the steel mold for easy demolding of the slab specimen.

Step 3: Casting and Material Testing – Concrete was supplied by a local ready mix plant approved by MDOT. Fresh concrete properties such as slump, air content, temperature, etc were recorded. Test specimens such as beams and cylinders were cast along with the test specimen for quality control of the MDOT approved paving mix. These beams and cylinder specimens were cured in a temperature controlled curing room and were tested at 3 days – when the specimen is demolded, 7 days – on day of specimen testing and 28 days.

Step 4: Demolding, setting up instrumentation and hydraulic cylinders, testing – The test specimens after casting were covered using plastic sheets and demolded after 3 days of curing. The specimens were demolded after ascertaining that the concrete has achieved at least 50% of the target 28-day uniaxial compressive strength (3500 psi).

A protocol was maintained during the entire testing regime: to continuously measure the induced load in the dowel bar due to joint opening of up to 1 in. The total load measured as the joint opened was divided by the number of dowels in the test specimen. The specimens were tested by pushing apart the concrete slabs using hydraulic actuators. The actuators applied a controlled monotonic longitudinal loading. The

hydraulic pressures in the actuators were synchronized using the split flow and needle valves. The concrete slabs were pushed apart very slowly at the approximate load rate of 20 lbs/min. followed by the opening displacement rate of approximately 0.02 in./min.

(a) Assembled Mold

(b) Surveying

(c) Casting of specimen

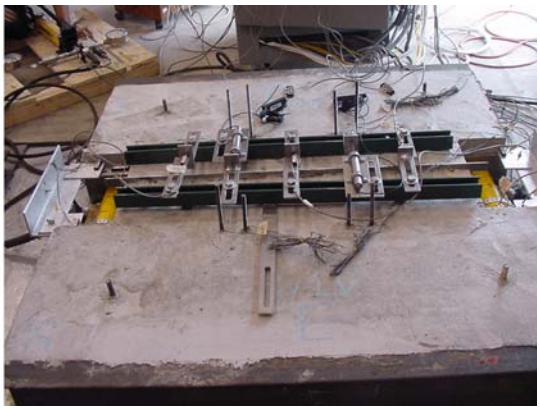

(d) Instrumented Slab

Figure 3.24: Typical cycle of specimen preparation and testing

In chapter 4, the results from the experimental investigations are presented. The types and severity of structural distresses observed during the laboratory investigation are also summarized in the next chapter.

CHAPTER 4

EXPERIMENTAL RESULTS AND EVALUATION

4.1 INTRODUCTION

This chapter presents results on the laboratory tests that were conducted on the concrete pavement specimens. A comparison of the dowel pullout force vs. joint opening behavior between the test specimens has been presented. Observations of structural distresses such as spalling around misaligned dowels at the joint face in the concrete, cracking and uplift of some test specimens with high misalignment magnitudes have been presented in this chapter.

4.2 LABORATORY TEST RESULTS

Table 4.1 presents the complete test matrix for the experimental investigation. As mentioned in Chapter 3, the parameters considered in the experimental investigations include (i) the number of dowel bars, (ii) the dowel misalignment type, (iii) magnitude and (iv) uniformity of the dowel bars. Additionally, Table 4.1 summarizes the structural distresses that were observed during the testing of the laboratory specimens.

TABLE 4.1(a): Test Matrix of the single dowel bar experiments conducted

Slab Dimensions	Number of Dowels	ID	Misalignment	Distresses Observed
2 slabs each 1220 x 610 x 250 mm	1	1A	Aligned	None
		1V9	Vertical	None
		1V12		
		1V18		
		1V36		
		1H9	Horizontal	None
		1H12		
		1H18		
		1H36		
		1C9	Combined	Spalling at end
		1C12		None
		1C18		None
		1C36		None

TABLE 4.1(b): Test Matrix of the two dowel bar experiments conducted

Slab Dimensions	Number of Dowels	ID	Misalignment	Distress Observed
2 slabs each 1220 x 610 x 250 mm	2 (Uniform)	2A	Aligned	None
		2V9U	Vertical	Spalling at end
		2V18U		None
		2H9U	Horizontal	Spalling at end
		2H18U		None
		2C9U	Combined	Spalling at end
		2C18U		None
	2 (Non - Uniform)	2V9NU	Vertical	Spalling at end
		2V12NU		Spalling at end
		2V18NU		Spalling at end
		2V36NU		Spalling at end
		2H9NU	Horizontal	Spalling and Transverse Cracking @ 0.67 in. joint opening
		2H12NU		Spalling and Transverse Cracking @ 0.7 in. joint opening
		2H18NU		Spalling at end
		2H36NU		Spalling at end
		2C9NU	Combined	Spalling and Transverse Cracking @ 0.43 in. joint opening
		2C12NU		Spalling and Transverse Cracking @ 0.95 in. joint opening
		2C18NU		Spalling at end
		2C36NU		Spalling at end
	2 (One Bar Misaligned)	2V12AM	Vertical	None
		2V18AM		None
		2H12AM	Horizontal	None
		2H18AM		None
		2C12AM	Combined	None
		2C18AM		None

TABLE 4.1(c) Test Matrix of the three and five dowel bar experiments conducted

Slab Dimensions	Number of Dowels	ID	Misalignment	Distresses Observed
2 slabs each 2440 x 915 x 250 mm	3 (Non - Uniform)	3V18NU	Vertical	Spalling around the dowel bars
		3H18NU	Horizontal	
		3C18NU	Combined	
	5 (Non - Uniform)	5V18NU	Vertical	Spalling @ 0.9 in. joint opening
		5H18NU	Horizontal	Spalling and Transverse Cracking @ 0.86 in. joint opening
		5C18NU	Combined	Spalling and Transverse Cracking @ 0.86 in. joint opening
	5 (Alternate Misaligned)	5V18AM	Vertical	Spalling around the outer and center dowel bars
		5H18AM	Horizontal	
		5C18AM	Combined	

The pullout behavior of dowel bars, as shown in Figure 4.1, is characterized by two distinct regions: (a) the initial fully bonded region (OA) and (b) the debonded / post – slip behavior region (AC). The bond stress τ, is then calculated by dividing the load by the circumferential area of the dowel bar (π*1.25*9). The magnitude of the bond stress at the point of debonding or initial slip is denoted as the initial slip/debonding stress (τ_b), and is calculated using the following equation:

Bond Stress: $\tau_b = \dfrac{F_b}{\pi DL}$

where F_b is the force at initial slip/debonding in lbs, D is the dowel bar diameter in inches and L is the embedment length of the dowel bar (9 in.).

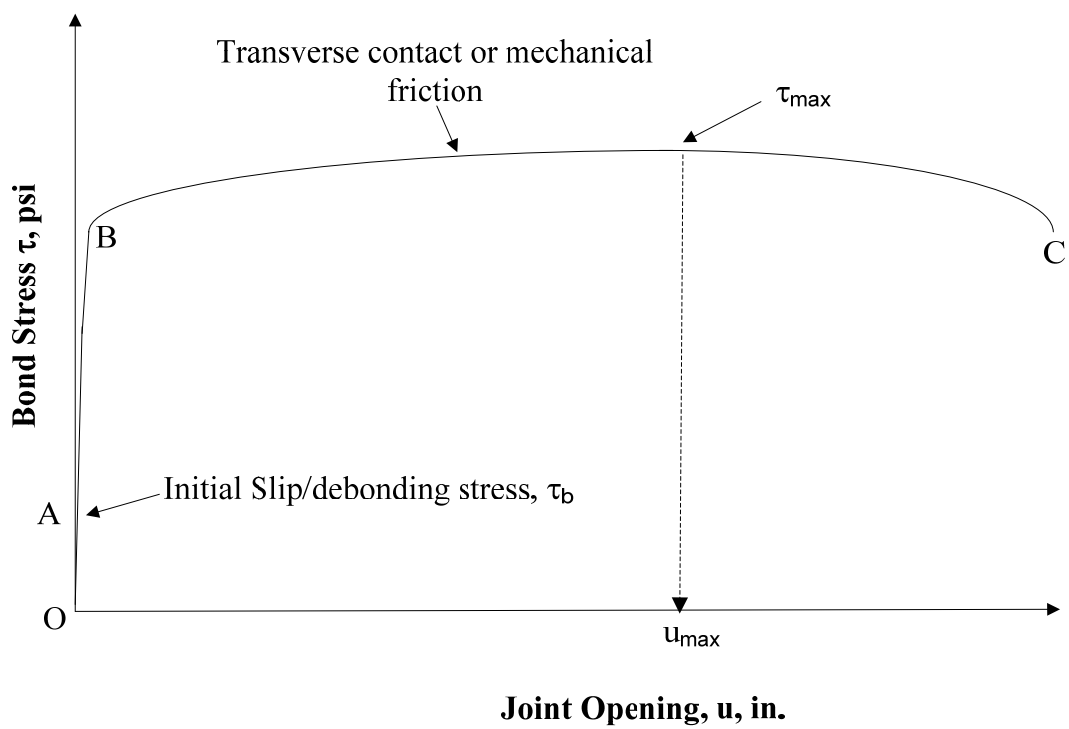

Figure 4.1: Typical Bond Stress versus Joint Opening curve

4.2.1 COMPARISON WITHIN A TYPE OF MISALIGNMENT

Vertically Misaligned dowel bar specimens

Figure 4.2 illustrates the comparisons of dowel pullout force per dowel bar vs. joint behavior for the one dowel (1A, 1V36, 1V18, 1V12 and 1V9) test specimens. Figures 4.3 through 4.5 present the comparisons of pullout force per dowel vs. joint opening behavior

of two dowels having non-uniform (2A, 2V36NU, 2V18NU, 2V12NU and 2V9NU), uniform (2A, 2V18U and 2V9U) and alternate misalignment (2V18AM and 2V12AM) orientations, respectively. Figures 4.6 and 4.7 present the comparisons of pullout force per dowel vs. joint opening behavior for three (3A and 3V18NU) and five (5A, 5V18NU, 5V18AM) dowel bar specimens, respectively. Figures 4.8 and 4.9 present the amount of dowel pullout force required to open the joint to ¼ in. and ½ in. respectively.

In the case of a single misaligned dowel bar, figure 4.2, a clear trend is observed in the post slip behavior. The amount of dowel pullout force required to open a joint increases as the misalignment magnitude is increased, from an aligned to a misalignment magnitude of 1/9 radians. From figures 4.8 and 4.9, an increasing trend in the dowel pullout force both at ¼ in. and ½ in. joint opening is observed. As the misalignment magnitude was increased, the amount force required to open the joint also increased.

In the two misaligned dowel bars test specimens, shown in figures 4.3 through 4.5, due to misalignment, the dowel pullout force per bar vs. joint opening behavior increases to a peak value and then plateaus as the joint is opened up to the end of the test. This trend was specially observed in the test specimens containing the non-uniform oriented dowel bars. The 2V9NU test specimen required the maximum amount of dowel pullout force, approximately 2900 lbs and 3400 lbs, to open a joint to ¼ in. and ½ in., respectively.

The results obtained for three and five dowel test specimens are shown in figures 4.6 and 4.7. From the dowel pullout force vs. joint opening behavior of 3V18NU and 5V18NU test specimens, it is clear that the slabs were undergoing restraint as the slabs were pushed apart. This was due to the fact that all the dowel bars in the test specimens

were misaligned with non-uniform orientation of misalignment causing joint locking. In the case of the 5V18NU test specimen, figure 4.9, at a dowel pullout force of 4000 lbs and joint opening of 0.85 in. the test specimen failed due to cracking of the slab.

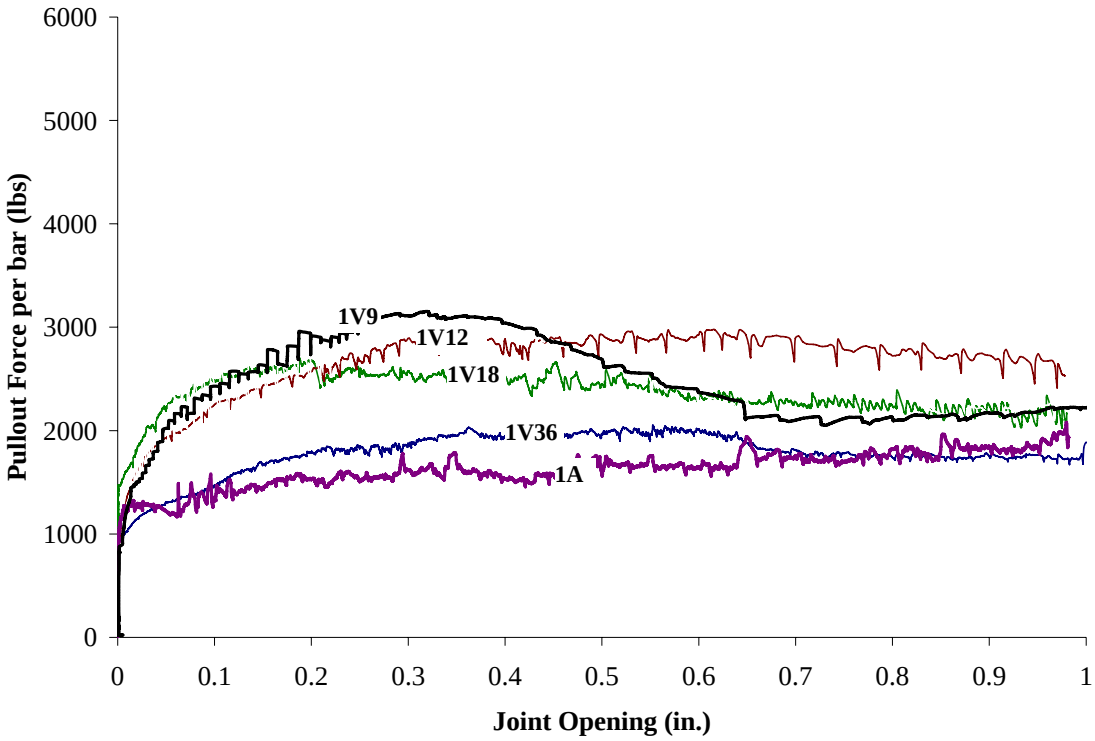

Figure 4.2: Comparison of pullout force vs. joint opening behavior for specimens with a single vertically misaligned dowel bar

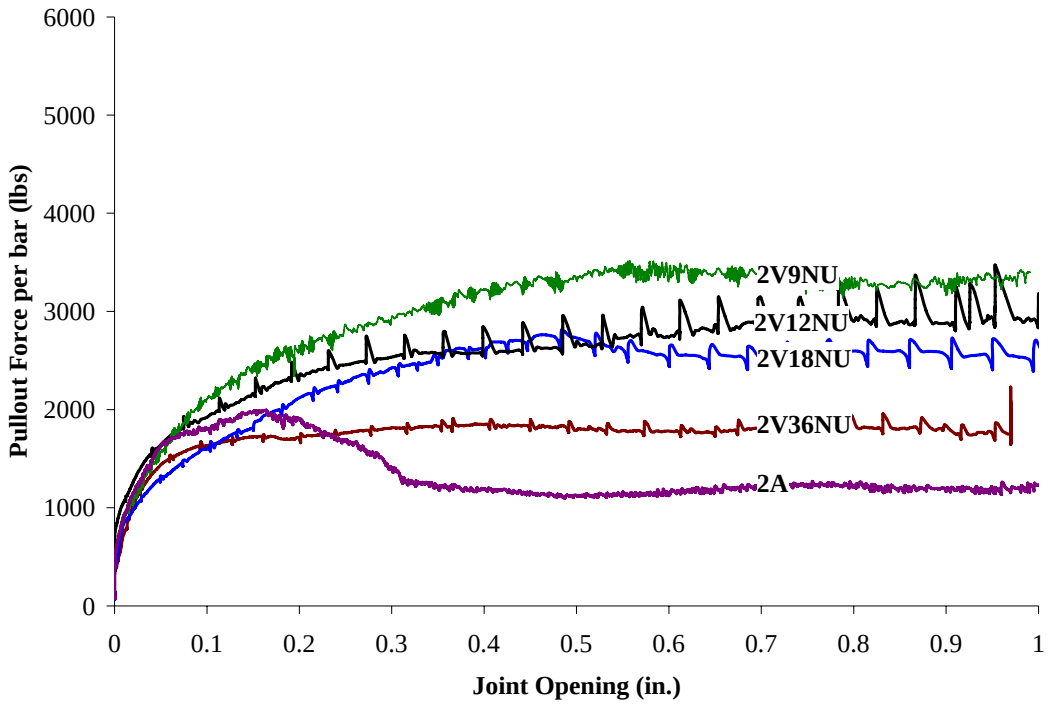

Figure 4.3: Comparison of pullout force vs. joint opening behavior for specimens with two vertically misaligned dowel bars having non-uniform (NU) orientation

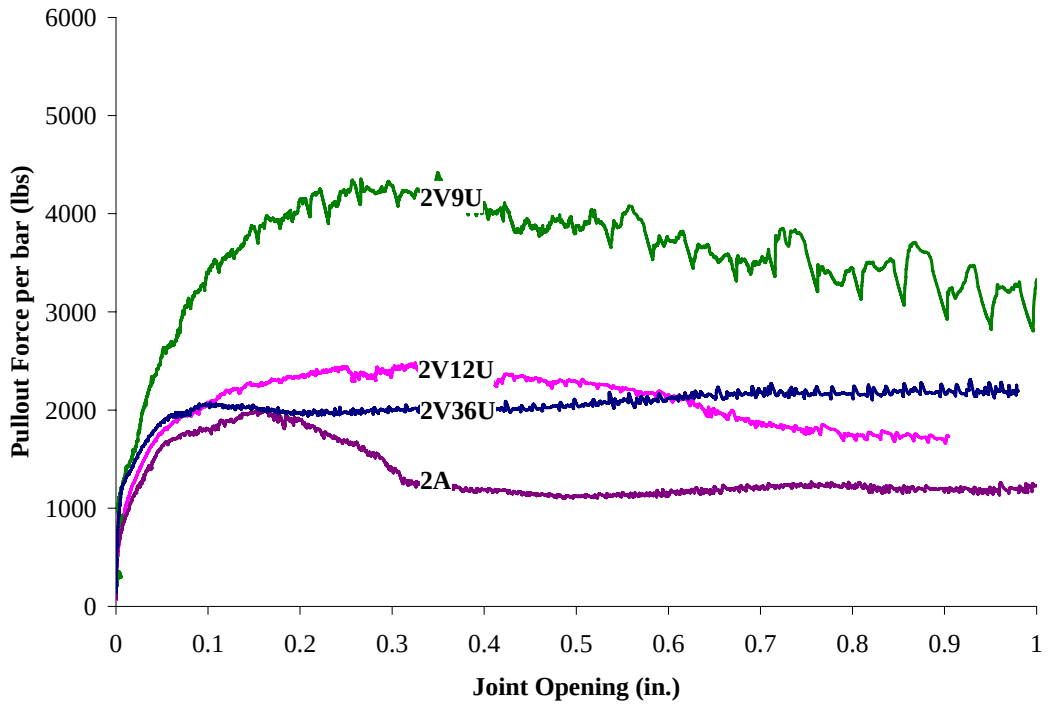

Figure 4.4: Comparison of pullout force vs. joint opening behavior for specimens with two vertically misaligned dowel bars and uniform (U) orientation

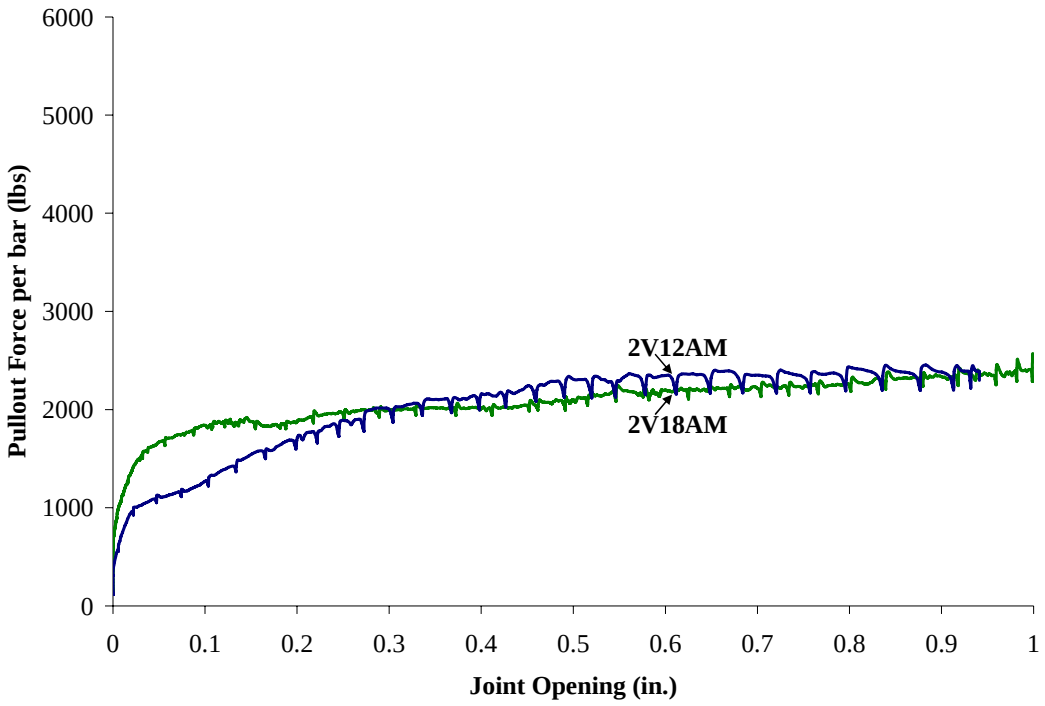

Figure 4.5: Comparison of pullout force vs. joint opening behavior for specimens with two vertically misaligned dowel bars and alternate (AM) orientation

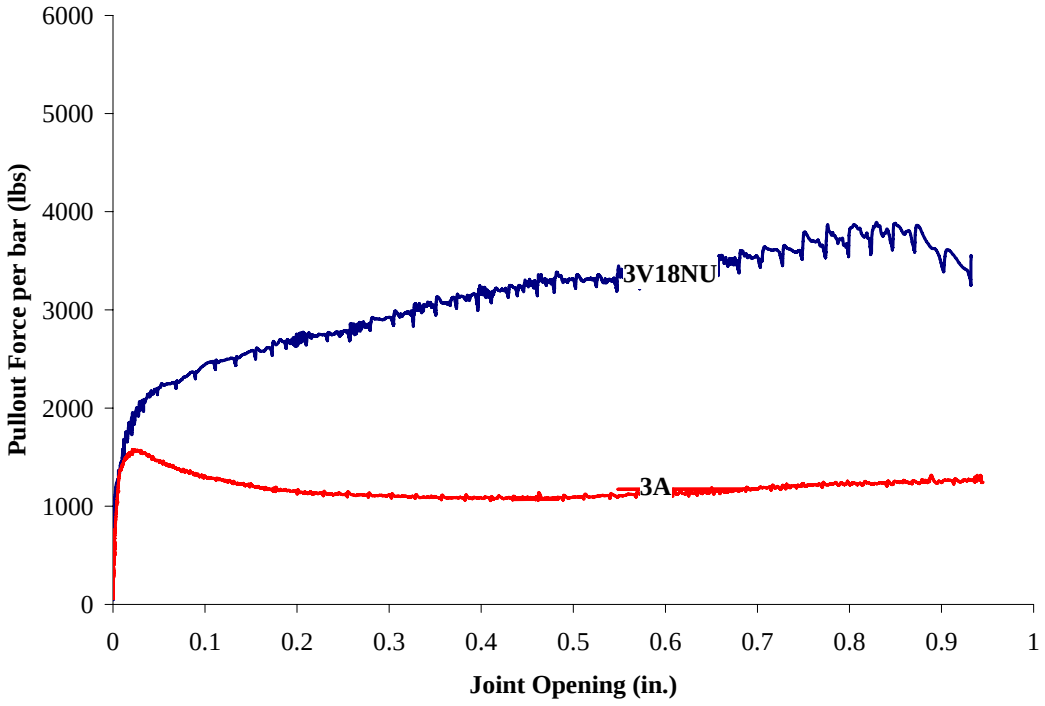

Figure 4.6: Comparison of pullout force per bar vs. joint opening behavior for specimens with three vertically misaligned dowel bars

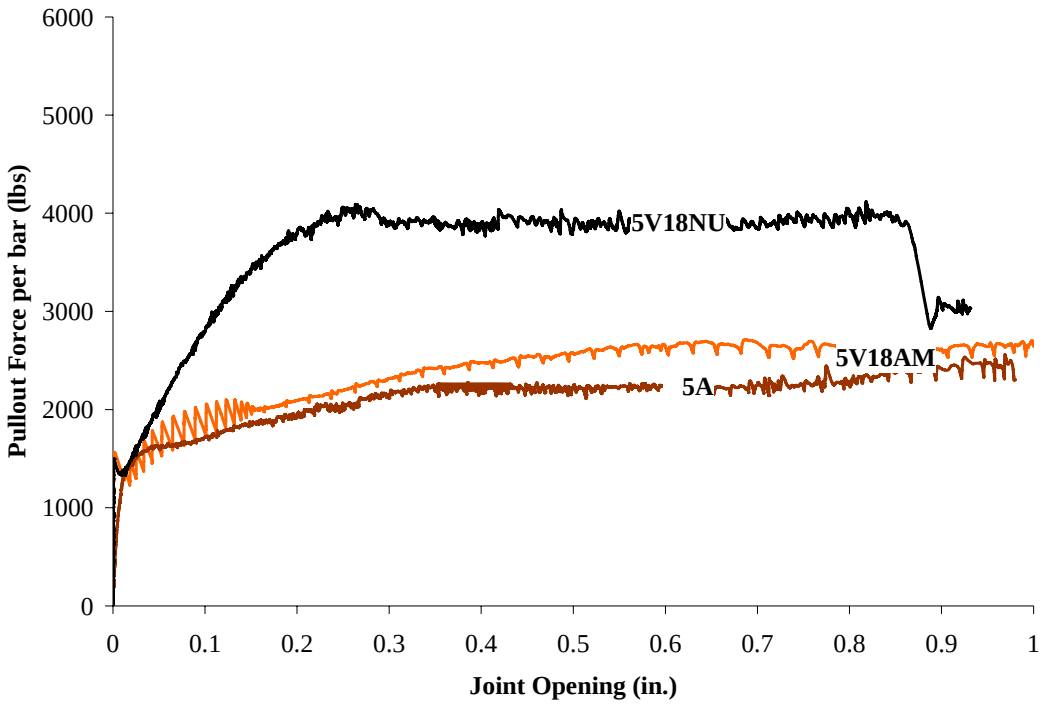

Figure 4.7: Comparison of pullout force per bar vs. joint opening behavior for specimens with five vertically misaligned dowel bars (5A, 5V18NU and 5V18AM)

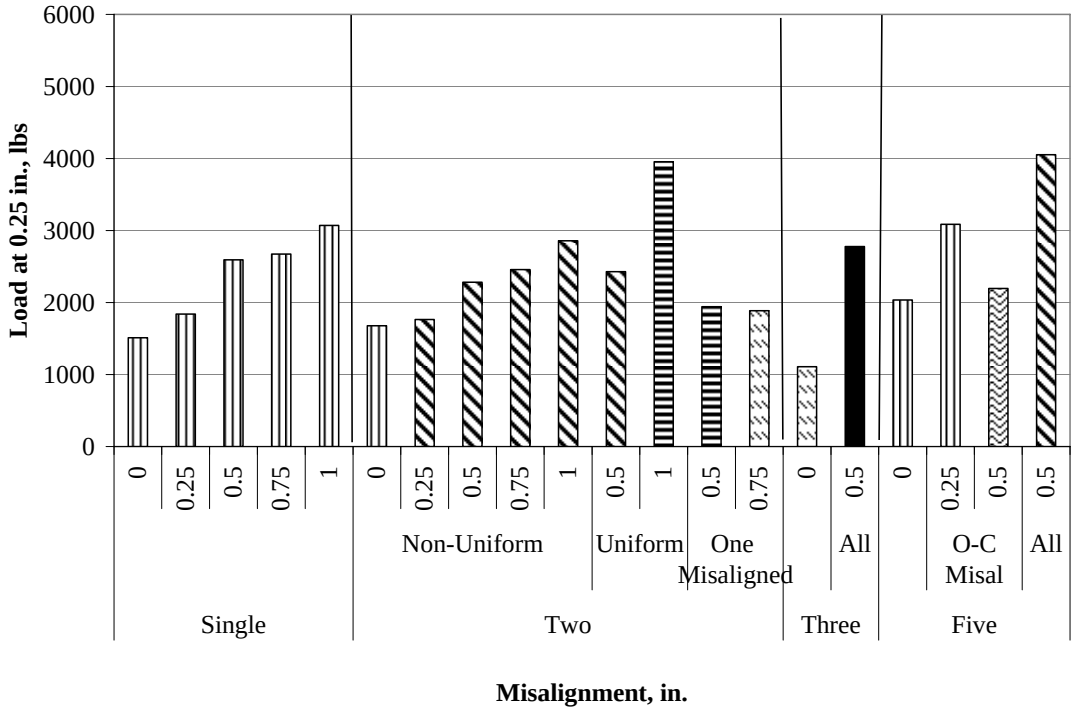

Figure 4.8: Comparison of pullout force per bar for vertically misaligned dowel bars at ¼ in joint opening

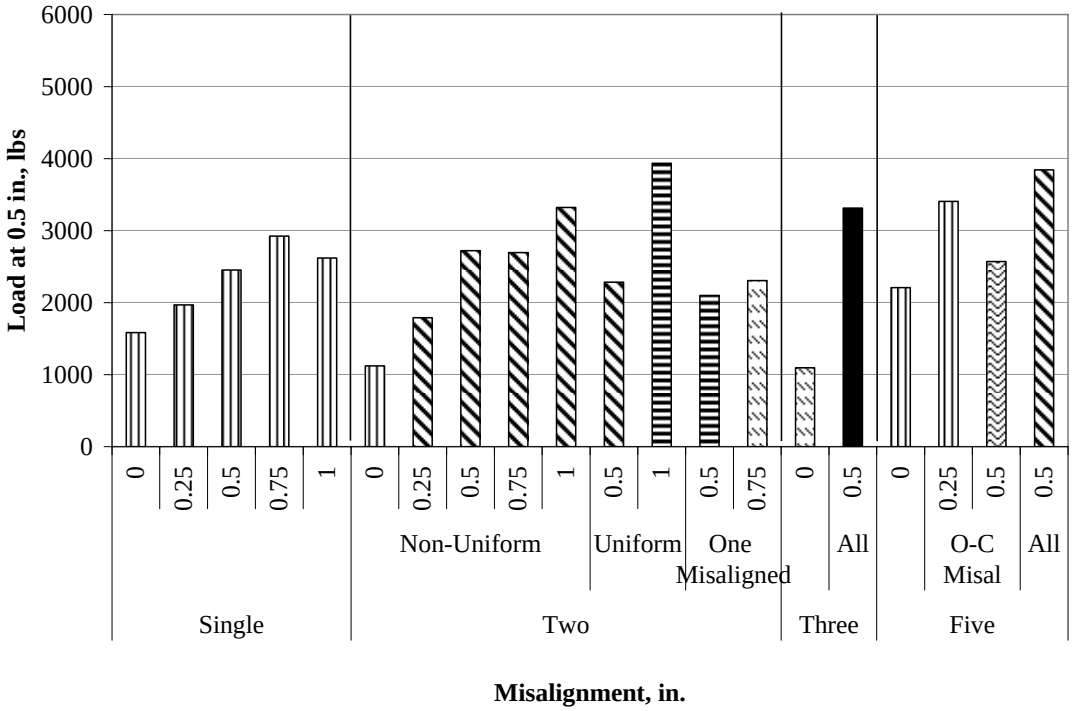

Figure 4.9: Comparison of pullout force per bar for vertically misaligned dowel bars at ½ in. joint opening

Horizontally Misaligned dowel bar specimens

Figure 4.10 illustrates the comparisons of dowel pullout force per dowel bar vs. joint behavior for the one dowel (1A, 1H36, 1H18, 1H12 and 1H9) test specimens. Figures 4.11 through 4.13 present the comparisons of pullout force per dowel vs. joint opening behavior of two dowels having non-uniform (2A, 2H36NU, 2H18NU, 2H12NU and 2H9NU), uniform (2A, 2H18U, 2H12U and 2H9U) and alternate misalignment (2H18AM and 2H12AM) orientations, respectively. Figures 4.14 and 4.15 present the comparison of the pullout force per dowel vs. joint opening behavior for three and five dowel bars respectively. Figures 4.16 and 4.17 present the amount of dowel pullout force required to open the joint to ¼ in. and ½ in. respectively.

Figure 4.10 shows the joint opening behavior for the single horizontally misaligned dowel bar test specimen. The overall magnitude of dowel pullout force

required to open a joint increased as the misalignment magnitude increases from an aligned to a misalignment magnitude of ⅙ radians. In case of 1H9 test specimen, the dowel pullout force reaches a peak value of 3000 lbs at a joint opening of ¼ in. and 3500 lbs at a joint opening of ½ in. as shown in figures 4.16 and 4.17.

In the two horizontally misaligned dowel bar test specimens, figures 4.11 through 4.13, due to misalignment, the dowel pullout force per bar vs. joint opening behavior increases to a certain peak value and then plateaus to the end of the test. Test specimens, 2H12NU and 2H9NU exhibited excessive spalling at joint in the concrete surrounding the misaligned dowel bars. The test specimens failed due to slab cracking at 0.7 in. joint opening.

In the three and five dowel test specimens, figures 4.16 and 4.17, the post slip behavior of the test specimen was characterized by an increasing dowel pullout force per bar. Structural distresses such as spalling in the concrete surrounding the misaligned dowel bars were observed in all the test specimens as mentioned in Table 4.1(c). Of the three and five dowel bar test specimens, maximum dowel pullout force of 3150 lbs and 3200 lbs corresponding to a joint opening of ¼ in. and ½ in. was observed in the 5H18AM test specimen.

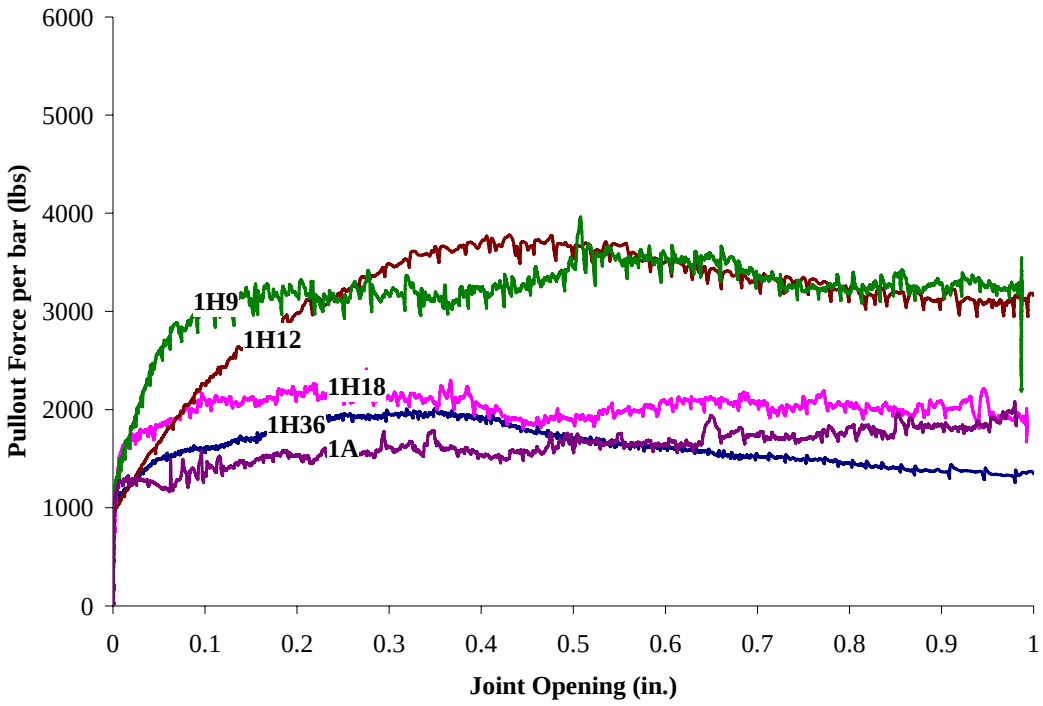

Figure 4.10: Comparison of pullout force vs. joint opening behavior for specimens with a single horizontally misaligned dowel bar

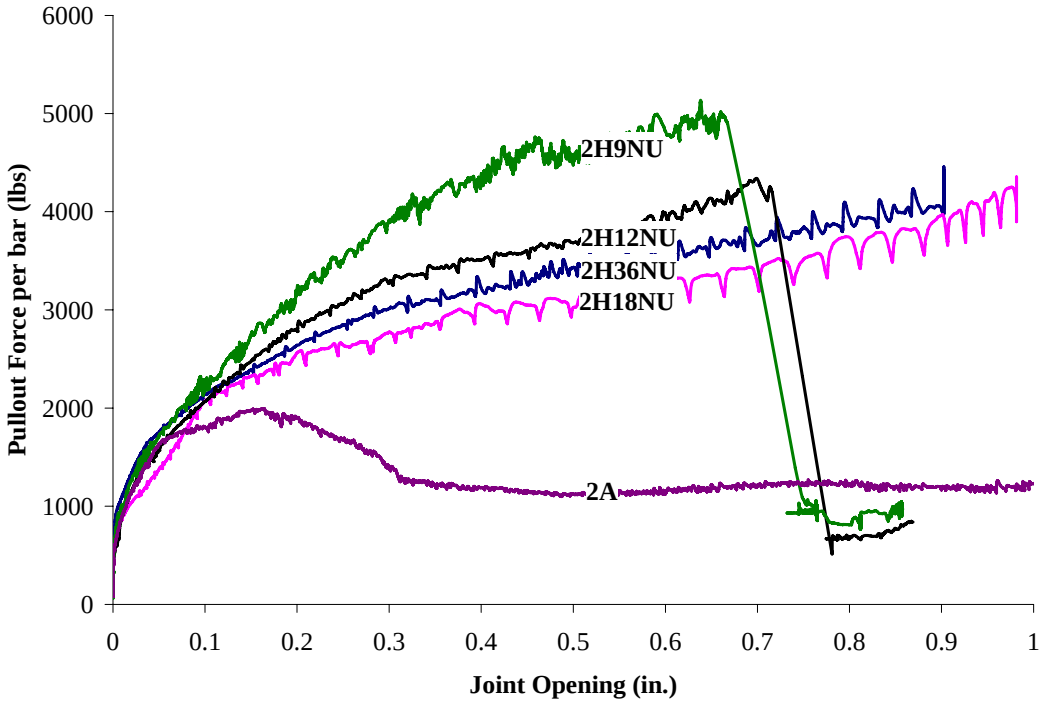

Figure 4.11: Comparison of pullout force vs. joint opening behavior for specimens with two horizontally misaligned dowel bars having non-uniform (NU) orientation

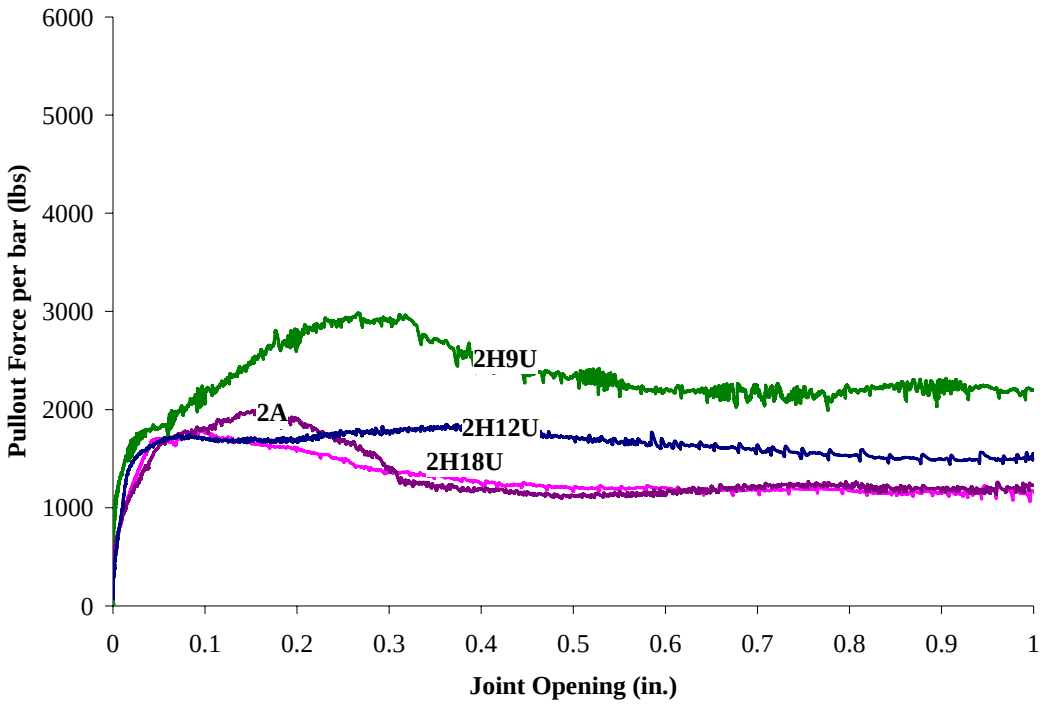

Figure 4.12: Comparison of pullout force vs. joint opening behavior for specimens with two horizontally misaligned dowel bars having uniform (U) orientation

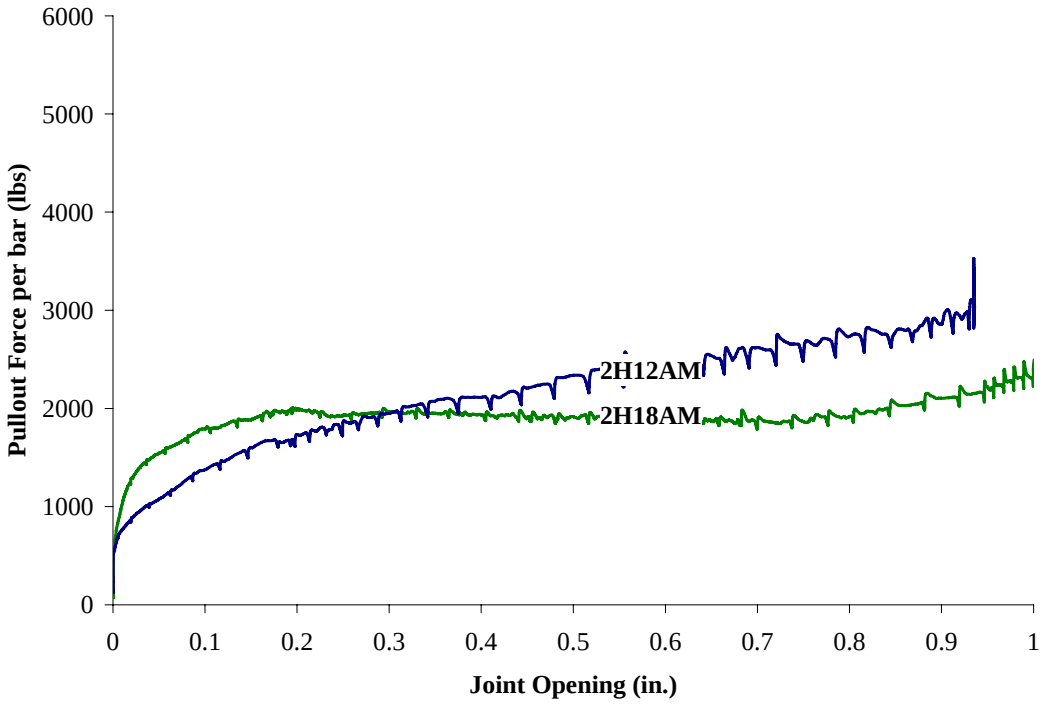

Figure 4.13: Comparison of pullout force vs. joint opening behavior for specimens with two horizontally misaligned dowel bars having alternate (AM) orientation

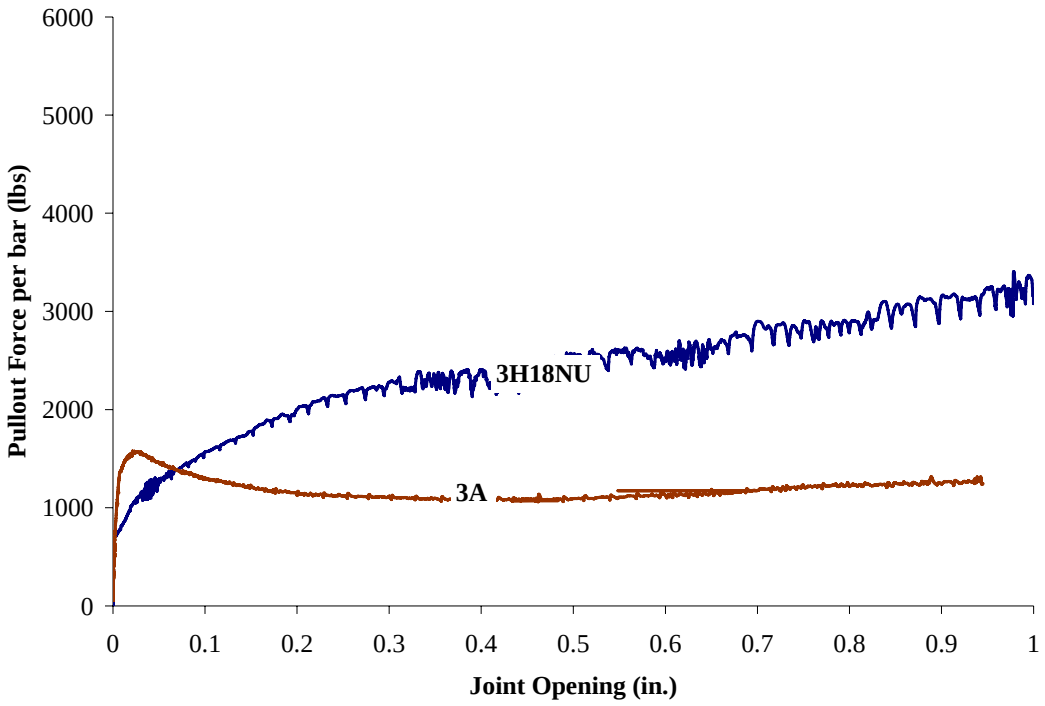

Figure 4.14: Comparison of pullout force per bar vs. joint opening behavior for specimens with three horizontally misaligned dowel bars

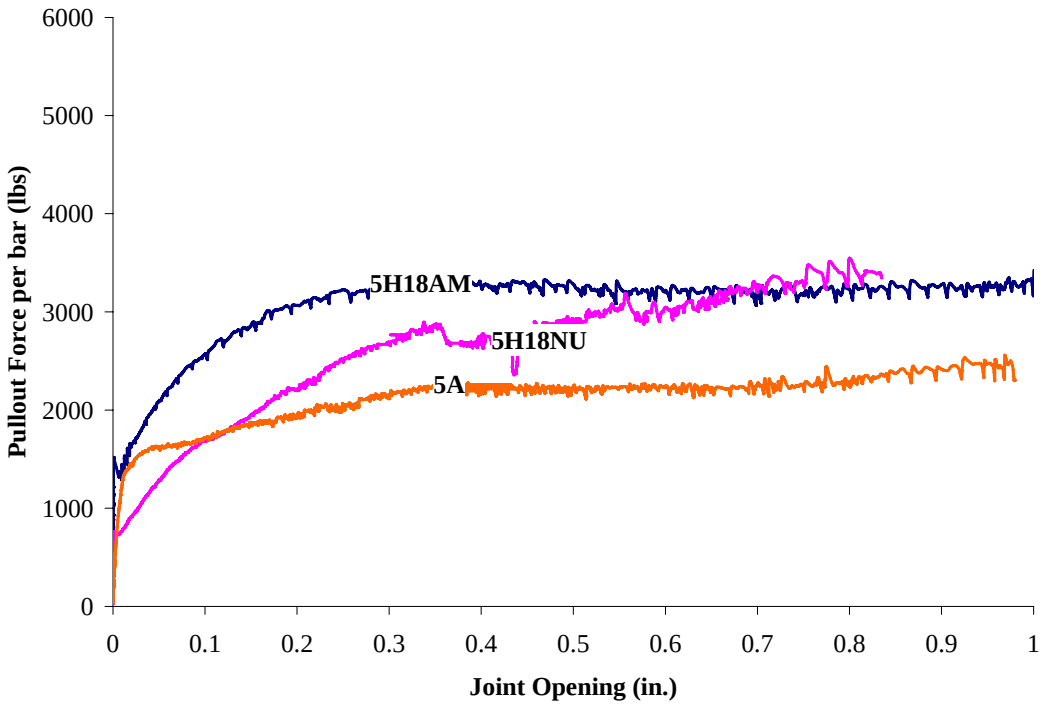

Figure 4.15: Comparison of pullout force per bar vs. joint opening behavior for specimens with five horizontally misaligned dowel bars (5A, 5H18NU and 5H18AM)

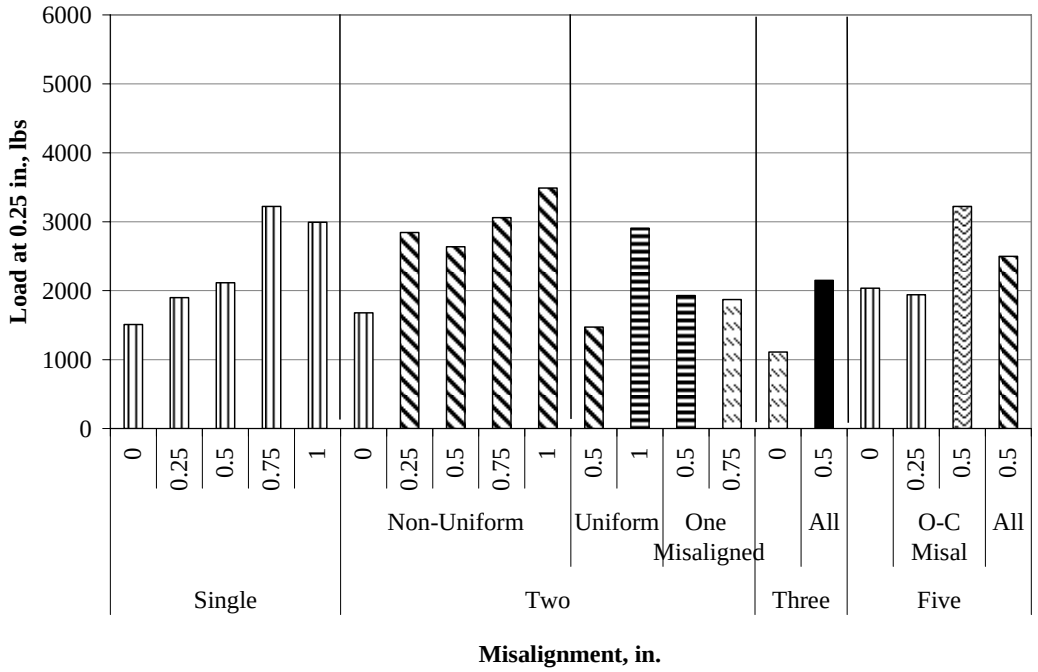

Figure 4.16: Comparison of pullout force per bar for horizontally misaligned dowel bars at ¼ in. joint opening

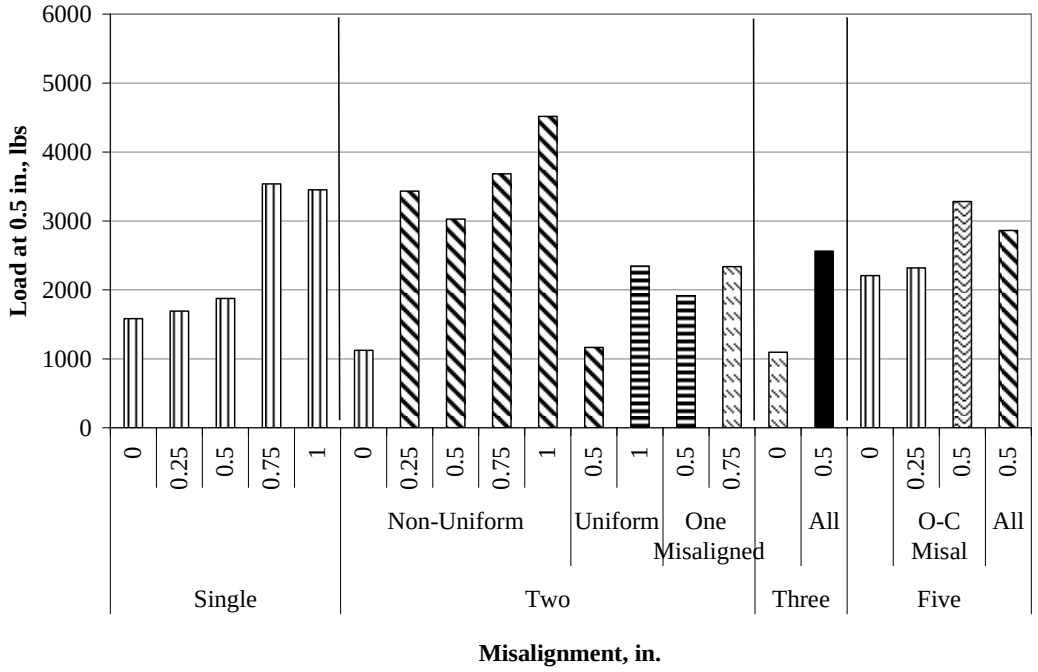

Figure 4.17: Comparison of pullout force per bar for horizontally misaligned dowel bars at ½ in. joint opening

Combined Misalignment type dowel bar specimens

Figure 4.18 illustrates the comparisons of dowel pullout force per dowel bar vs. joint opening behavior for the one dowel (1A, 1C36, 1C18, 1C12 and 1C9) test specimens. Figures 4.19 through 4.21 present the comparisons of pullout force per dowel vs. joint opening behavior of two dowels having non-uniform (2A, 2C36NU, 2C18NU, 2C12NU and 2C9NU), uniform (2A, 2C18U and 2C9U) and alternate misalignment (2C18AM and 2C12AM) orientations, respectively. Figures 4.22 and 4.23 present the comparison of the pullout force per dowel vs. joint opening behavior for three and five dowel bars respectively. Figures 4.24 and 4.25 present the amount of dowel pullout force required to open the joint to ¼ in. and ½ in. respectively.

Figure 4.18, shows the joint opening behavior for test specimens with a single dowel bar having combined misalignment type. For each of the test specimens, the amount of dowel pullout force required increased with increase in joint opening. In case of 1C9 test specimen, the dowel pullout force reached a peak value of 3500 lbs at a joint opening of 0.35 in. as shown in figure 4.18.

In the two dowel bar test specimens with combined misalignment, figures 4.19 through 4.21, due to misalignment the dowel pullout force per bar vs. joint opening behavior increases to a peak value and then a plateau or a sudden drop in the force due to structural distresses was observed. The dowel pullout force per bar dropped sharply in test specimen 2C9NU at a joint opening of 0.95 in. Some spalling around the misaligned dowel bars at the joint face was also observed at dowel pullout force of 5500 lbs per bar and joint opening of 0.45 in.

In the three and five dowel test specimens, figures 4.22 and 4.23, the post slip behavior of the test specimen was characterized by an increase in the dowel pullout force per bar. Spalling of the concrete surrounding the misaligned dowel bars was observed in all the test specimens as mentioned in Table 4.1(c). In test specimen 5C18NU a significant amount of spalling was observed at a pullout force of 4250 lbs and 0.6 in. joint opening and the test specimen failed due to brittle cracking of concrete at 0.85 in. joint opening, as shown in figure 4.23.

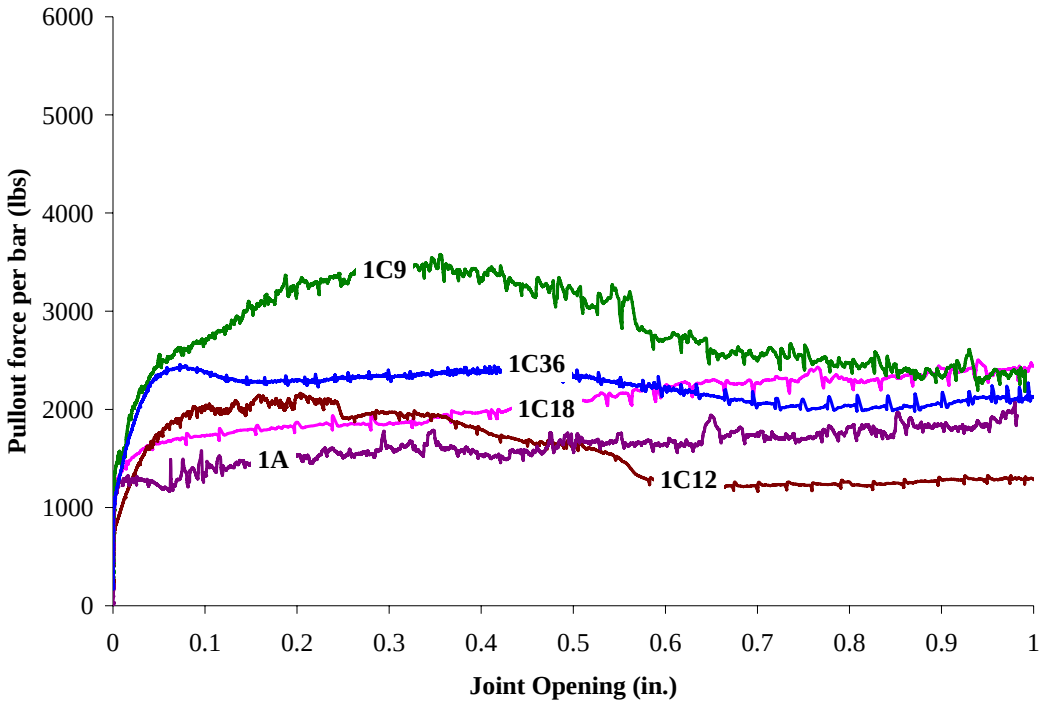

Figure 4.18: Comparison of pullout force vs. joint opening behavior for specimens with a single combined misaligned dowel bar

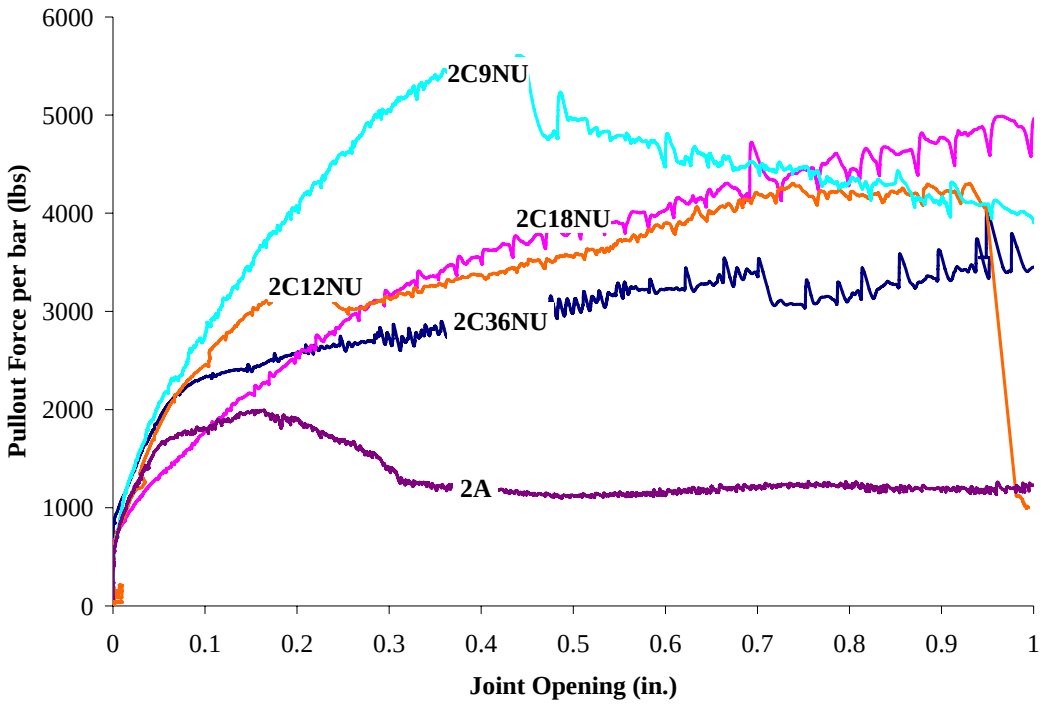

Figure 4.19: Comparison of pullout force vs. joint opening behavior for specimens with two combined misaligned dowel bars having non-uniform (NU) orientation

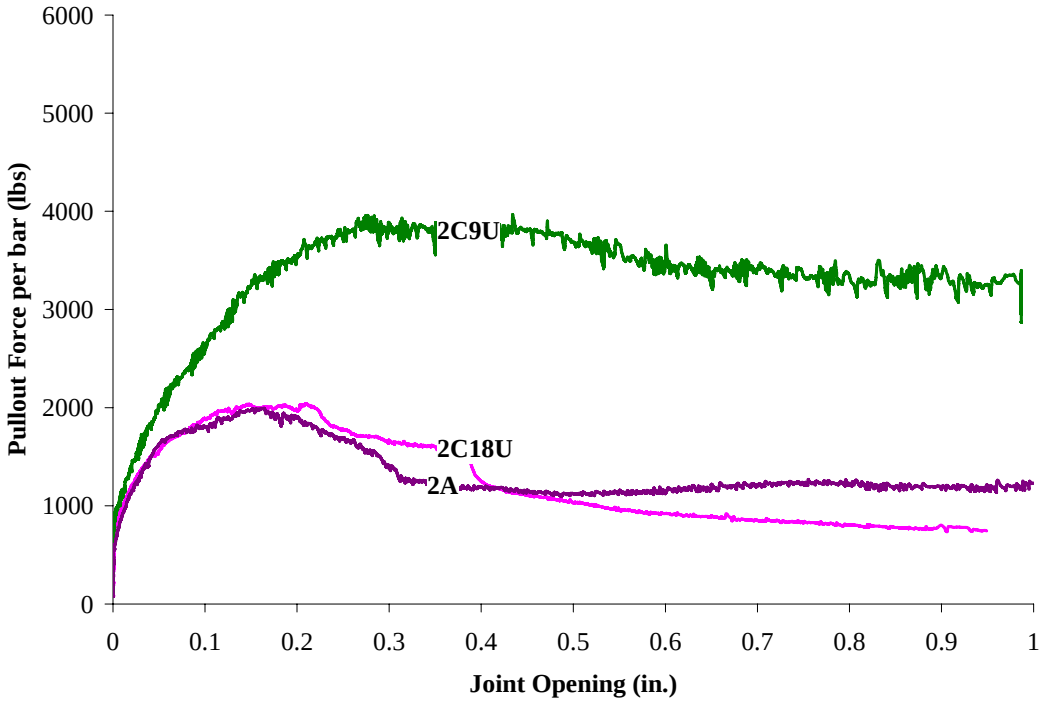

Figure 4.20: Comparison of pullout force vs. joint opening behavior for specimens with two combined misaligned dowel bars having non-uniform (U) orientation

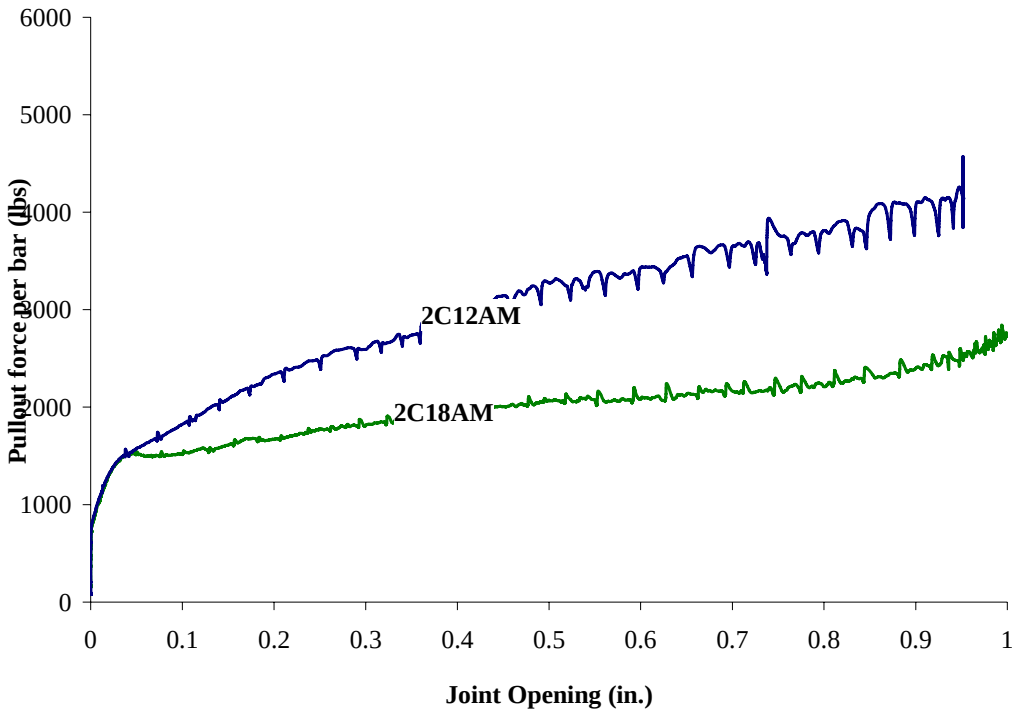

Figure 4.21: Comparison of pullout force vs. joint opening behavior for specimens with two combined misaligned dowel bars having alternate (AM) orientation

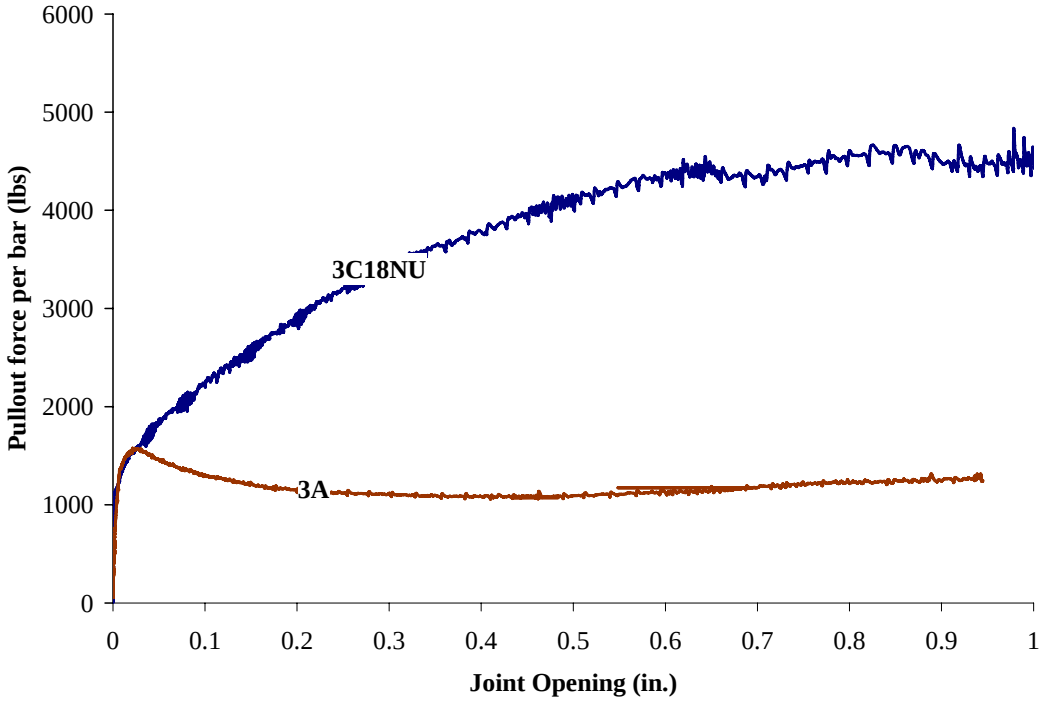

Figure 4.22: Comparison of pullout force vs. joint opening behavior for specimens with three combined misaligned dowel bars

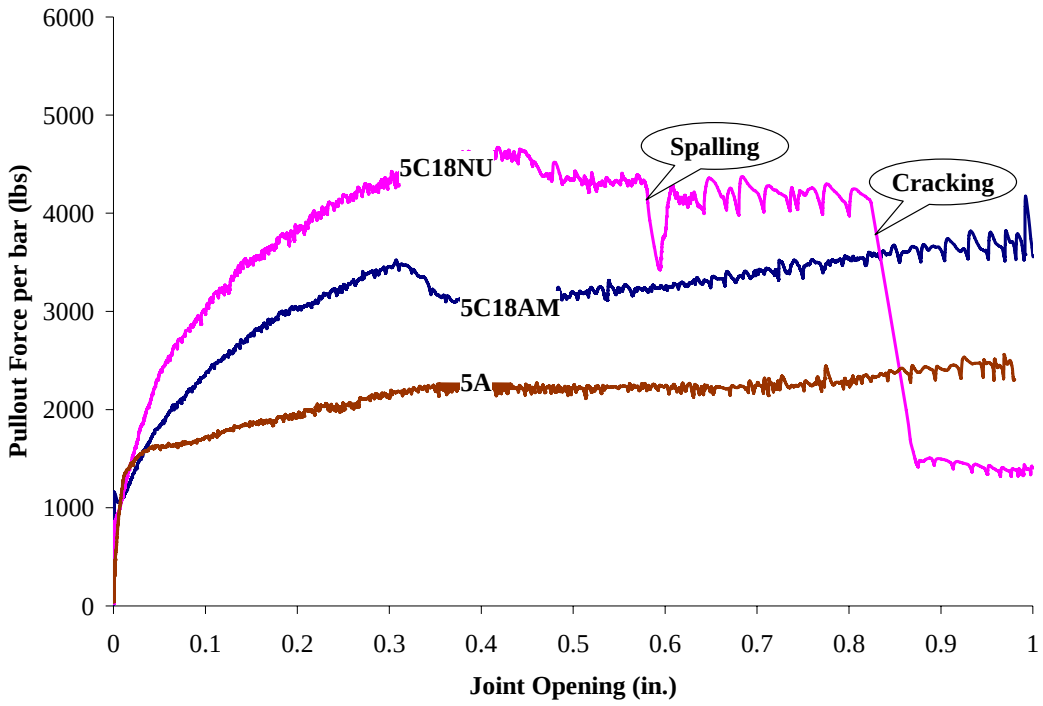

Figure 4.23: Comparison of pullout force vs. joint opening behavior for specimens with five combined misaligned dowel bars (5A, 5C18NU and 5C18AM)

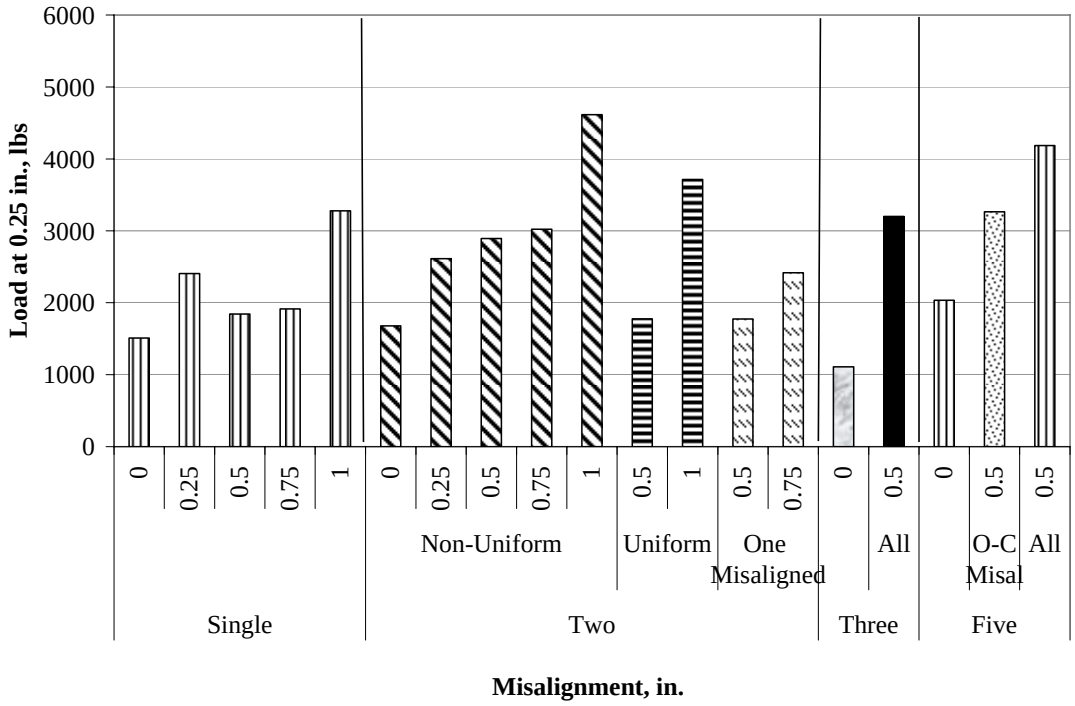

Figure 4.24: Comparison of pullout force per bar for combined misaligned dowel bars at ¼ in. joint opening

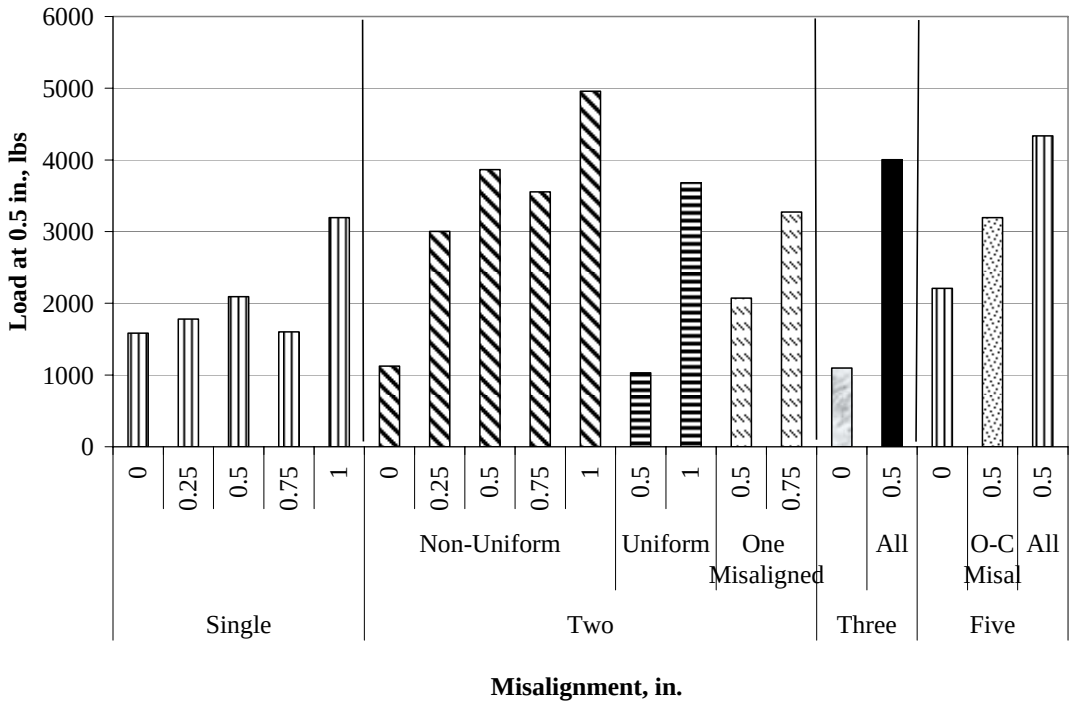

Figure 4.25: Comparison of pullout force per bar for combined misaligned dowel bars at ½ in. joint opening

4.2.2 COMPARISONS BETWEEN THE ORIENTATION OF MISALIGNED DOWEL BARS

The orientation of dowel bars in a multiple dowel bar test specimen could be one of three types, namely, non-uniform orientation (NU), uniform orientation (U) and alternate misaligned (AM). Comparison of the behavior between results of test specimens with same magnitude of misalignment, number of dowels in a test specimen, etc. have been presented.

Same Magnitude of misalignment

Figures 4.26 compares the pullout behavior of test specimens with two horizontally misaligned dowel bars of 1/18 radians misalignment magnitude and having different orientations. The dowel pullout force per dowel in the 2H18NU test specimen due to its

non-uniform orientation of misaligned dowels requires higher dowel pullout force compared to the 2H18AM and the 2H18U test specimens. A similar trend is observed in the results obtained from the joint opening behavior of 2V18NU, 2V18AM and 2V18U test specimens as shown in figure 4.27 and 2C18NU, 2C18AM and 2C18U test specimens shown in figure 4.28. The dowel pullout force vs. joint opening behavior for 1/12 radians magnitude of misalignment as shown in figures 4.29 through 4.31, show the same trend as observed in the 1/18 radians misaligned dowel bars. For the specimens with 1/12 radians with all three types of misalignments, the force required to open a joint with non-uniform orientation of misalignment is overall higher compared to the alternate misaligned dowel bars.

In the five dowel bar test specimens, comparison of the results were made with respect to the 1/18 radians magnitude and misalignment type. The alternate misaligned dowel bars in horizontally misaligned test specimen, 5H18AM, yielded higher values of pullout force compared to the no-uniform, 5H18NU, misaligned dowel bars, shown in figure 4.32. In results obtained from test specimens with vertical and combined misalignments, the forces in the specimens with non-uniform misaligned bars were higher compared to the alternate misalignment, as shown in figures 4.33 and 4.34.

In general, it can be concluded that for a given misalignment magnitude, the load induced per dowel increases as the number of dowels misaligned increases. Overall, it indicates that irrespective of the dowel misalignment type (vertical, horizontal or combined) and magnitude (1/18 radians, 1/12 radians), the force required to open the joint in a pavement slab with non-uniform misaligned dowel bars is higher compared to

alternate and uniform orientation of misalignments. Generally, more spalling was observed in test specimens with non-uniform orientation of dowel bars.

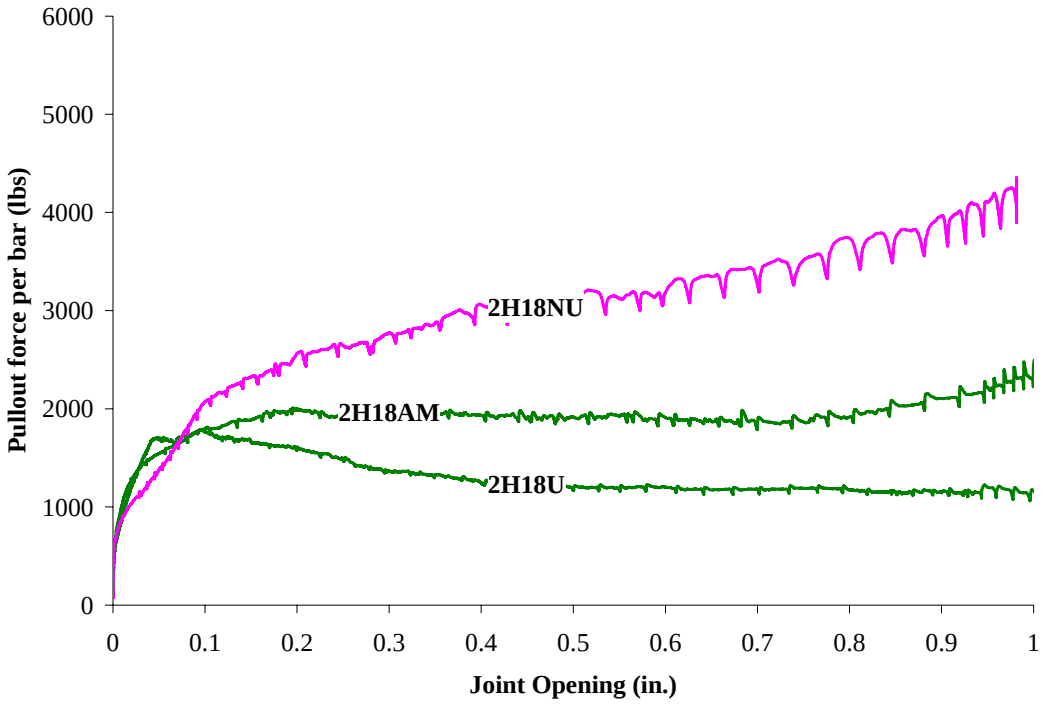

Figure 4.26: Comparison of pullout force vs. joint opening curves of 2-dowel ½ in. Horizontal Misalignment (2H18NU, 2H18U, and 2H18AM)

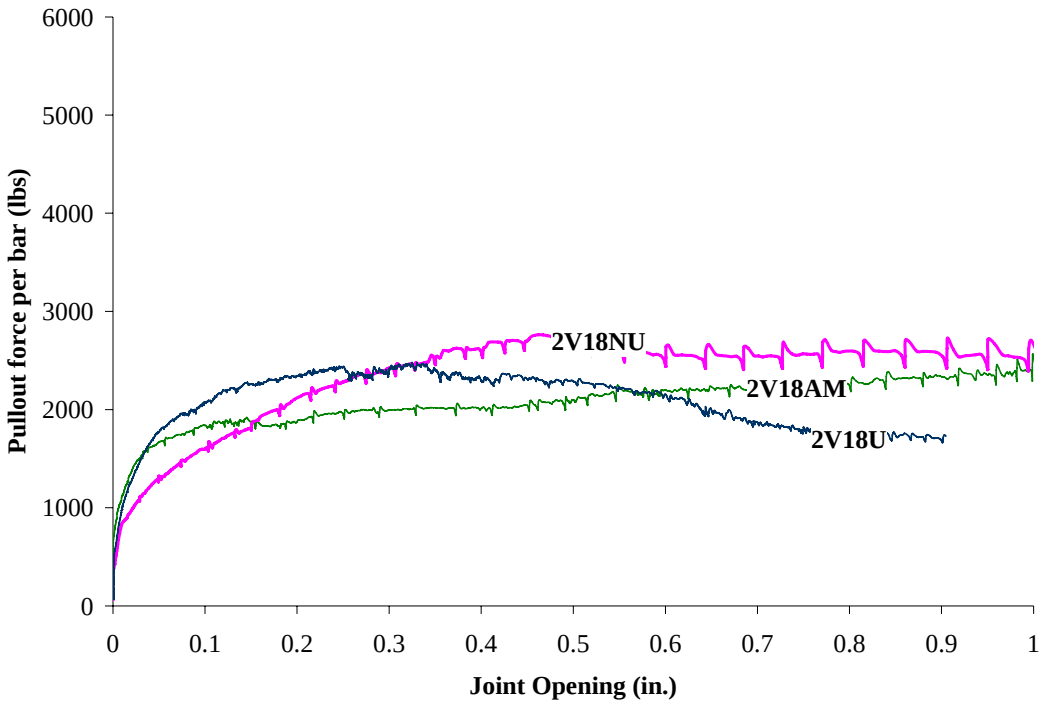

Figure 4.27 Comparison of pullout force vs. joint opening curves of 2-dowel ½ in. Vertical Misalignment (2V18NU, 2V18U, and 2V18AM)

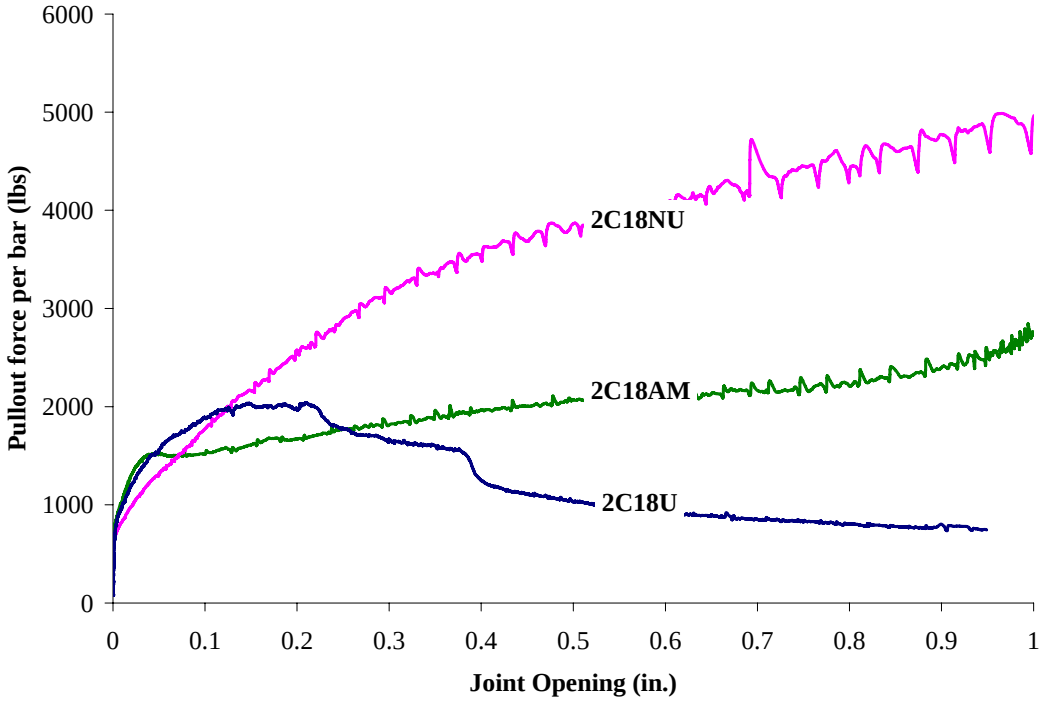

Figure 4.28: Comparison of pullout force vs. joint opening curves of 2-dowel ½ in. Combined Misalignment (2C18NU, 2C18U, and 2C18AM)

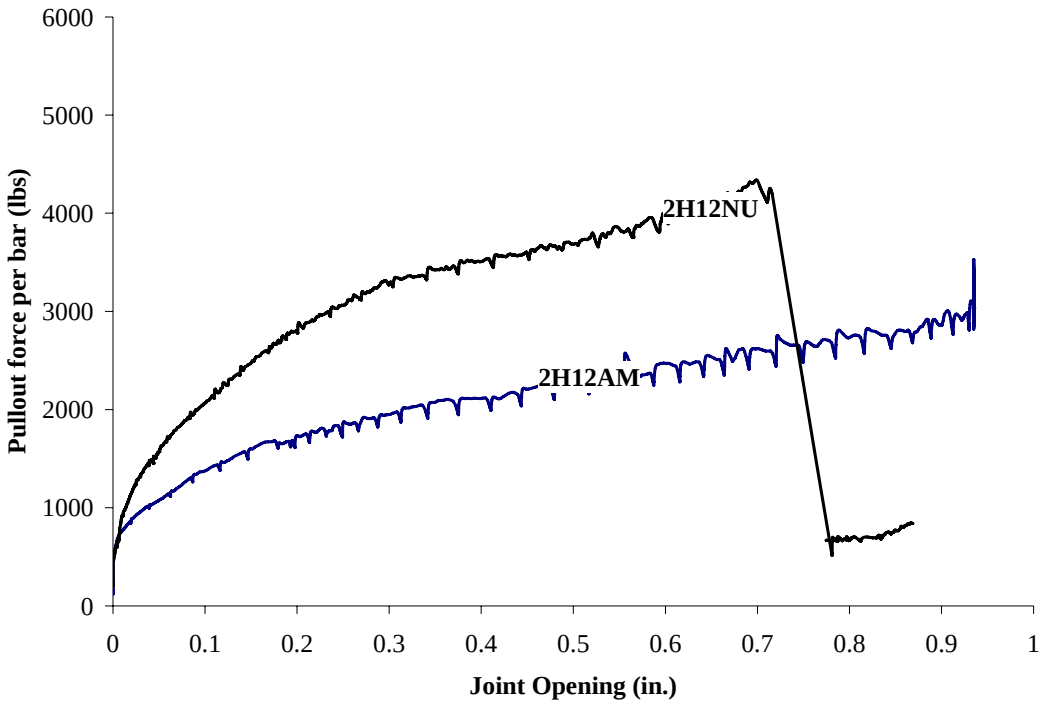

Figure 4.29: Comparison of pullout force vs. joint opening curves of 2-dowel ¾ in. Horizontal Misalignment (2H12NU and 2H12AM)

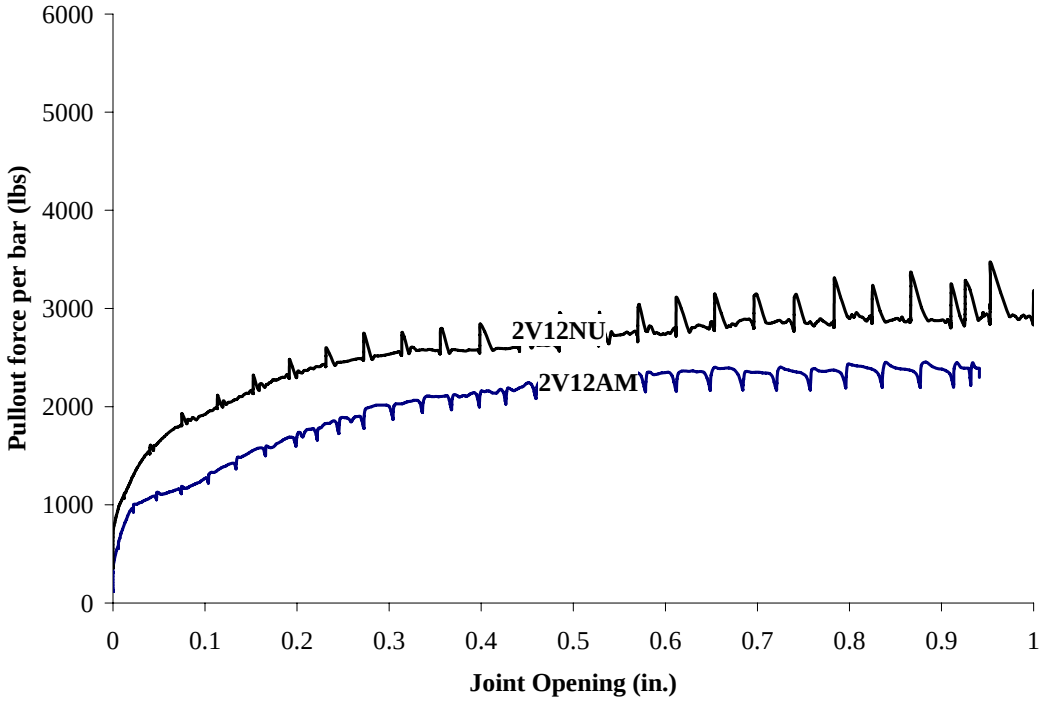

Figure 4.30: Comparison of pullout force vs. joint opening curves of 2-dowel ¾ in. Vertical Misalignment (2V12NU and 2V12AM)

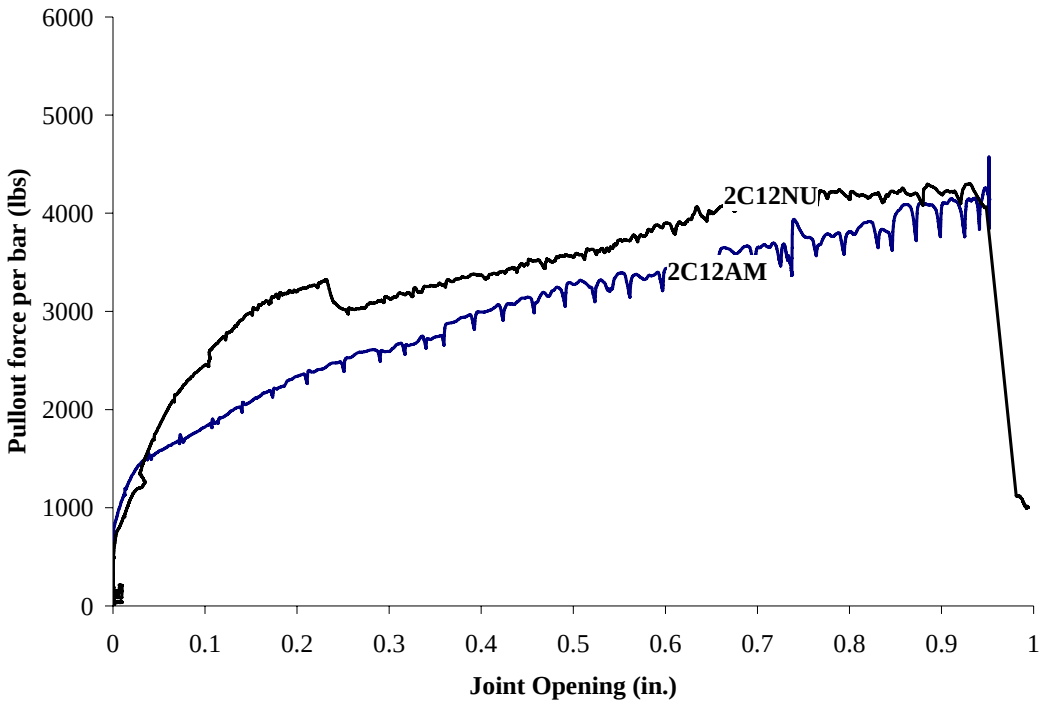

Figure 4.31 Comparison of pullout load vs. joint opening curves of 2-dowel ¾ in. Combined Misalignment (2C12NU and 2C12AM)

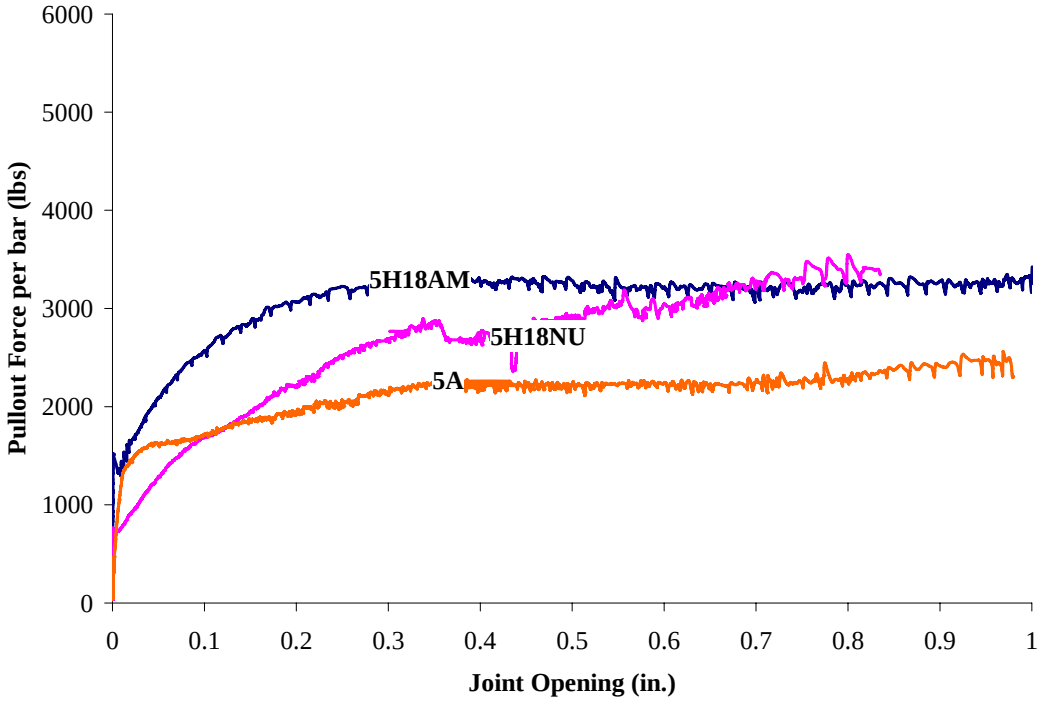

Figure 4.32 Comparison of pullout load vs. joint opening curves of 5H18NU and 5H18AM

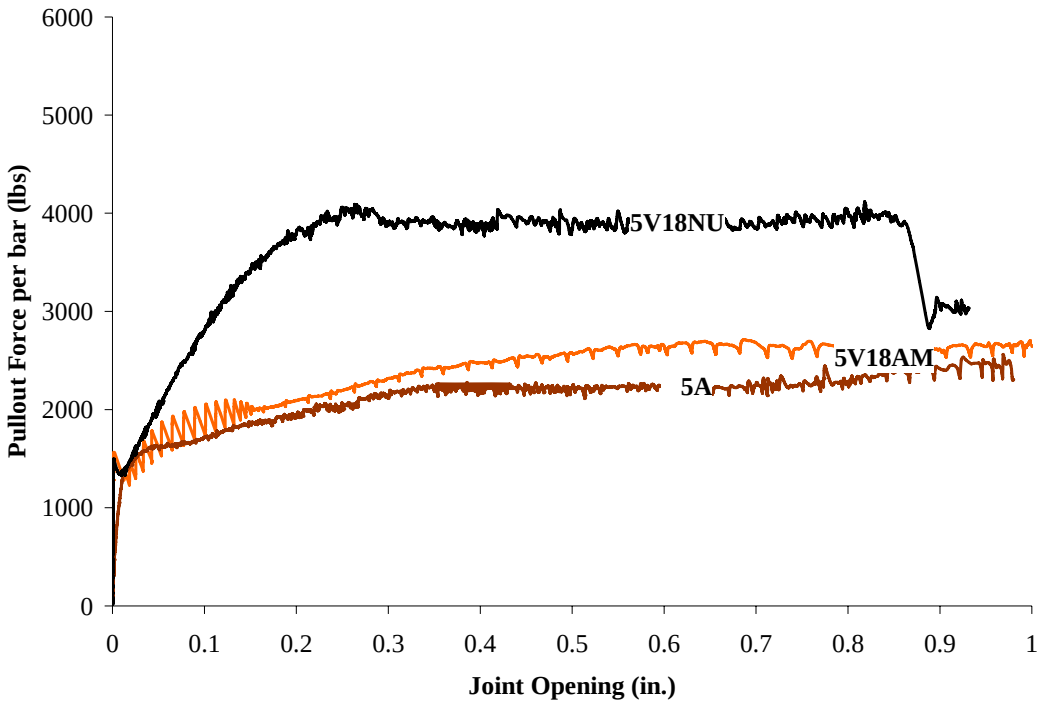

Figure 4.33 Comparison of pullout force vs. joint opening curves of 5V18NU and 5V18AM

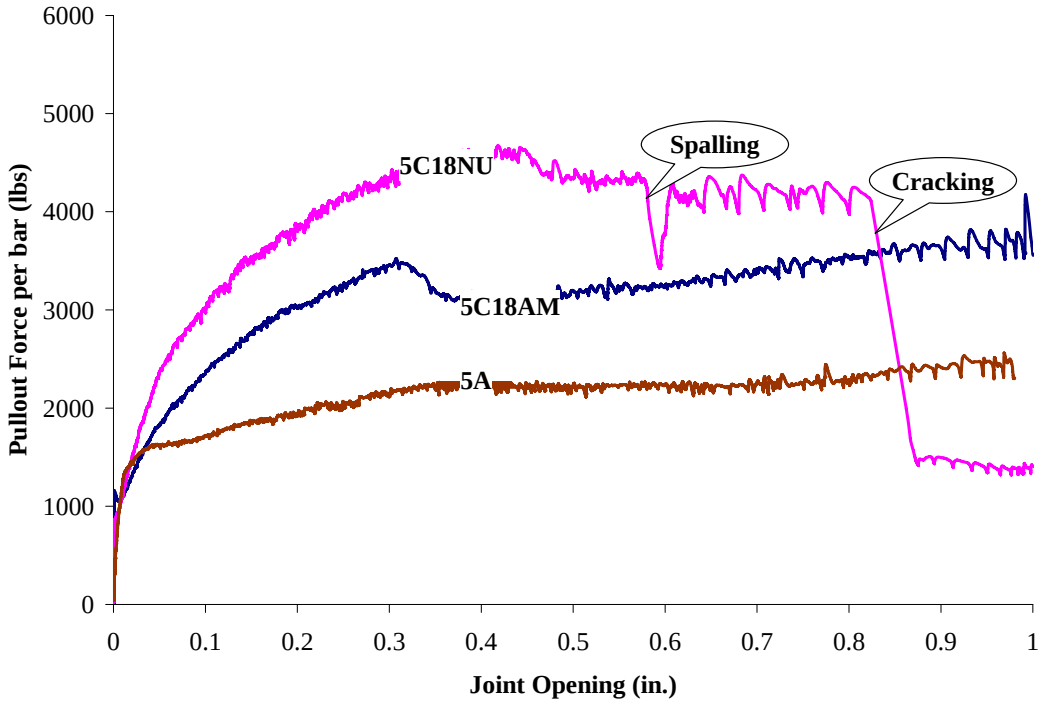

Figure 4.34 Comparison of pullout force vs. joint opening curves of 5C18NU and 5C18AM

Number of Dowels in Test Specimen Size

A comparison of the pullout force per dowel vs. joint opening behavior of one vs. two dowels and three vs. five dowels is presented in this section. Basically, the comparison is made due to difference in specimen size and concrete volume. The smaller specimen could accommodate one or two dowel bars whereas the larger specimen could accommodate three and five dowels.

Horizontal Misalignment

Figure 4.35 and 4.36 compare the results obtained for the test specimens with one and two dowel bars having horizontal misalignment of 1/18 radians and 1/9 radians respectively. In figure 4.35, the pullout force per bar to produce joint opening was higher in the 2H18NU followed by the 1H18 and the 2H18U test results. A similar trend was observed in figure 4.36, that illustrates the pullout force per bar in the 2H9NU was greater than the 1H9 and the 2H9U test results. In the slab specimen containing three and five dowel bars, the pullout force per dowel required by the 5H18NU test specimen was consistently higher compared to the results obtained for the 3H18NU test specimen, shown in figure 4.37.

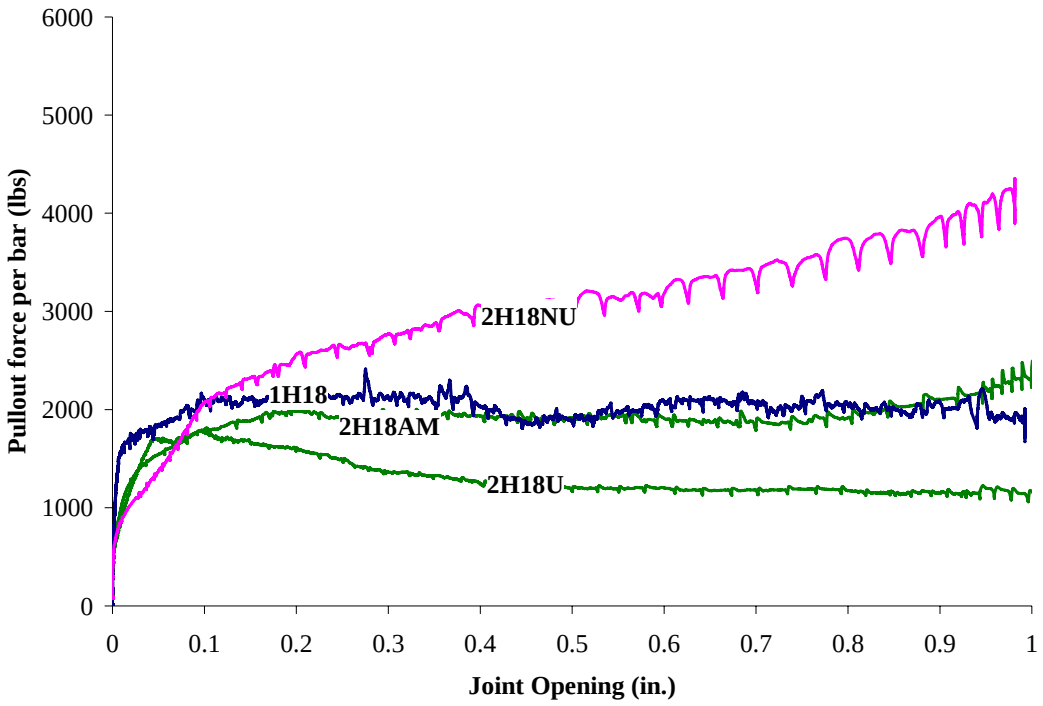

Figure 4.35 Comparison of pullout force vs. joint opening curves of 1H18 and 2-dowel ½ in. Horizontal Misalignment (2H18NU, 2H18U, 2H18AM)

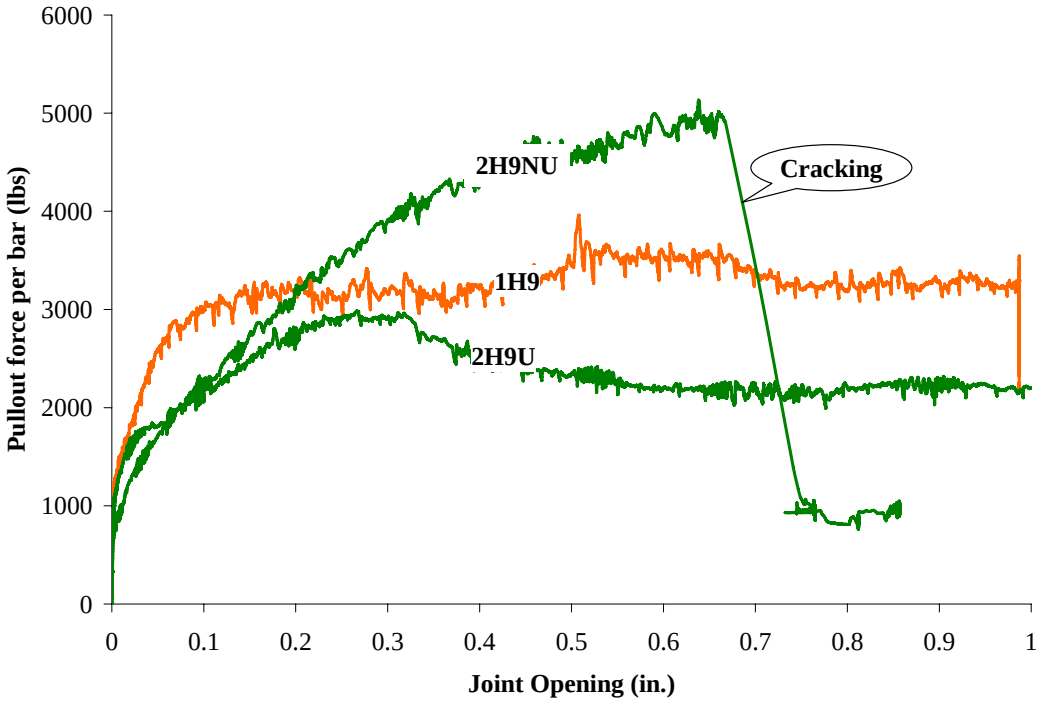

Figure 4.36 Comparison of pullout force vs. joint opening curves of 1H9 and 2-dowel 1 in. Horizontal Misalignment (2H9NU, 2H9U)

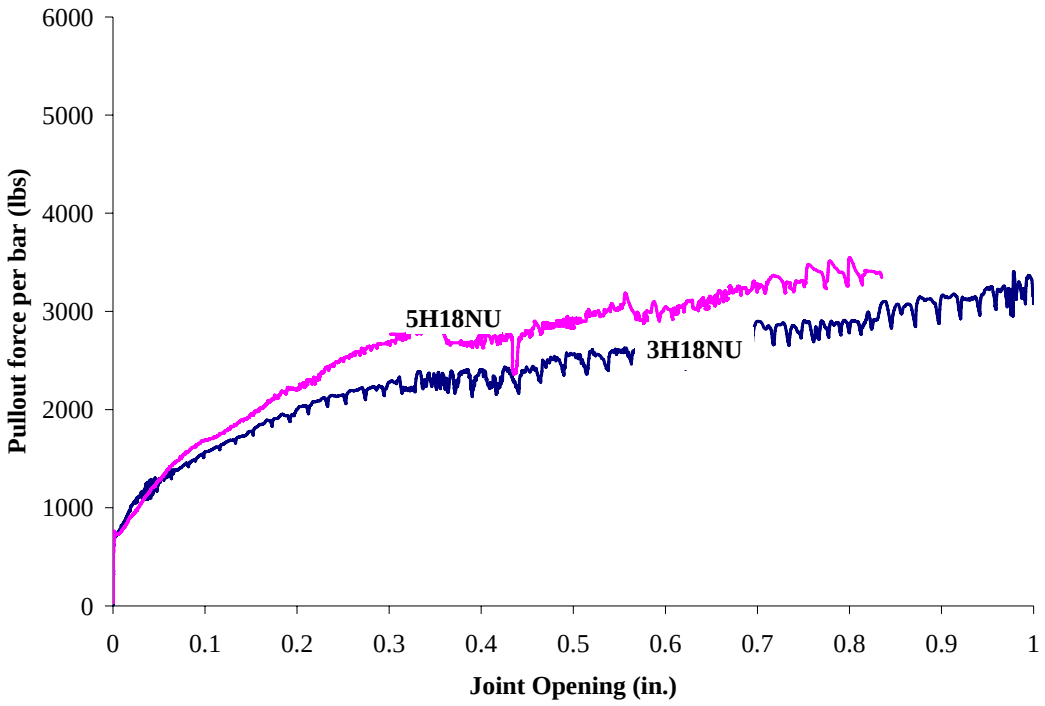

Figure 4.37 Comparison of pullout force vs. joint opening curves of 3H18NU and 5H18NU

Vertical Misalignment:

Figure 4.38 and 4.39 compare the results obtained for the test specimens with one and two dowel bars having vertical misalignment of 1/18 radians and 1/9 radians, respectively. In figure 4.38, similar to the horizontally misaligned dowel bar specimens, the pullout force per bar to produce joint opening was higher in the 2V18NU followed by the 1V18 and the 2V18U test results. In Figure 4.39, the post slip behavior with vertically misaligned bars with a magnitude of 1/9 radians shows that the pullout force per bar in the 2V9U was greater than the 2V9NU followed by the 1V9 test results. In the slab specimen containing three and five dowel bars, the pullout force per dowel required by the 5V18NU test specimen was consistently higher compared to the results obtained for the 3V18NU test specimen, shown in figure 4.40. The 5V18NU test specimen failed due cracking of the concrete slab towards the end of the test.

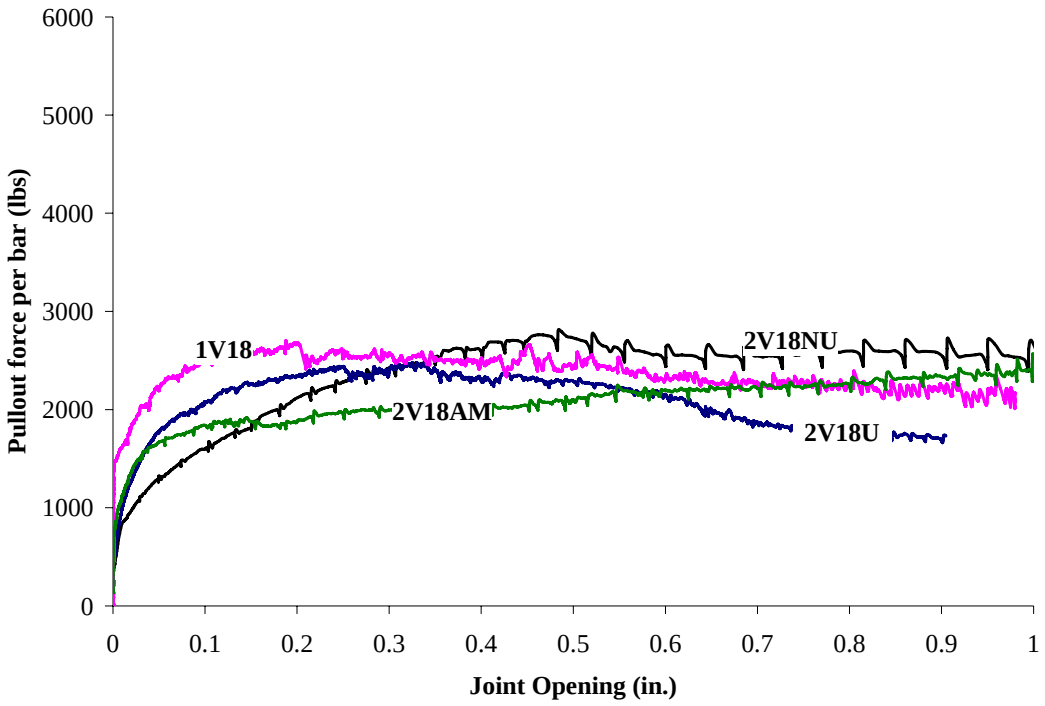

Figure 4.38: Comparison of pullout force vs. joint opening curves of 1V18 and 2-dowel ½ in. Vertical Misalignment (2V18NU, 2V18U, 2V18AM)

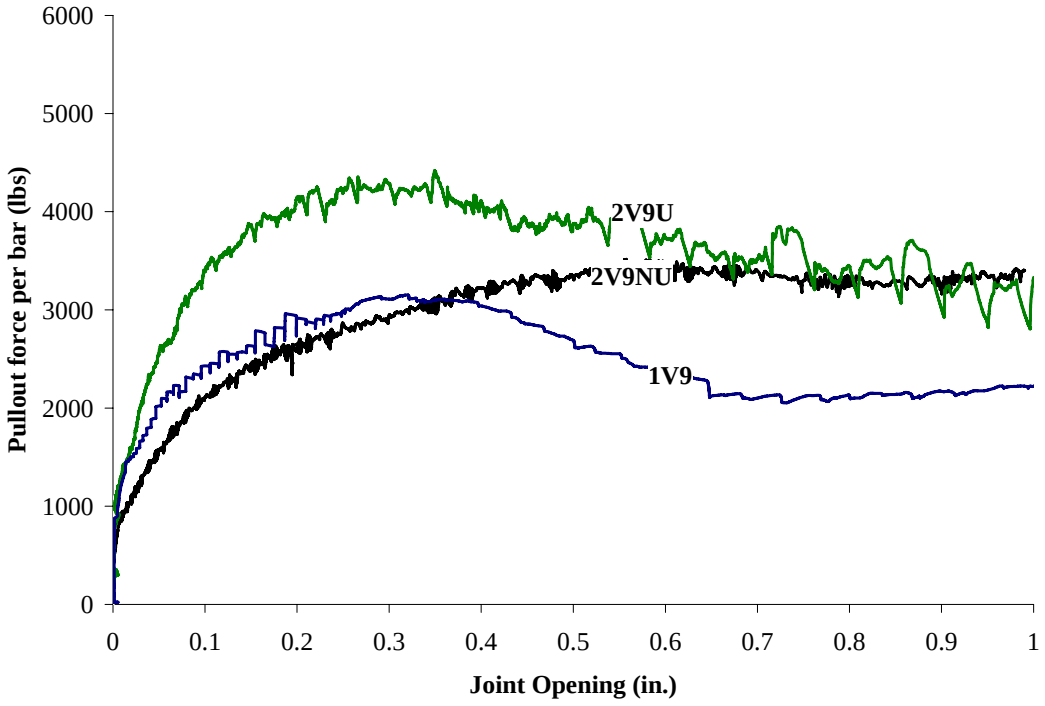

Figure 4.39 Comparison of pullout force vs. joint opening curves of 1V9 and 2-dowel 1 in. Vertical Misalignment (2V9NU, 2V9U)

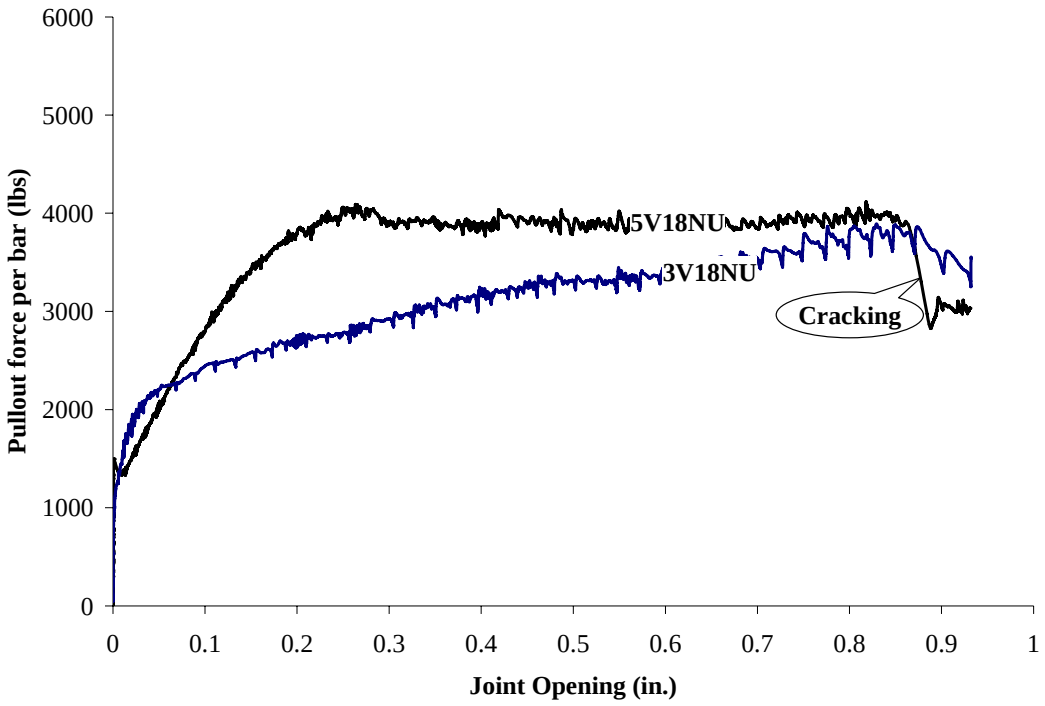

Figure 4.40 Comparison of pullout force vs. joint opening curves of 3V18NU and 5V18NU

Combined Misalignment

Figure 4.41 and 4.42 compare the results obtained for the test specimens with one and two dowel bars having a combined misalignment type of 1/18 radians and 1/9 radians, respectively. In figure 4.41, a trend similar to the horizontal and vertical misaligned dowel bars is seen. The pullout force per bar to produce joint opening in the 2C18NU test specimen is much higher followed by the 1C18 and the 2C18U test results. In figure 4.42, the post slip behavior with vertically misaligned bars with a magnitude of 1/9 radians shows that the pullout force per bar in the 2C9NU was greater than the 2C9U and the 1C9 test results. In the slab specimen containing three and five dowel bars, the pullout force per dowel required by the 5C18NU test specimen was higher compared to the results obtained for the 3C18NU test specimen, shown in figure 4.43. Most of the test

specimens with multiple combined misalignment type showed spalling in the concrete around the dowel bars at the joint. The 5C18NU test specimen failed due to significant spalling and finally cracking of the concrete slab at a very high joint opening.

A comparison of the loads at ¼ and ½ in. joint openings for different misalignment scenario has been presented in figures 4.44 and 4.45.

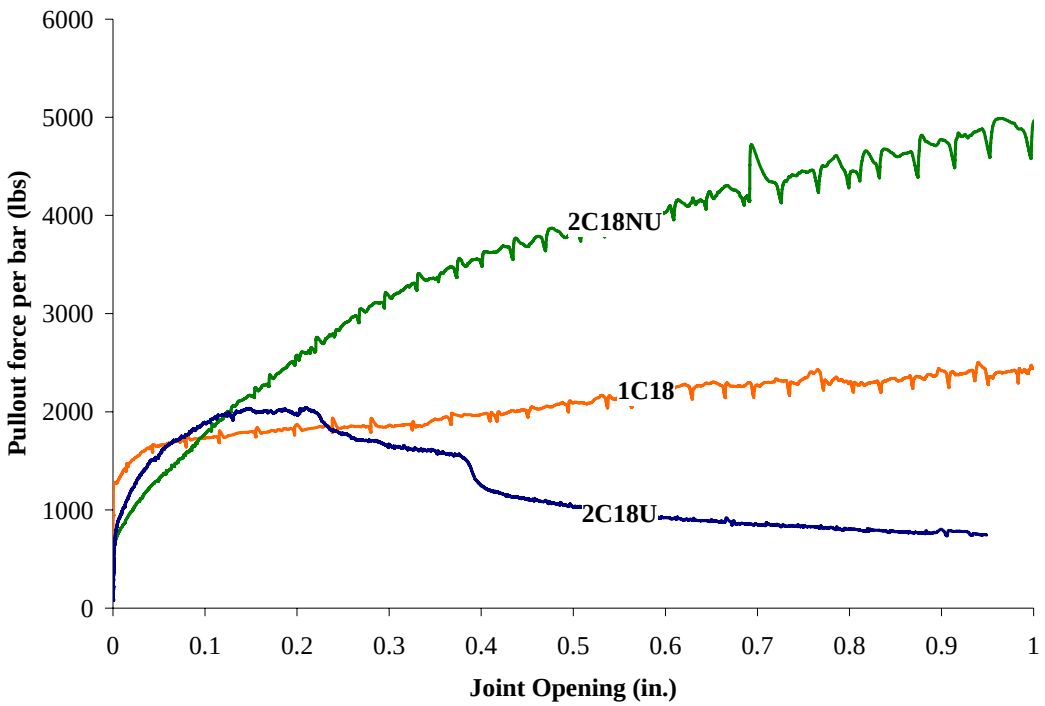

Figure 4.41: Comparison of pullout force vs. joint opening curves of 1C18 and 2-dowel ½ in. Combined Misalignment (2C18NU, 2C18U)

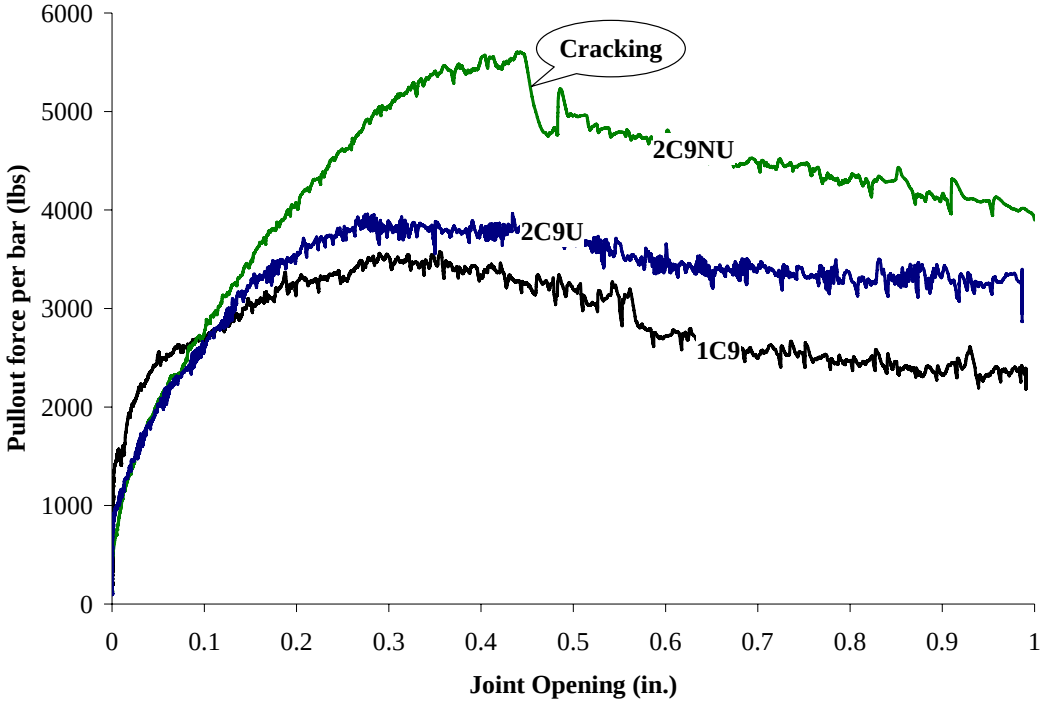

Figure 4.42: Comparison of pullout force vs. joint opening curves of 1C9 and 2-dowel 1 in. Combined Misalignment (2C9NU, 2C9U)

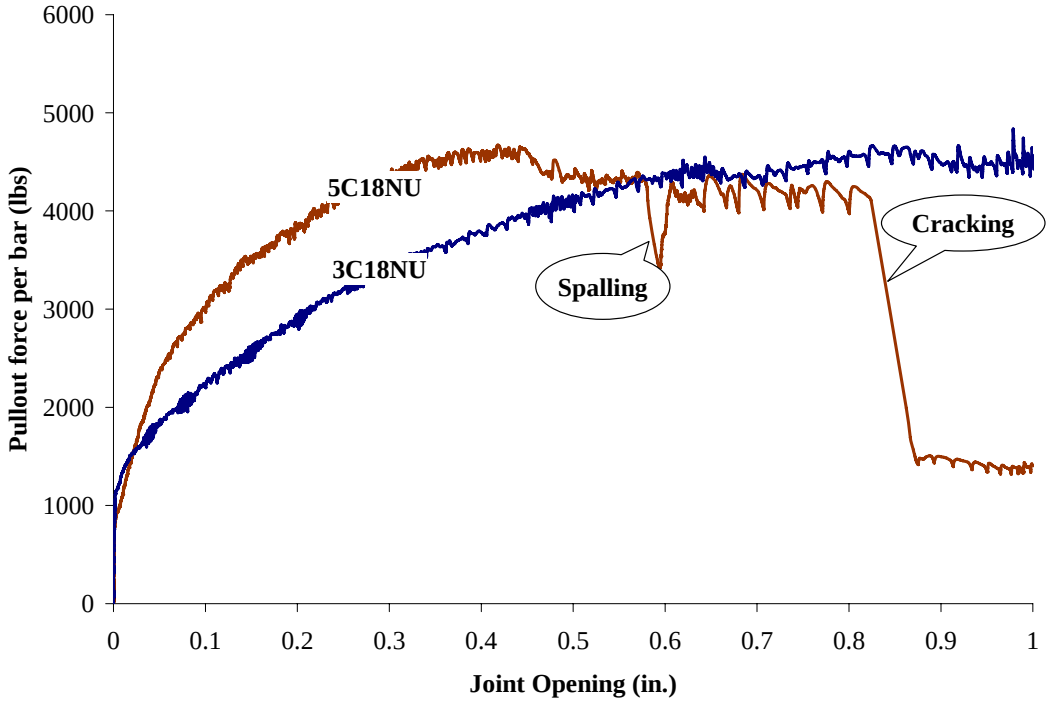

Figure 4.43 Comparison of pullout force vs. joint opening curves of 3C18NU and 5C18NU

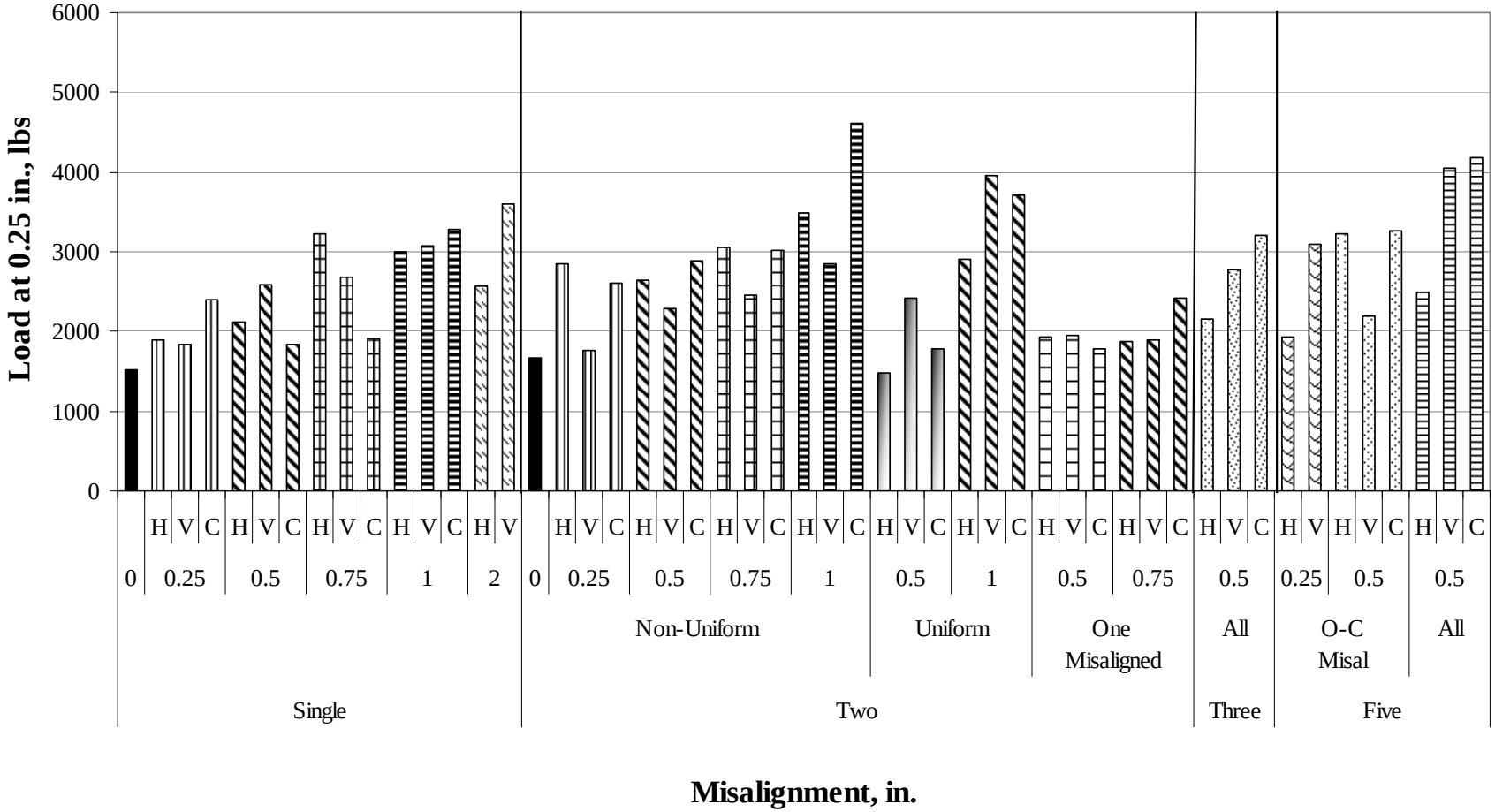

Figure 4.44: Comparison of loads at ¼ in. across different tests of misalignment

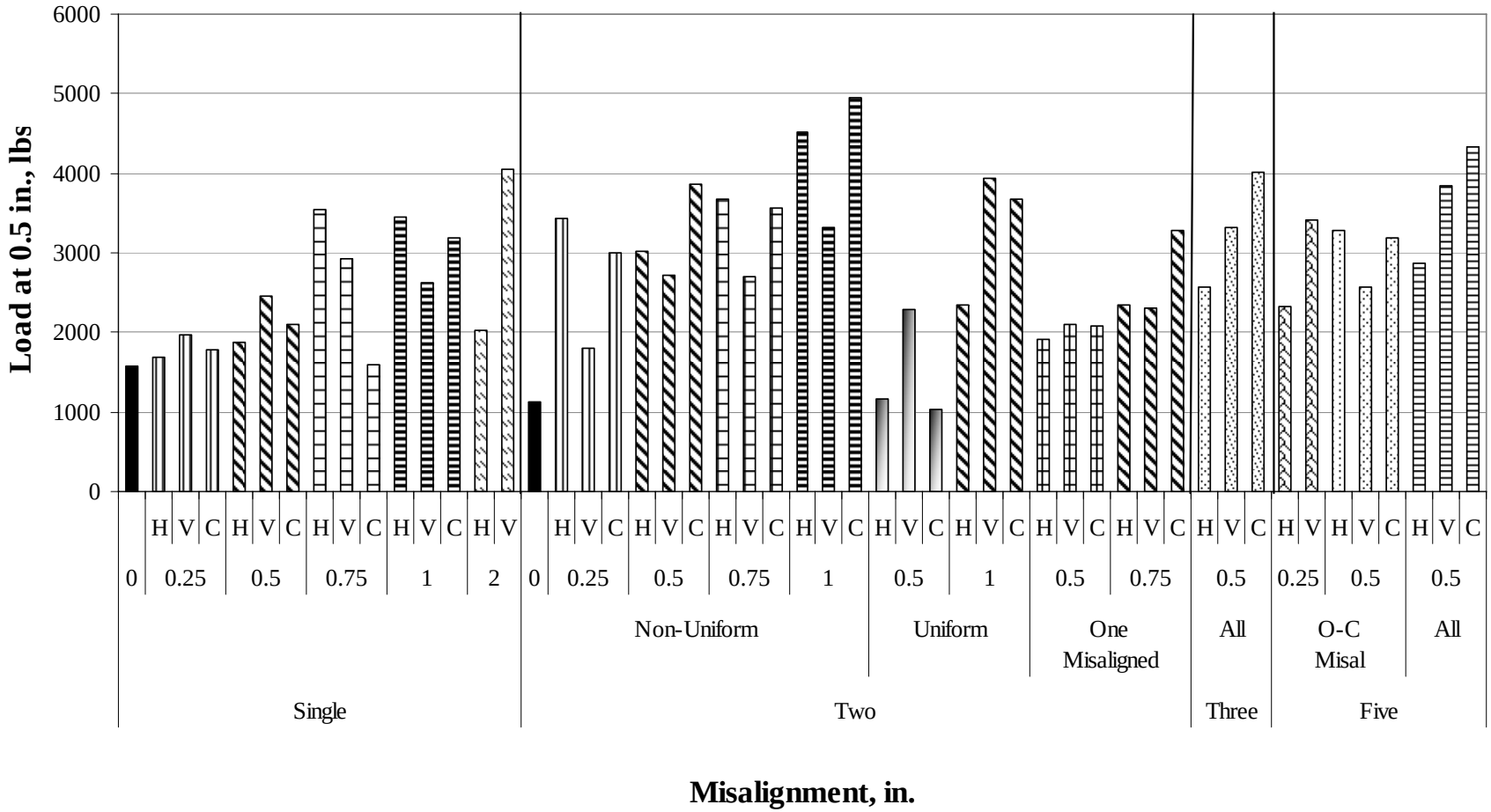

Figure 4.45: Comparison of loads at ½ in. across different tests of misalignment

4.2.3 DISTRESSES OBSERVED IN THE TEST SPECIMENS

The distresses observed in all the test specimens during the laboratory investigation can be found in Table 4.1 (a), (b) and (c). Some of the "significant" structural distresses such as spalling of concrete, crack patterns, specimen uplift and slab rotation that were documented during the experimental investigation are presented in this section.

Vertically Misaligned Test Specimens

The visual observations in the vertical misaligned dowel bar test specimens are presented below. No distresses such as spalling were observed in the one dowel bar test specimens. In the two, three and five dowel test specimens, different orientation of misaligned dowel bars resulted in different types of distresses such as spalling at the dowel-concrete interface, vertical uplift and cracking of the concrete specimens.

In the 2V9NU test, in addition to surface spalling, the northwest and southeast ends of the slabs lifted up (the ungreased of the two dowel bars). Figure 4.46 (a) gives a diagrammatic representation of the uplift and figures 4.46 (b) and (c) corresponds to the actual vertical uplift at the NW and SE corners of the slab. A similar observation was made in the 2V12NU and 2V18NU test specimens but the magnitude of uplift was not measured.

Cracking of the slab in later stages of the test (at joint openings higher than ½ in.) was observed in the 5V18NU test, shown in figure 4.47. As further load was applied, the crack continued to open, pushing the two halves of the slab apart rather than opening the joint. Thus the test was terminated at a joint opening of 0.93 in.

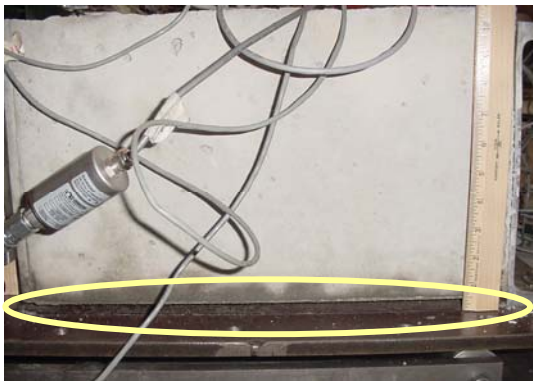

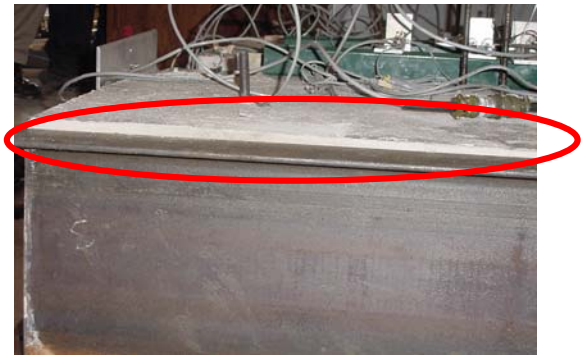

(b) NW side **(c) SE side**

Figure 4.46: Vertical Uplift (2V9NU)

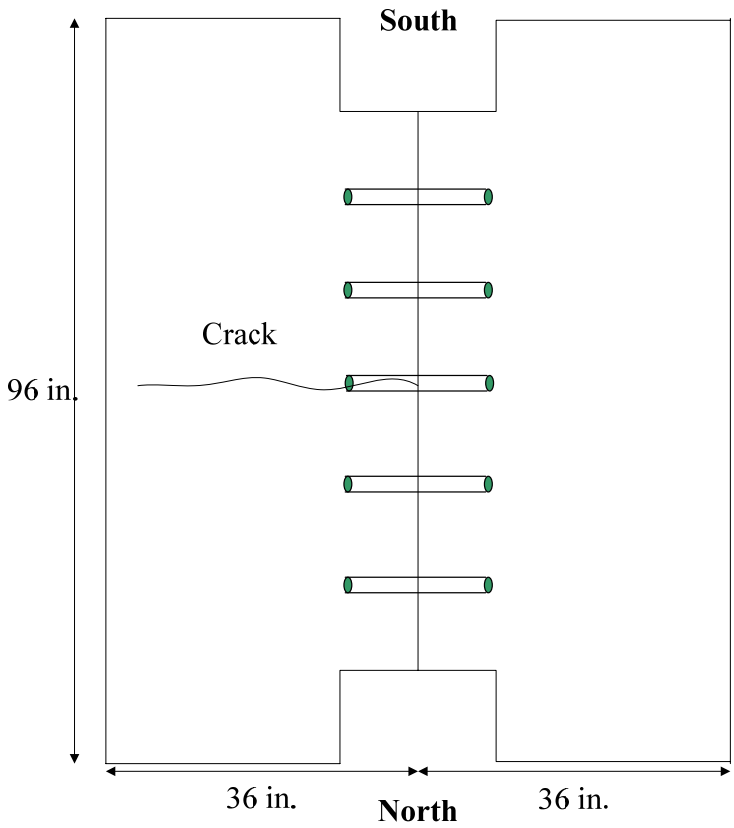

Figure 4.47: Diagrammatic representation of Crack in 5V18NU

Horizontal Misalignment Test Specimens

This section discusses the visual observations documented during the horizontal misalignment tests. In the two, three and five dowel bar test specimens, different combination of misalignment orientation resulted in different distresses such as spalling at the dowel-concrete interface, non-uniform joint opening, and cracking. Spalling was the predominant distress in these tests. The spalls ranged from 2 in. by 2 in. to more than half-depth of the slab. Typical illustrations of spalling and non-uniform joint opening observed in the 2H9U test are shown in figures 4.48 and 4.49, respectively.

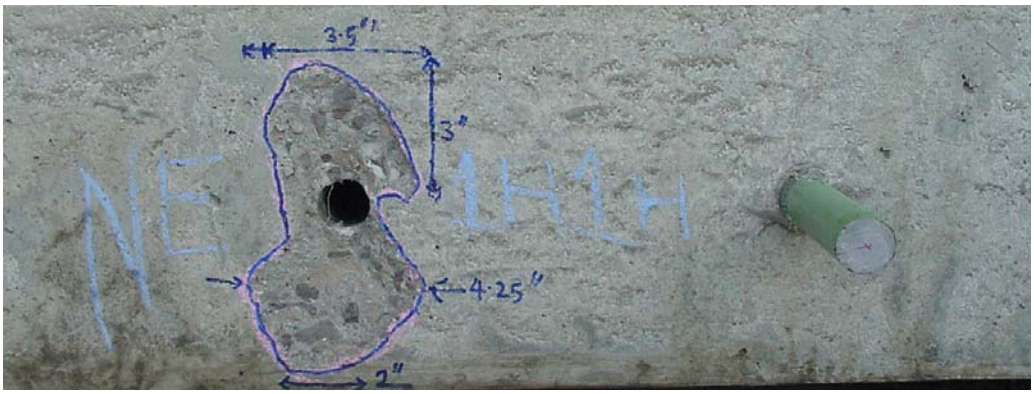

Figure 4.48: Spalling in the 2H9U test

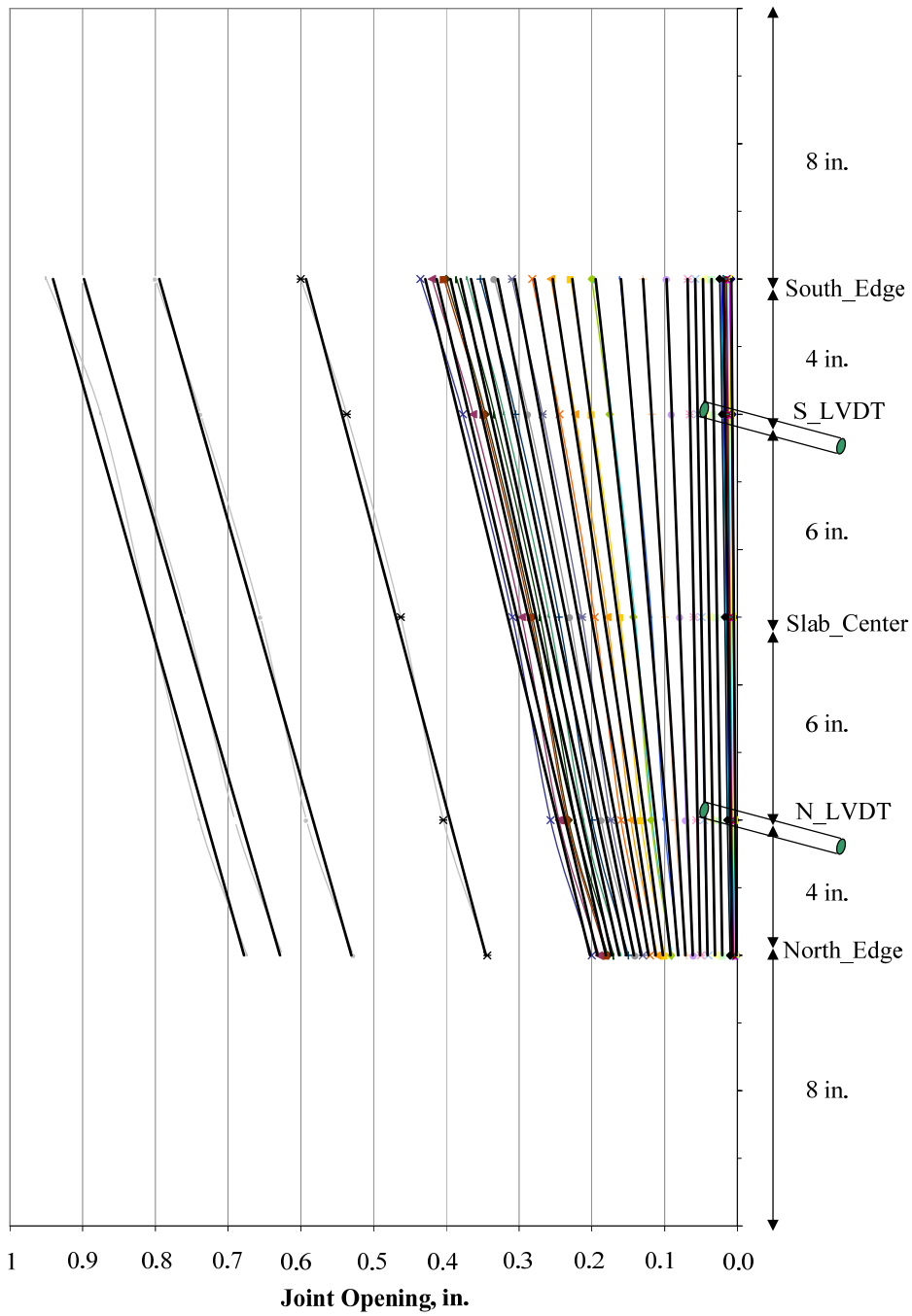

Figure 4.49: Joint opening as a function of distance along the joint (2H1U)

Cracking in the 2H12NU test: At a joint opening of 0.716 in., cracking occurred in the west slab, which resulted in a sudden drop of load from 4198 to 515 lbs, shown in figure 4.11. One full depth crack appeared instantaneously and it split the west slab into two

parts at the dowel bar on the north side. The location of the crack pattern and cracked test specimen is shown in figure 4.50.

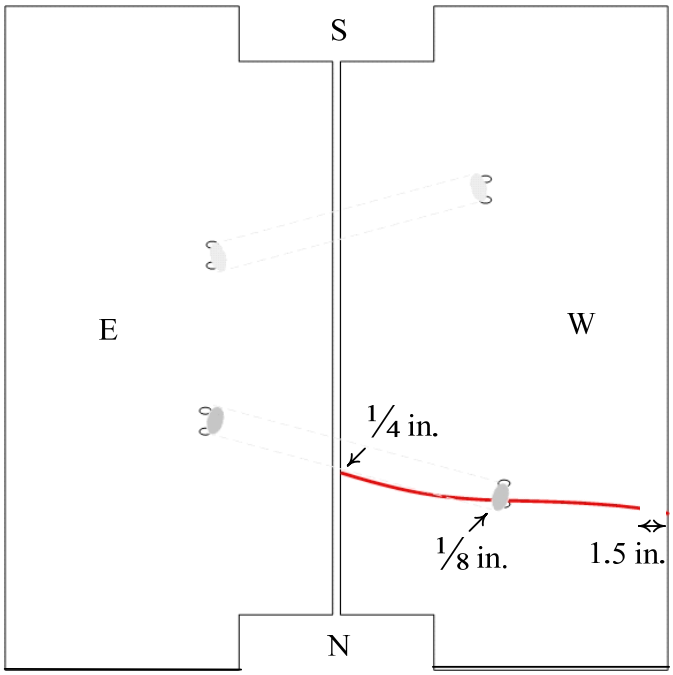

(a) Crack Pattern and Initial dimensions

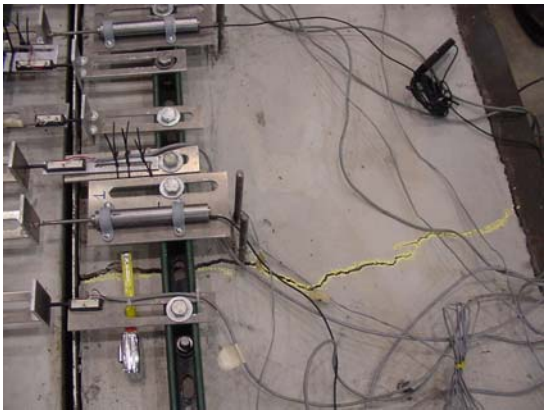

(b) Crack initiation **(c) Crack at end of test**

Figure 4.50: Cracking in 2H12NU

Cracking in the 2H9NU test: At a joint opening of 0.668 in., cracking occurred in the west slab, which resulted in a sudden drop in load from 4891 to 1476 lbs. One full depth

crack appeared instantaneously and it split the west slab into two parts at the position of the dowel bar on the north side. The dimensions and position of the crack are shown in figure 4.51. Since the pattern is to the similar to the 2H9NU test, the photographs have not been provided here.

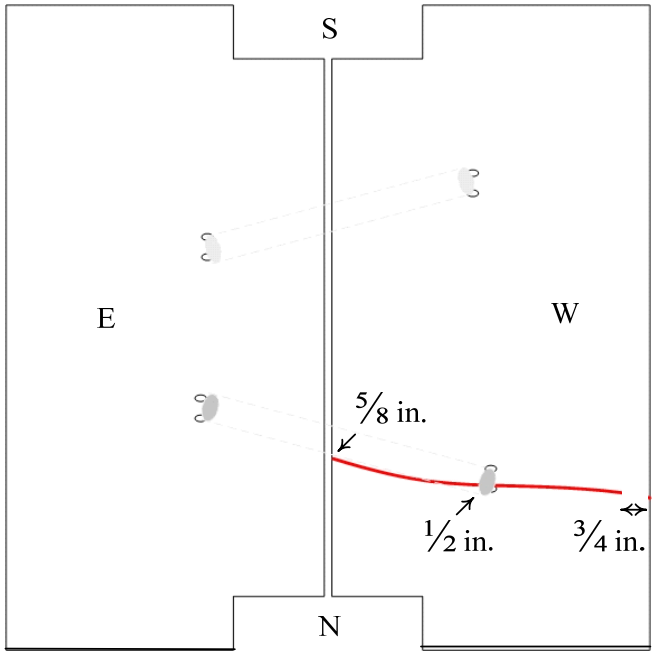

Figure 4.51: Crack pattern and Initial dimensions in 2H9NU

The sudden drop in pressure is captured in the load versus joint opening curve as seen in figure 4.11. As further load was applied, the crack continued to open, pushing the concrete pieces apart rather than opening the joint. Thus the test was stopped at a joint opening of 0.857 in. and the crack width at the joint at the end of the test was ¾ in.

Combined Misalignment Test Specimens

In the single dowel bar test specimens, the only distress observed was spalling at the dowel-concrete interface in the 1C9 test specimen. In the two, three, and five dowel tests, different orientation of misaligned dowel bars resulted in different distresses such as

spalling at the dowel-concrete interface, non-uniform joint opening, and cracking. Spalling was the predominant distress in these tests. The spalls ranged from 2 in. by 2 in. to more than half-depth of the slab. Cracking of slabs observed in the 2C12NU and 2C9NU tests are described below.

Cracking in the 2C12NU test: At a joint opening of 0.949 in., cracking occurred in the west slab, which resulted in a sudden drop of load from 4060 to 1124 lbs, shown in figure 4.19. Two cracks formed on the concrete above the north dowel bar, the schematics of the crack pattern are shown in figure 4.52. One of the cracks was a full-depth crack that appeared instantaneously and split the west slab into two part at the position of the dowel bar on the north side.

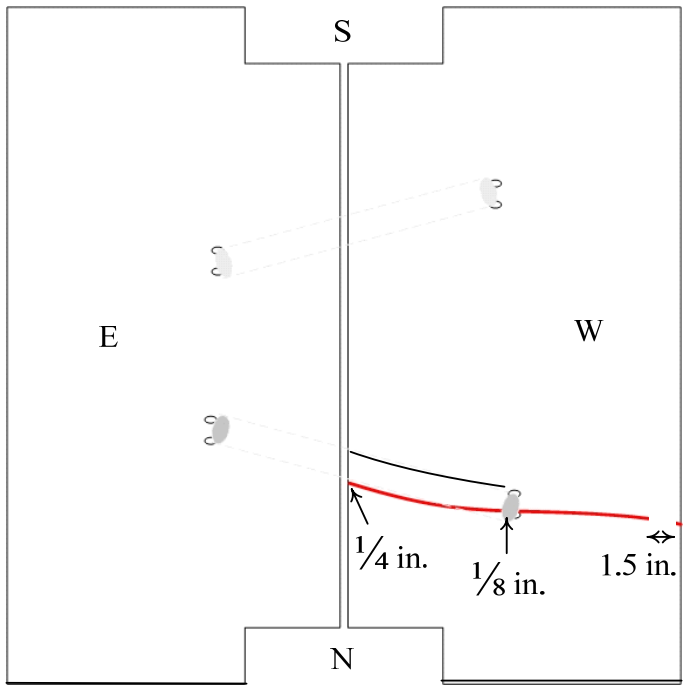

(a) Crack Pattern and Initial dimensions

(b) Crack initiation on top of the north dowel

Figure 4.52: Cracking in 2C12NU

Cracking in the 2C9NU test: At a joint opening of 0.447 in., two closely spaced cracks formed in the west slab near the south box cutout, which resulted in a sudden drop of load from 5550 to 4691 lbs, shown in figure 4.19. On further separation of the slabs, it was seen that the crack observed at the surface was a result of the crack that was initiated near the south dowel bar. At the surface, the cracks did not open significantly, but at the west joint face, the crack propagated from one dowel bar to the other. No further cracks were formed. The schematics of the crack pattern and actual cracks are shown in figure 4.53.

(a) Corner cracks observed in the test specimen

(c) Concrete spalling and cracking around misaligned dowel bar in test specimen

Figure 4.53: Corner Cracking in 2C9NU on west side

Cracking in the 5C18NU test: At a joint opening of 0.58 in., spalling occurred near the outer dowels which resulted in a drop in pressure. Cracking of the slab in later stages of the test (at joint openings higher than ½ in.) was also observed. At a joint opening of 0.824 in., a hairline crack occurred in the east slab, near the center dowel bar, the location similar to the location in the 5V18NU test. This crack resulted in a drop in load from 4108 to 1568 lbs, shown in figure 4.23.

The results obtained in the experimental investigation indicate that the distress in the concrete surrounding the misaligned dowel bars depends on the magnitude, orientation and uniformity of misalignment. It is hypothesized that the same effects will be observed when the slab thickness is increased to 12 in. with 1.5 in. diameter dowel bars.

4.3 SUMMARY OF RESULTS

To summarize the results of the laboratory investigations:

- In general, for a given misalignment type, as the magnitude of misalignment was increased, the amount of pullout force per bar to produce joint opening also increased. Test specimens with non-uniform orientation of misaligned dowels required a higher force per bar to produce joint opening compared to the alternate or the uniform orientation of misaligned dowel bars.
- For a given misalignment magnitude, the load induced per dowel to produce joint opening increased as the number of misaligned dowels increased.
- The results indicate that irrespective of the dowel misalignment type (vertical, horizontal or combined) and magnitude (shown in the 1/18 radians and 1/12 radians), the force required to open the joint in a pavement slab with non-uniform misaligned dowel bars is higher as compared to alternate and uniform orientation of misalignments.
- Structural distress such as spalling was observed in the test specimens with non-uniform orientation of dowel bars. Test specimens especially with greater than 1/12 radians non-uniform misalignment magnitude exhibited cracking.

4.4 PULLOUT BEHAVIOR OF MISALIGNED DOWEL BARS

It is hypothesized that an initial bond exists between the dowel and the hardening concrete. This bond is present due to (i) the volumetric changes in the hydrating cement paste and (ii) irregularities along dowel surface. This initial bond generates contact stresses at the dowel concrete interface. These contact stresses generate frictional and axial forces in the dowel bar that resist the free axial movement of the pavement slab

when exposed to thermal expansion and contraction. There are no bearing stresses produced in the concrete during dowel pullout in the case of an aligned dowel bar subjected to pure thermal expansion, as shown in figure 4.54.

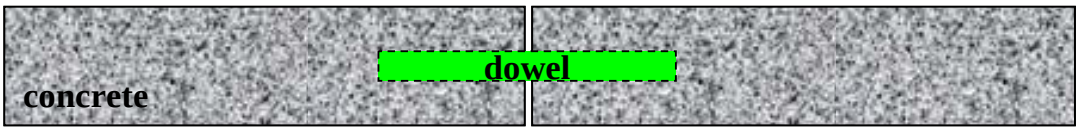

Figure 4.54: Aligned dowel bar in concrete pavement slab

However, bearing stresses and frictional shear stresses are produced at the dowel-concrete interface, for joints with misaligned dowel bars, as shown in figure 4.55.

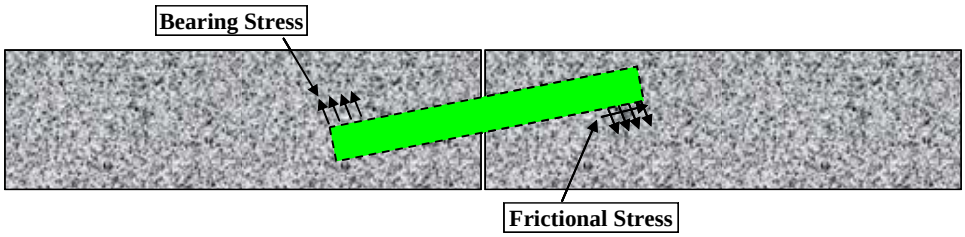

Figure 4.55: Misaligned dowel bar in a concrete pavement slab

Furthermore, as the joint opens due to thermal expansion, the bond between the dowel and concrete is a function of the kinematic friction between the two contacting surfaces. Each of the misalignment type, magnitude, and orientation would cause a certain stress state zone at the interface along the length of the bar and at the joint, which cannot be studied directly through lab observations/tests. There is a need to conduct an analytical study on the dowel concrete interaction to understand the joint opening behavior of misaligned dowel bars.

4.5 DOWEL-CONCRETE INTERACTION

The experimental results presented in the previous sections provide basic information regarding the overall joint opening behavior of concrete pavements with aligned or misaligned dowel bars. The pullout force per dowel-joint opening response of all pavement specimens consists of two regions: (1) the initial fully bonded region, and (2) the post-slip debonded region. In the initial fully bonded region, the load applied across the joint increases without any slip or joint opening. Slip occurs after the pullout force per dowel increases beyond a certain threshold value (1124 lbs -1574 lbs). In the post-slip region, as the joint is opened to 1 in., the pullout force per dowel undergoes hardening (increases) and softening (decreases) depending on the misalignment type, magnitude, and distribution. The effects of these parameters on the post-slip joint opening behavior have been presented in the previous section.

The pullout force per dowel-joint opening behavior of the pavement specimens can be used to estimate averaged bond shear stress-slip strain behavior of the dowel-concrete interfaces. The averaged bond shear stress can be estimated as the pullout force per dowel divided by the surface area ($\pi \times 1.25 \times 9$ in^2) of the greased (debonding) side of the dowel. The slip strain can be estimated by dividing the joint opening by the embedded length (9 in.) of the greased side of the dowel. The averaged bond shear stress-slip strain responses for specimens 1A and 2A (with zero misalignment) provide information regarding the overall longitudinal bond interaction between straight (aligned) dowels and the surrounding concrete; see Figure 4.56(a). The averaged bond shear stress-slip strain responses for the remaining specimens provide information regarding the overall longitudinal bond between the misaligned dowel and the surrounding concrete,